AN ABSTRACT OF THE THESIS OF

Caihua Yan for the degree of Doctor of Philosophy in Physics presented February 23, 1994.

Title: Electronic Structure and Optical Properties of ZnO: Bulk and Surface

Abstract approved: Henri J. F. Jansen William M. Hetherington

To understand and describe optical phenomena microscopically has always been an interesting challenge in theoretical physics. This thesis contributes a full-band-structure calculation of the frequency-dependent dielectric and second harmonic response functions of ZnO. These functions characterize certain optical properties of the material and they are related to the microscopic structure of the material. In our calculation for ZnO, we use a linear combination of atomic orbitals (LCAO) technique to obtain the electronic energy band structure and wave functions semiempirically.

In order to include the surface contributions to the optical properties of ZnO, we proposed a "layered" model and carried out the full-band-structure calculation of the frequency-dependent linear and nonlinear susceptibilities for both a ZnO bulk crystal and for our ZnO layered model. By comparing the results of the bulk and layered model, we find that the surface plays a significant role in determining the second harmonic response of ZnO but has no significant effects on the dielectric function. The calculated results for the dielectric function are compared to the experiment results.

Also in this thesis, the electronic surface states are calculated using our layered model. The technique of numerical integration used in the susceptibility calculation is presented and discussed.

Electronic Structure and Optical Properties of ZnO: Bulk and Surface

by

Caihua Yan

A THESIS

submitted to

Oregon State University

in partial fulfillment of the
requirements for the degree of

Doctor of Philosophy

Completed February 23, 1994

Commencement June 1994

Approved:

Redacted for Privacy

Co-Professor of Physics in charge of major

Redacted for Privacy

Co-Professor of Physics in charge of major

Redacted for Privacy

Head of Department of Physics

Redacted for Privacy

Dean of Graduate School

Date thesis is presented February 23, 1994

Typed by Caihua Yan

Table of Contents

List of Figures

List of Tables

Electronic Structure and Optical Properties of ZnO: Bulk and Surface

Chapter 1
Introduction

Second harmonic generation of optical frequencies was observed in 1961 by P.A.Franken[1]. Since then, numerous nonlinear optical phenomena have been discovered. These phenomena are very well understood and described macroscopically through Maxwell's equations together with the constitutive equations. The observation of these phenomena was facilitated by a revolutionary change in optical technology right after the advent of the laser. On the other side, however, physicists have been trying to understand and describe these phenomena microscopically. Although a large amount of research has been conducted and our knowledge about the interaction of light with matter has been greatly enhanced, a few full band-structure calculations of nonlinear optical properties of matter have appeared in the literature[2][3] only recently. A full band-structure calculation of the nonlinear optical properties of matter has been a challenge for over three decades. In particular, there is no such full band-structure calculation for ZnO over a wide range of frequencies and including matrix elements. We chose ZnO as the subject to carry out our systematic computation of optical properties of atomic matter because it has potential[4] in the electro-optical technology, together with other wurtzite structure crystals.

An optical phenomenon, whether it is linear or nonlinear, involves light and a medium[5]. The underlying process is simple. Light first induces a response in the medium, and then the medium, in reaction, modifies the electromagnetic fields.

Hence, we have two problems. One problem is how to describe the response in terms of intrinsic properties of the medium. Another is to find out how the electromagnetic fields are modified by the response of the medium.

N. Bloembergen and co-workers[6] developed in 1962 a semi-classical theory to connect the macroscopic Maxwell's field quantities with the intrinsic properties of dielectric matter. Via such a connection, the polarization, which accounts for the response of the medium in the macroscopic Maxwell's equations, is expressed microscopically in terms of eigenvalues and wave functions of the system. Those expressions have been widely used in calculations of optical properties, and we will also use them to carry out our calculations. We assume that the response function is independent of the space variable $\vec{r}$ for a non-localized system.

Once we have obtained the connection between the macroscopic properties of Maxwell's field quantities and the intrinsic properties of matter, we are ready to carry out the computations if we know how to obtain the intrinsic properties of atomic matter. For a material like ZnO, its intrinsic properties need to be characterized by its electronic band structure. The LCAO (Linear Combination of Atomic Orbitals) method[7] will be used in our calculations of the electronic band structure and corresponding wave functions.

Also of interest are the electronic structure and optical properties of the ZnO surface. A "layered" model is proposed. The idea is that surface states can be identified by comparing the results of a bulk ZnO calculation with those of a layered model calculation, and optical properties of the surface can be included using our layered model.

So far we claimed that we are going to calculate optical properties and we mentioned that optical properties are related to the polarizability. In Chapter 2 we present the fundamentals defining the polarizability and nonlinear polarizabilities and how they can be used to explain various optical phenomena such as refraction, second

harmonic generation, third harmonic generation, stimulated Raman scattering, etc. The general formalism used in our calculations will be given following these fundamentals in that chapter. Since we need the electronic band structure and electron wave functions to compute optical properties of ZnO, Chapter 3 provides a description of the LCAO method, followed by a description of the ZnO crystal structure and the bulk band structure calculation. In Chapter 4 we discuss finite one-dimensional models in order to make some simple observations about surface states. Then, in Chapter 5 we present our "layered" model for the ZnO surface and calculate the surface electronic structure. In Chapter 6 we present our calculation of the first order susceptibility. Our calculation of second harmonic response functions is given in Chapter 7.

Chapter 2
Semiclassical Theory of Polarizability

As pointed out in chapter 1, all optical phenomena involve light and a medium. The light first induces a response in the medium, then the medium in reacting modifies the electromagnetic fields. A response is linear if its amplitude is proportional to the amplitude of the incident light. Otherwise, a response is considered nonlinear. In the case of linear response, the electromagnetic fields of the light will be modified linearly, but the electromagnetic fields will be modified nonlinearly if the response is nonlinear.

So, if we can find a way to describe the response and to define at the same time how the response will modify the electromagnetic fields of the light, then we are in the position to understand and predict optical phenomena. A phenomenological theory based upon such a philosophy exists. It is the well-known theory of classical electrodynamics[8][9] of continuous media.

2.1 Maxwell's Equations in a Medium

Microscopically, a medium consists of nuclei and electrons. The size of a nucleus is about 10^{-14} m and the size of an electron is much smaller. They can be treated as charged point particles. When the medium is described as charged point particles the interaction between such a medium and light is described by the microscopic Maxwell's equations which are, in Gaussian unit, as follows:

$$\vec{\nabla} \cdot \vec{b} = 0 \qquad (2.1)$$

$$\vec{\nabla} \times \vec{e} + \frac{1}{c}\frac{\partial \vec{b}}{\partial t} = 0 \qquad (2.2)$$

$$\vec{\nabla} \cdot \vec{e} = 4\pi\rho \qquad (2.3)$$

$$\vec{\nabla} \times \vec{b} - \frac{1}{c}\frac{\partial \vec{e}}{\partial t} = \frac{4\pi}{c}\vec{j} \qquad (2.4)$$

where $\vec{e}$ and $\vec{b}$ are the microscopic electric and magnetic fields, ρ is the microscopic charge density, $\vec{j}$ is the microscopic current density and c is the vacuum speed of light.

Unfortunately, those equations are unsolvable because a macroscopic system contains a huge number of electrons and nuclei (on the order of 10^{23}). The details of changes in those physical quantities are too overwhelming. It is not of interest, however, to explore the detailed changes over very small ranges of both time and space in our case. So, we average those microscopic quantities over a small volume of space which is a little bit smaller than the smallest volume we can macroscopically distinguish. We end up with the macroscopic Maxwell's equations,

$$\vec{\nabla} \cdot \vec{B} = 0 \qquad (2.5)$$

$$\vec{\nabla} \times \vec{E} + \frac{1}{c}\frac{\partial \vec{B}}{\partial t} = 0 \qquad (2.6)$$

$$\vec{\nabla} \cdot \vec{D} = 4\pi\rho \qquad (2.7)$$

$$\vec{\nabla} \times \vec{H} - \frac{1}{c}\frac{\partial \vec{D}}{\partial t} = \frac{4\pi}{c}\vec{J} \qquad (2.8)$$

where $\vec{E}$ and $\vec{B}$ are the macroscopic electric and magnetic field quantities, ρ and $\vec{J}$ are macroscopic charge and current densities, $\vec{D}$ and $\vec{H}$ are macroscopic quantities which are related to $\vec{E}$ and $\vec{B}$ through the macroscopic polarization $\vec{P}$ and magnetization $\vec{M}$ of the matter as follows,

$$\vec{D} = \vec{E} + 4\pi\vec{P} \qquad (2.9)$$

$$\vec{H} = \vec{B} - 4\pi\vec{M} \qquad (2.10)$$

As it is shown from equations from (2.5) to (2.10), the response of the medium is accounted for by the macroscopic polarization $\vec{P}$ and magnetization $\vec{M}$. At the same time, the modification of the electromagnetic fields by the response is also clearly

defined through those equations. Equations (2.9 and 2.10) are often called the constitutive equations.

By following the process of averaging the microscopic Maxwell's equations, we find out[8] that $\vec{P}$ and $\vec{M}$ should contain macroscopic multipole terms. In this thesis, we keep the electric dipole term only, and we assume that there is no electric current and no net charge in the medium. Then, the macroscopic Maxwell's equations become,

$$\vec{\nabla}\times\vec{E}=-\frac{1}{c}\frac{\partial\vec{B}}{\partial t} \qquad (2.11)$$

$$\vec{\nabla}\times\vec{B}=\frac{1}{c}\frac{\partial}{\partial t}\left(\vec{E}+4\pi\vec{P}\right) \qquad (2.12)$$

$$\vec{\nabla}\cdot\left(\vec{E}+4\pi\vec{P}\right)=0 \qquad (2.13)$$

$$\vec{\nabla}\cdot\vec{B}=0 \qquad (2.14)$$

where $\vec{P}$, the polarization is the only source for the electromagnetic fields in the equations above.

$\vec{P}$ is not well defined on a surface, near a region of impurities or on an interface between two different media because $\vec{P}$ is defined as a macroscopic quantity by averaging the electric dipole moments over the volume of space which is macroscopically small but microscopically large. We have to be very cautious when we focus on the inhomogeneous region of a medium.

It should now be clear that we intend to describe the response of the medium to the light by the macroscopic polarization $\vec{P}$. Later on in this chapter we will see how $\vec{P}$ can be formulated in terms of the intrinsic properties of the medium according to its macroscopic definition. But first, we examine the possible dependency of $\vec{P}$ on the external electric fields and discuss how the fields can be modified by such a response $\vec{P}$ by studying equations (2.11-2.14) in more detail.

2.2 The Polarizability

After substitution of equation (2.12) into the equation of $\vec{\nabla}\times(2.11)$, we obtain,

$$\nabla\times\left(\nabla\times\vec{E}\right)+\frac{1}{c^2}\frac{\partial^2}{\partial t^2}\vec{E}=-\frac{4\pi}{c^2}\frac{\partial^2}{\partial t^2}\vec{P} \qquad (2.15)$$

This equation shows clearly that $\vec{P}$ is a source for $\vec{E}$. This equation is linear.

On the other hand, the electric fields are causing the polarization. The most general form of $\vec{P}$ is,

$$\vec{P}(\vec{r},t)=\int_{-\infty}^{+\infty}d\vec{r}_1\int_0^{\infty}dt_1\vec{\vec{\chi}}^{(1)}(\vec{r}-\vec{r}_1,t-t_1)\vec{E}(\vec{r}_1,t_1)+$$

$$\int_{-\infty}^{+\infty}d\vec{r}_1d\vec{r}_2\int_0^{\infty}dt_1dt_2\vec{\vec{\vec{\chi}}}^{(2)}(\vec{r}-\vec{r}_1,t-t_1;\ \vec{r}-\vec{r}_2,t-t_2)\vec{E}(\vec{r}_1,t_1)\vec{E}(\vec{r}_2,t_2)+$$

$$\int_{-\infty}^{+\infty}d\vec{r}_1d\vec{r}_2d\vec{r}_3\int_0^{\infty}dt_1dt_2dt_3\vec{\vec{\vec{\vec{\chi}}}}^{(3)}(\vec{r}-\vec{r}_1,t-t_1;\ \vec{r}-\vec{r}_2,t-t_2;\vec{r}-\vec{r}_3,t-t_3)\vec{E}(\vec{r}_1,t_1)\vec{E}(\vec{r}_2,t_2)\vec{E}(\vec{r}_3,t_3)$$

$$+\cdots \qquad (2.16)$$

This is just a functional expansion of $\vec{P}(\vec{r},t)$ in terms of the electric field $\vec{E}(\vec{r},t)$. The coefficients $\vec{\vec{\chi}}^{(1)}$, $\vec{\vec{\vec{\chi}}}^{(2)}$ and $\vec{\vec{\vec{\vec{\chi}}}}^{(3)}$ are called first, second and third order susceptibilities. We have to bear in mind that $\vec{P}(\vec{r},t)$ and $\vec{E}(\vec{r},t)$ are macroscopic quantities. The combination of equations (2.15) and (2.16) determines the actual fields in the medium. The properties of the material are embedded in the susceptibilities.

Now, in order to better see the effect of each term in equation (2.16), we take the Fourier transform of equation (2.15). That is we substitute the following equations,

$$\vec{E}(\vec{r},t)=\int_{-\infty}^{+\infty}\vec{E}\left(\omega,\vec{k}\right)e^{i\left(\vec{k}\cdot\vec{r}-\omega t\right)}d\omega d\vec{k} \qquad (2.17)$$

$$\vec{P}(\vec{r},t)=\int_{-\infty}^{+\infty}\vec{P}\left(\omega,\vec{k}\right)e^{i\left(\vec{k}\cdot\vec{r}-\omega t\right)}d\omega d\vec{k} \qquad (2.18)$$

into equation (2.15). This gives,

$$\vec{k}\times\left(\vec{k}\times\vec{E}\left(\omega,\vec{k}\right)\right)+\frac{\omega^2}{c^2}\vec{E}\left(\omega,\vec{k}\right)=-\frac{4\pi\omega^2}{c^2}\vec{P}\left(\omega,\vec{k}\right) \qquad (2.19)$$

where $\vec{E}\left(\omega,\vec{k}\right)$ and $\vec{P}\left(\omega,\vec{k}\right)$ are the Fourier transforms of $\vec{E}(\vec{r},t)$ and $\vec{P}(\vec{r},t)$ respectively. The Fourier transform of equation (2.16) gives $\vec{P}\left(\omega,\vec{k}\right)$ expanded into a series,

$$\vec{P}\left(\omega,\vec{k}\right)=\vec{P}^{(1)}\left(\omega,\vec{k}\right)+\vec{P}^{(2)}\left(\omega,\vec{k}\right)+\vec{P}^{(3)}\left(\omega,\vec{k}\right)+\cdots \qquad (2.20)$$

where

$$\vec{P}^{(1)}\left(\omega,\vec{k}\right)=\frac{1}{(2\pi)^4}\int d\vec{r}dt\int d\vec{r}_1dt_1\bar{\bar{\chi}}^{(1)}(\vec{r}-\vec{r}_1,t-t_1)\vec{E}(\vec{r}_1,t_1)e^{-i\left(\vec{k}\cdot\vec{r}-\omega t\right)}$$

$$\equiv\bar{\bar{\chi}}^{(1)}\left(\omega,\vec{k}\right)\vec{E}\left(\omega,\vec{k}\right) \qquad (2.21)$$

$$\vec{P}^{(2)}\left(\omega,\vec{k}\right)$$

$$=\frac{1}{(2\pi)^4}\int d\vec{r}dte^{-i\left(\vec{k}\cdot\vec{r}-\omega t\right)}\int d\vec{r}_1d\vec{r}_2dt_1dt_2\bar{\bar{\bar{\chi}}}^{(2)}(\vec{r}-\vec{r}_1,t-t_1;\vec{r}-\vec{r}_2,t-t_2)\vec{E}(\vec{r}_1,t_1)\vec{E}(\vec{r}_2,t_2)$$

$$\equiv\int d\omega_1d\vec{k}_1d\omega_2d\vec{k}_2\bar{\bar{\bar{\chi}}}^{(2)}\left(\omega_1,\vec{k}_1,\omega_2,\vec{k}_2\right)\vec{E}\left(\omega_1,\vec{k}_1\right)\vec{E}\left(\omega_2,\vec{k}_2\right)\delta\left(\vec{k}-\vec{k}_1-\vec{k}_2\right)\delta(\omega-\omega_1-\omega_2)$$

$$=\int d\omega_1d\vec{k}_1\bar{\bar{\bar{\chi}}}^{(2)}\left(\omega_1,\vec{k}_1,\omega-\omega_1,\vec{k}-\vec{k}_1\right)\vec{E}\left(\omega_1,\vec{k}_1\right)\vec{E}\left(\omega-\omega_1,\vec{k}-\vec{k}_1\right) \qquad (2.22)$$

$$\vec{P}^{(3)}\left(\omega,\vec{k}\right)=\frac{1}{(2\pi)^4}\int d\vec{r}dte^{-i\left(\vec{k}\cdot\vec{r}-\omega t\right)}\int d\vec{r}_1d\vec{r}_2d\vec{r}_3dt_1dt_2dt_3$$

$$\bar{\bar{\bar{\bar{\chi}}}}^{(3)}(\vec{r}-\vec{r}_1,t-t_1;\vec{r}-\vec{r}_2,t-t_2;\vec{r}-\vec{r}_3;t-t_3)\vec{E}(\vec{r}_1,t_1)\vec{E}(\vec{r}_2,t_2)\vec{E}(\vec{r}_3,t_3)$$

$$=\int d\omega_1d\vec{k}_1d\omega_2d\vec{k}_2\bar{\bar{\bar{\bar{\chi}}}}^{(3)}\left(\omega_1,\vec{k}_1,\omega_2,\vec{k}_2,\omega-\omega_1-\omega_2,\vec{k}-\vec{k}_1-\vec{k}_2\right)$$

$$\vec{E}\left(\omega_1,\vec{k}_1\right)\vec{E}\left(\omega_2,\vec{k}_2\right)\vec{E}\left(\omega-\omega_1-\omega_2,\vec{k}-\vec{k}_1-\vec{k}_2\right) \qquad (2.23)$$

where $\bar{\bar{\chi}}^{(1)}(\omega,\vec{k})$, $\bar{\bar{\bar{\chi}}}^{(2)}(\omega_1,\vec{k}_1;\omega_2,\vec{k}_2)$, $\bar{\bar{\bar{\bar{\chi}}}}^{(3)}(\omega_1,\vec{k}_1;\omega_2,\vec{k}_2;\omega_3,\vec{k}_3)$ are the Fourier transforms of the susceptibilities, defined as,

$$\bar{\bar{\chi}}^{(1)}(\omega,\vec{k})=\frac{1}{(4\pi)^4}\int\bar{\bar{\chi}}^{(1)}(\vec{r},t)e^{-i(\vec{k}\cdot\vec{r}-\omega t)}d\vec{r}dt \qquad (2.24)$$

$$\bar{\bar{\bar{\chi}}}^{(2)}(\omega_1,\vec{k}_1;\omega_2,\vec{k}_2)=\frac{1}{(4\pi)^8}\int\bar{\bar{\bar{\chi}}}^{(2)}(\vec{r}_1,t_1;\vec{r}_2,t_2)e^{-i(\vec{k}_1\cdot\vec{r}_1-\omega_1t_1)}e^{-i(\vec{k}_2\cdot\vec{r}_2-\omega_2t_2)}d\vec{r}_2dt_2d\vec{r}_1dt_1 \qquad (2.25)$$

$$\bar{\bar{\bar{\bar{\chi}}}}^{(3)}(\omega_1,\vec{k}_1;\omega_2,\vec{k}_2;\omega_3\vec{k}_3)=\frac{1}{(4\pi)^{12}}\times$$
$$\int\bar{\bar{\bar{\bar{\chi}}}}^{(3)}(\vec{r}_1,t_1;\vec{r}_2,t_2;\vec{r}_3,t_3)e^{-i(\vec{k}_1\cdot\vec{r}_1-\omega_1t_1)}e^{-i(\vec{k}_2\cdot\vec{r}_2-\omega_2t_2)}e^{-i(\vec{k}_3\cdot\vec{r}_3-\omega_3t_3)}d\vec{r}_3dt_3d\vec{r}_2dt_2d\vec{r}_1dt_1 \qquad (2.26)$$

2.2.1 Linear response and dispersion

First we ignore higher order terms and keep $\vec{P}^{(1)}(\omega,\vec{k})$ only. Then we obtain from equation (2.19) and (2.21) the following equation,

$$\vec{k}\times\left(\vec{k}\times\vec{E}(\omega,\vec{k})\right)+\frac{\omega^2}{c^2}\vec{E}(\omega,\vec{k})=-\frac{4\pi\omega^2}{c^2}\bar{\bar{\chi}}^{(1)}(\omega,\vec{k})\vec{E}(\omega,\vec{k}) \qquad (2.27)$$

Obviously, this equation is a linear equation in $\vec{E}$. From now on, we will suppose that the susceptibility $\bar{\bar{\chi}}^{(n)}$ is independent of $\vec{k}$. Furthermore, in the case of linear response we choose the coordinate system such that $\bar{\bar{\chi}}^{(1)}$ is a diagonalized tensor. Then equation (2.27) becomes,

$$\vec{k}\times\left(\vec{k}\times\vec{E}(\omega,\vec{k})\right)+\frac{\omega^2}{c^2}\varepsilon(\omega)\vec{E}(\omega,\vec{k})=0 \qquad (2.28)$$

where $$\varepsilon(\omega)=1+4\pi\chi^{(1)}(\omega) \qquad (2.29)$$

Equation (2.29) is called a dispersion relation, $\varepsilon(\omega)$ is called the permittivity or dielectric function. By solving equation (2.28) and discussing the solutions for various cases one finds out that $\bar{\bar{\chi}}^{(1)}$ is responsible for phenomena such as absorption and

refraction. The change in the shape of a traveling light beam through the medium can also be explained by $\bar{\bar{\chi}}^{(1)}$.

For later convenience, we give the formulas for the refractive index n and absorption coefficient κ:

$$n=\sqrt{\frac{1}{2}\left[1+4\pi\chi_R^{(1)}+\sqrt{\left(1+4\pi\chi_R^{(1)}\right)^2+\left(4\pi\chi_I^{(1)}\right)^2}\right]} \qquad (2.30a)$$

$$\kappa=\sqrt{\frac{1}{2}\left[-(1+4\pi\chi_R^{(1)})+\sqrt{\left(1+4\pi\chi_R^{(1)}\right)^2+\left(4\pi\chi_I^{(1)}\right)^2}\right]} \qquad (2.30b)$$

where $\chi_R^{(1)}$ and $\chi_I^{(1)}$ are real and imaginary parts of $\bar{\bar{\chi}}^{(1)}(\omega)$ respectively.

2.2.2 Second order response

If we include $\vec{P}^{(2)}(\omega,\vec{k})$, then we obtain from equations of (2.19), (2.21), (2.22) and (2.29):

$$\vec{k}\times\left(\vec{k}\times\vec{E}(\omega,\vec{k})\right)+\frac{\omega^2}{c^2}\varepsilon(\omega)\vec{E}(\omega,\vec{k})=$$
$$-\frac{4\pi\omega^2}{c^2}\int d\omega_1 d\vec{k}_1\bar{\bar{\chi}}^{(2)}(\omega_1,\omega-\omega_1)\vec{E}(\omega_1,\vec{k}_1)\vec{E}(\omega-\omega_1,\vec{k}-\vec{k}_1) \qquad (2.31)$$

Equation (2.31) gives us a group of equations which couple different components of the electric fields. The integration on the right hand side of equation (2.31) becomes a summation if the electric field contains only a couple of discrete monochromatic components. Equation (2.31) tells us that the response of the medium to the components of the electric fields at frequencies ω_1 and $\omega-\omega_1$ with wave vectors $\vec{k}_1$ and $\vec{k}-\vec{k}_1$ becomes a driving source for the component of the electric field of frequency ω and wave vector $\vec{k}$. Generally, equation (2.31) couples three components of the electric field. Equation (2.31) also shows that only those three components which

satisfy the following conditions can be coupled.

$$\vec{k} = \vec{k}_1 + \vec{k}_2 \qquad (2.32)$$

$$\omega = \omega_1 + \omega_2 \qquad (2.33)$$

Equation (2.33) is simply conservation of energy. Equation (2.32) is commonly interpreted as momentum conservation. It is the so-called phase matching condition.

Now, suppose that we have three electric field components with frequencies and wave vectors of $(\omega_1, \vec{k}_1)$, $(\omega_2, \vec{k}_2)$, $(\omega_3, \vec{k}_3)$ and that they are coupled through a second order nonlinear response. Then, from equation (2.31), the coupled wave equations can be written as,

$$\vec{k}_1 \times \left(\vec{k}_1 \times \vec{E}(\omega_1, \vec{k}_1)\right) + \frac{\omega_1^2}{c^2}\varepsilon(\omega_1)\vec{E}(\omega_1, \vec{k}_1) = -\frac{4\pi\omega_1^2}{c^2}\vec{\vec{\chi}}^{(2)}(\omega_2, \omega_3)\vec{E}(\omega_2, \vec{k}_2)\vec{E}(\omega_3, \vec{k}_3) \qquad \text{..... (2.34)}$$

$$\vec{k}_2 \times \left(\vec{k}_2 \times \vec{E}(\omega_2, \vec{k}_2)\right) + \frac{\omega_2^2}{c^2}\varepsilon(\omega_2)\vec{E}(\omega_2, \vec{k}_2) = -\frac{4\pi\omega_2^2}{c^2}\vec{\vec{\chi}}^{(2)}(\omega_1, -\omega_3)\vec{E}(\omega_1, \vec{k}_1)\vec{E}(-\omega_3, -\vec{k}_3) \qquad \text{..... (2.35)}$$

$$\vec{k}_3 \times \left(\vec{k}_3 \times \vec{E}(\omega_3, \vec{k}_3)\right) + \frac{\omega_3^2}{c^2}\varepsilon(\omega_3)\vec{E}(\omega_3, \vec{k}_3) = -\frac{4\pi\omega_3^2}{c^2}\vec{\vec{\chi}}^{(2)}(\omega_1, -\omega_2)\vec{E}(\omega_1, \vec{k}_1)\vec{E}(-\omega_2, -\vec{k}_2) \qquad \text{..... (2.36)}$$

with the conditions,

$$\omega_1 = \omega_2 + \omega_3 \qquad (2.37)$$

$$\vec{k}_1 = \vec{k}_2 + \vec{k}_3 \qquad (2.38)$$

If $\omega_2 = \omega_3 \equiv \omega$, $\omega_1 = 2\omega$, $\vec{k}_2 = \vec{k}_3 \equiv \vec{k}$ and $\vec{k}_1 = 2\vec{k}$, then the three coupled equations reduce to the following two coupled equations for Second Harmonic Generation (SHG):

$$\vec{k} \times \left(\vec{k} \times \vec{E}(2\omega, 2\vec{k})\right) + \frac{\omega^2}{c^2}\varepsilon(2\omega)\vec{E}(2\omega, 2\vec{k}) = -\frac{4\pi\omega^2}{c^2}\vec{\vec{\chi}}^{(2)}(\omega, \omega)\vec{E}(\omega, \vec{k})\vec{E}(\omega, \vec{k}) \qquad \text{..... (2.39)}$$

$$\vec{k}\times\left(\vec{k}\times\vec{E}(\omega,\vec{k})\right)+\frac{\omega^2}{c^2}\varepsilon(\omega)\vec{E}(\omega,\vec{k})=-\frac{4\pi\omega^2}{c^2}\vec{\vec{\chi}}^{(2)}(2\omega,-\omega)\vec{E}(2\omega,2\vec{k})\vec{E}(-\omega,-\vec{k}) \quad \text{..... (2.40)}$$

In conclusion, the second order nonlinear response $\vec{P}^{(2)}(\omega,\vec{k})$ results in second harmonic generation which is a special case of sum frequency generation. The phase matching condition must be satisfied in these processes.

2.2.3 Third order response

If we ignore the second order response $\vec{P}^{(2)}(\omega,\vec{k})$, but include the third order response $\vec{P}^{(3)}(\omega,\vec{k})$, then from equations (2.19), (2.21), (2.23) and (2.29) we find:

$$\vec{k}\times\left(\vec{k}\times\vec{E}(\omega,\vec{k})\right)+\frac{\omega^2}{c^2}\varepsilon(\omega)\vec{E}(\omega,\vec{k})=-\frac{4\pi\omega^2}{c^2}\times$$
$$\int d\omega_1 d\vec{k}_1 d\omega_2 d\vec{k}_2\vec{\vec{\chi}}^{(3)}(\omega_1,\omega_2,\omega-\omega_1-\omega_2)\vec{E}(\omega_1,\vec{k}_1)\vec{E}(\omega_2,\vec{k}_2)\vec{E}(\omega-\omega_1-\omega_2,\vec{k}-\vec{k}_1-\vec{k}_2) \quad \text{..... (2.41)}$$

It is not difficult to deduce from equation (2.41) that the third order response leads to the coupling of two, three or four components of the electric field.

In the case where two different components couple, there is no condition imposed upon their frequencies and wave vectors. Especially, there is no phase matching condition required. This is the case of the Stimulated Raman Scattering (SRS) phenomena. The coupling equations for the stimulated Raman scattering are derived from equation (2.41):

$$\vec{k}_1\times\left(\vec{k}_1\times\vec{E}(\omega_1,\vec{k}_1)\right)+\frac{\omega_1^2}{c^2}\varepsilon(\omega_1)\vec{E}(\omega_1,\vec{k}_1)=-\frac{4\pi\omega_1^2}{c^2}\times$$
$$\vec{\vec{\chi}}^{(3)}(\omega_1,\omega_2,-\omega_2)\vec{E}(\omega_1,\vec{k}_1)\vec{E}(\omega_2,\vec{k}_2)\vec{E}(-\omega_2,-\vec{k}_2) \qquad (2.42)$$

$$\vec{k}_2 \times \left(\vec{k}_2 \times \vec{E}\left(\omega_2, \vec{k}_2\right)\right) + \frac{\omega_2^{\,2}}{c^2}\varepsilon(\omega_2)\vec{E}\left(\omega_2, \vec{k}_2\right) = -\frac{4\pi\omega_2^{\,2}}{c^2} \times$$
$$\vec{\vec{\vec{\chi}}}^{(3)}(\omega_1, \omega_2, -\omega_1)\vec{E}\left(\omega_1, \vec{k}_1\right)\vec{E}\left(\omega_2, \vec{k}_2\right)\vec{E}\left(-\omega_1, -\vec{k}_1\right) \qquad (2.43)$$

Three component coupling is a special case of four component coupling. The equations for four component coupling take the form

$$\vec{k}_1 \times \left(\vec{k}_1 \times \vec{E}\left(\omega_1, \vec{k}_1\right)\right) + \frac{\omega_1^{\,2}}{c^2}\varepsilon(\omega_1)\vec{E}\left(\omega_1, \vec{k}_1\right) = -\frac{4\pi\omega_1^{\,2}}{c^2} \times$$
$$\vec{\vec{\vec{\chi}}}^{(3)}(\omega_2, \omega_3, \omega_4)\vec{E}\left(\omega_2, \vec{k}_2\right)\vec{E}\left(\omega_3, \vec{k}_3\right)\vec{E}\left(\omega_4, \vec{k}_4\right) \qquad (2.44)$$

$$\vec{k}_2 \times \left(\vec{k}_2 \times \vec{E}\left(\omega_2, \vec{k}_2\right)\right) + \frac{\omega_2^{\,2}}{c^2}\varepsilon(\omega_2)\vec{E}\left(\omega_2, \vec{k}_2\right) = -\frac{4\pi\omega_2^{\,2}}{c^2} \times$$
$$\vec{\vec{\vec{\chi}}}^{(3)}(\omega_1, -\omega_3, -\omega_4)\vec{E}\left(\omega_1, \vec{k}_1\right)\vec{E}\left(-\omega_3, -\vec{k}_3\right)\vec{E}\left(-\omega_4, -\vec{k}_4\right) \qquad (2.45)$$

$$\vec{k}_3 \times \left(\vec{k}_3 \times \vec{E}\left(\omega_3, \vec{k}_3\right)\right) + \frac{\omega_3^{\,2}}{c^2}\varepsilon(\omega_3)\vec{E}\left(\omega_3, \vec{k}_3\right) = -\frac{4\pi\omega_3^{\,2}}{c^2} \times$$
$$\vec{\vec{\vec{\chi}}}^{(3)}(\omega_1, -\omega_2, -\omega_4)\vec{E}\left(\omega_1, \vec{k}_1\right)\vec{E}\left(-\omega_2, -\vec{k}_2\right)\vec{E}\left(-\omega_4, -\vec{k}_4\right) \qquad (2.46)$$

$$\vec{k}_4 \times \left(\vec{k}_4 \times \vec{E}\left(\omega_4, \vec{k}_4\right)\right) + \frac{\omega_4^{\,2}}{c^2}\varepsilon(\omega_4)\vec{E}\left(\omega_4, \vec{k}_4\right) = -\frac{4\pi\omega_4^{\,2}}{c^2} \times$$
$$\vec{\vec{\vec{\chi}}}^{(3)}(\omega_1, -\omega_2, -\omega_3)\vec{E}\left(\omega_1, \vec{k}_1\right)\vec{E}\left(-\omega_2, -\vec{k}_2\right)\vec{E}\left(-\omega_3, -\vec{k}_3\right) \qquad (2.47)$$

with the restrictions of ,

$$\omega_1 = \omega_2 + \omega_3 + \omega_4 \qquad (2.48)$$
$$\vec{k}_1 = \vec{k}_2 + \vec{k}_3 + \vec{k}_4 \qquad (2.49)$$

As we can see from equations (2.44) - (2.49), the phase matching conditions have to be satisfied in the four component coupling through third order response in addition to the conservation of energy requirement. If $\omega_2 = \omega_3 = \omega_4 \equiv \omega$, equations (2.44) - (2.49) describe third harmonic generation (THG).

So, we have demonstrated that some phenomena resulting from the third order response need phase matching to take place, but others need not.

2.3 Formal Expressions of Polarizability

Next, we turn to the formulation of polarizations in terms of the intrinsic properties of the medium. Even without external electromagnetic fields the atomic matter is a complex system which consists of a large number of particles interacting with each other. Since those internal interactions among the particles are very strong, the external electric fields introduce only a small perturbation in the atomic matter system. Based on this judgment, the expressions of polarization can be formulated using perturbation theory.

In the mean field approximation, a many-body system is described by particles in single-particle eigenstates. Hence, there is an electron occupation distribution of the eigenstates. The perturbing of the external electromagnetic field changes the electron occupation distribution of the system by mixing those eigenstates or inducing transitions from one eigenstate to another. It would be straightforward to calculate the polarization if the distribution and the wave functions of the eigenstates were known. We could simply take a quantum average of the dipole moments. A statistical ensemble average of dipole moments, instead of a quantum average, should be taken if thermal effects are considered. For such a calculation, it is convenient to use the density matrix formalism.

Let ρ denote the density matrix operator. The equation of motion for ρ is the following Liouville equation.[5][20]

$$i\hbar\frac{\partial\rho}{\partial t}=[H,\rho] \qquad (2.50)$$

where the single electron Hamiltonian H includes external influences. The Hamiltonian H consists of three parts,

$$H = H_0 + H_{\text{int}} + H_{random} \qquad (2.51)$$

where H_0 is the Hamiltonian of the unperturbed material system, H_{int} is the Hamiltonian describing the interaction of light with the electrons, and H_{random} is a Hamiltonian describing the random perturbation on the system by the thermal reservoir around the system. There is no simple expression for H_{random}. However, the Hamiltonian H_{random} is responsible for the relaxation of the perturbed ρ back to thermal equilibrium. Hence, $[H_{random}, \rho]$ can be handled approximately using the concept of a relaxation time. In our calculation, H_{random} is simply ignored.

In this case, the Liouville equation becomes,

$$i\hbar \frac{\partial \rho}{\partial t} = [H_0 + H_{\text{int}}, \rho] \qquad (2.52)$$

In the semiclassical approximation the interaction Hamiltonian is,

$$H_{\text{int}} = -e\vec{r} \cdot \vec{E} \qquad (2.53)$$

In principle, the Liouville equation (2.52) can be solved and we can obtain the density matrix operator ρ. Then the ensemble average of a physical quantity $\vec{P}$ is given by

$$\langle \vec{P} \rangle = Tr(\rho \vec{P}) \qquad (2.54)$$

$\vec{P}$ stands for electric polarization in our calculation and $\vec{P} = -Ne\vec{r}$.

We use the perturbation theory to solve equation (2.52) for the density matrix operator. We expand the density matrix operator ρ into the following series,

$$\rho = \rho^{(0)} + \rho^{(1)} + \rho^{(2)} + \rho^{(3)} + \cdots \qquad (2.55)$$

where $\rho^{(0)}$ is the density matrix operator for the system at thermal equilibrium without the external electromagnetic perturbation. We suppose that a $\rho^{(n)}$ corresponds to the n^{th} order correction and it is proportional to $(H_{\text{int}})^n$. Substituting equation (2.55) into (2.52) and collecting terms of the same order with respect to H_{int}, we obtain,

$$\frac{\partial \rho^{(0)}}{\partial t} = \frac{1}{i\hbar}\left[H_0, \rho^{(0)}\right] \tag{2.56}$$

$$\frac{\partial \rho^{(1)}}{\partial t} = \frac{1}{i\hbar}\left(\left[H_0, \rho^{(1)}\right] + \left[H_{\text{int}}, \rho^{(0)}\right]\right) \tag{2.57}$$

$$\frac{\partial \rho^{(2)}}{\partial t} = \frac{1}{i\hbar}\left(\left[H_0, \rho^{(2)}\right] + \left[H_{\text{int}}, \rho^{(1)}\right]\right) \tag{2.58}$$

$$\frac{\partial \rho^{(3)}}{\partial t} = \frac{1}{i\hbar}\left(\left[H_0, \rho^{(3)}\right] + \left[H_{\text{int}}, \rho^{(2)}\right]\right) \tag{2.59}$$

and so on. If the electric field contains only a few of discrete monochromatic components, we have

$$H_{\text{int}} = -\sum_{\alpha} V^{(\alpha)} e^{-i\omega_\alpha t} \tag{2.60}$$

where $V^{(\alpha)} = e r_a \varepsilon_a^{\alpha}$. So, we can also expand the density matrix operator $\rho^{(n)}$ into a Fourier series

$$\rho^{(n)} = \sum_{\alpha} \rho^{(n)}(\omega_\alpha) e^{-i\omega_\alpha t} \tag{2.61}$$

Inserting equations (2.60), (2.61) into equations (2.57) to (2.59) and taking the matrix element between two single-particle eigenvectors of $\langle i|$ and $|j\rangle$, we obtain the solutions for $\rho^{(1)}, \rho^{(2)}, \rho^{(3)}$:

$$\rho_{ij}^{(1)}(\omega_\alpha) = G_{ij}^{(1)}(\alpha) V_{ij}^{(\alpha)} e^{-i\omega_\alpha t} \tag{2.62}$$

$$\rho_{ij}^{(2)}(\omega_\alpha + \omega_\beta) = \left(G_{ijk}^{(2)}(\alpha,\beta) V_{ik}^{(\alpha)} V_{kj}^{(\beta)} + G_{ijk}^{(2)}(\beta,\alpha) V_{ik}^{(\beta)} V_{kj}^{(\alpha)}\right) e^{-i(\omega_\alpha + \omega_\beta)t} \tag{2.63}$$

$$\begin{aligned} \rho_{ij}^{(3)}(\omega_\alpha + \omega_\beta + \omega_\gamma) = (&G_{ijkl}^{(3)}(\alpha,\beta,\gamma) V_{ik}^{(\alpha)} V_{kl}^{(\beta)} V_{lj}^{(\gamma)} + \\ &G_{ijkl}^{(3)}(\alpha,\gamma,\beta) V_{ik}^{(\alpha)} V_{kl}^{(\gamma)} V_{lj}^{(\beta)} + \\ &G_{ijkl}^{(3)}(\beta,\alpha,\gamma) V_{ik}^{(\beta)} V_{kl}^{(\alpha)} V_{lj}^{(\gamma)} + \\ &G_{ijkl}^{(3)}(\beta,\gamma,\alpha) V_{ik}^{(\beta)} V_{kl}^{(\gamma)} V_{lj}^{(\alpha)} + \\ &G_{ijkl}^{(3)}(\gamma,\beta,\alpha) V_{ik}^{(\gamma)} V_{kl}^{(\beta)} V_{lj}^{(\alpha)} + \\ &G_{ijkl}^{(3)}(\gamma,\alpha,\beta) V_{ik}^{(\gamma)} V_{kl}^{(\alpha)} V_{lj}^{(\beta)}) e^{-i(\omega_\alpha + \omega_\beta + \omega_\gamma)t} \end{aligned} \tag{2.64}$$

where the indices k and l are summed over, and where

$$G_{ij}^{(1)}(\alpha)=\frac{f_{ji}^{(0)}}{\hbar\left(\omega_\alpha-\omega_{ij}\right)} \tag{2.65}$$

$$G_{ijk}^{(2)}(\alpha,\beta)=\frac{1}{\hbar\left(\omega_\alpha+\omega_\beta-\omega_{ij}\right)}\left[\frac{f_{jk}^{(0)}}{\hbar\left(\omega_\beta-\omega_{kj}\right)}+\frac{f_{ik}^{(0)}}{\hbar\left(\omega_\alpha-\omega_{ik}\right)}\right] \tag{2.66}$$

$$G_{ijkl}^{(3)}(\alpha,\beta)=\frac{1}{\hbar\left(\omega_\alpha+\omega_\beta+\omega_\gamma-\omega_{ij}\right)}\left[\frac{1}{\hbar\left(\omega_\beta+\omega_\gamma-\omega_{kj}\right)}\left[\frac{f_{jl}^{(0)}}{\hbar\left(\omega_\gamma-\omega_{lj}\right)}+\frac{f_{kl}^{(0)}}{\hbar\left(\omega_\beta-\omega_{kl}\right)}\right]\right.$$

$$\left.+\frac{1}{\hbar\left(\omega_\alpha+\omega_\beta-\omega_{il}\right)}\left[\frac{f_{kl}^{(0)}}{\hbar\left(\omega_\beta-\omega_{kl}\right)}+\frac{f_{ki}^{(0)}}{\hbar\left(\omega_\alpha-\omega_{ik}\right)}\right]\right] \tag{2.67}$$

with no summation implied. Here, $\omega_\alpha,\omega_\beta$, and ω_γ are the monochromatic frequencies of the external fields; ω_{ij} is defined as $\omega_{ij}=\frac{\langle i|H_0|i\rangle-\langle j|H_0|j\rangle}{\hbar}$; $f_{ij}^{(0)}$ is defined as $f_{ij}^{(0)}=\rho_{ii}^{(0)}-\rho_{jj}^{(0)}$ and $\rho_{ii}^{(0)}$ is the probability that the single-particle state $|i\rangle$ is occupied when there is no external field.

Combining equations (2.54), (2.62), (2.63), and (2.64), we obtain

$$\begin{aligned}\langle\vec{P}\rangle&=Tr\left(\rho^{(1)}\vec{P}\right)+Tr\left(\rho^{(2)}\vec{P}\right)+Tr\left(\rho^{(3)}\vec{P}\right)+\cdots\\&=\vec{P}^{(1)}+\vec{P}^{(2)}+\vec{P}^{(3)}+\cdots\end{aligned} \tag{2.68}$$

Finally, we write the macroscopic polarizability as[6][10]

$$\vec{P}_a^{(1)}(t)=\sum_{b,\alpha}\vec{\vec{\chi}}_{ab}^{(1)}(\omega_\alpha)E_b^\alpha e^{-i\omega_\alpha t} \tag{2.69}$$

$$\vec{P}_a^{(2)}(t)=\sum_{b,c;\alpha,\beta}\vec{\vec{\vec{\chi}}}_{abc}^{(2)}\left(\omega_\alpha+\omega_\beta\right)E_b^\alpha E_c^\beta e^{-i(\omega_\alpha+\omega_\beta)t} \tag{2.70}$$

$$\vec{P}_a^{(3)}(t)=\sum_{b,c,d;\alpha,\beta,\gamma}\vec{\vec{\vec{\vec{\chi}}}}_{abc}^{(3)}\left(\omega_\alpha+\omega_\beta+\omega_\gamma\right)E_b^\alpha E_c^\beta E_d^\gamma e^{-i(\omega_\alpha+\omega_\beta+\omega_\gamma)t} \tag{2.71}$$

where $\bar{\bar{\chi}}^{(1)}_{ab}(\omega_\alpha)$, $\bar{\bar{\chi}}^{(2)}_{abc}(\omega_\alpha+\omega_\beta)$, and $\bar{\bar{\bar{\chi}}}^{(3)}_{abc}(\omega_\alpha+\omega_\beta+\omega_\gamma)$ are the susceptibilities defined as

$$\bar{\bar{\chi}}^{(1)}_{ab}(\omega_\alpha) = -\sum_{i,j}\left[\frac{e}{m\omega_\alpha}\right]^2 G^{(1)}_{ij}(\alpha)\, p^b_{ij} p^a_{ji} \qquad (2.72)$$

$$\bar{\bar{\chi}}^{(2)}_{abc}(\omega_\alpha+\omega_\beta) = -\sum_{i,j,k}\frac{ie^3}{m^3\omega_\alpha\omega_\beta(\omega_\alpha+\omega_\beta)} G^{(2)}_{ijk}(\alpha,\beta)\, p^a_{ij} p^b_{jk} p^c_{ki} \qquad (2.73)$$

$$\bar{\bar{\bar{\chi}}}^{(3)}_{abc}(\omega_\alpha+\omega_\beta+\omega_\gamma) = \sum_{i,j,k,l}\frac{e^4}{m^4\omega_\alpha\omega_\beta\omega_\gamma(\omega_\alpha+\omega_\beta+\omega_\gamma)} G^{(3)}_{ijkl}(\alpha,\beta,\gamma)\, p^a_{ij} p^b_{jk} p^c_{kl} p^d_{li} \qquad (2.74)$$

where p is the momentum operator. We have used the identity of $[\bar{r}, H_0] = \frac{i\hbar}{m}\bar{p}$ in deriving these expressions. Equations (2.72) and (2.73) will be used to calculate the susceptibilities in Chapter 6 and Chapter 7.

2.4 Comments on the Semiclassic Theory

In the semiclassical theory of interactions between electromagnetic fields and atomic matter presented above, the electromagnetic field is described classically. As a result, the polarizations have been defined as macroscopic averages of a dipole moment density over a small volume. This approach is very useful and it describes the optical phenomena very well. One might, however, want to describe the underlying microscopic processes of those optical phenomena in terms of transition probabilities per unit time or cross sections for scattering or absorption. In that case one needs to quantize the electromagnetic fields.

As mentioned in section 2.3.3, stimulated Raman scattering is one of the nonlinear phenomena accounted for by the third order polarizability. As it is shown in figure 2.1, the corresponding microscopic process is that one photon is absorbed by the

medium, another photon with different energy is emitted from the medium and the medium changes its internal configuration to keep the energy conserved in this process.

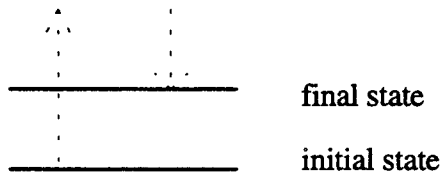

Figure 2.1 microscopic process of stimulated Raman scattering

One can calculate the gain of the Raman wave ω_2 by calculating the transition probability of such processes. The result is in agreement with the result of the semiclassical approach[5][11], as it should be.

Unfortunately, describing the electromagnetic fields in terms of a prescribed number of photons, as we just did for stimulated Raman scattering, will lose phase information of the electromagnetic waves. In the process of stimulated Raman scattering, the relative phases of components ω_1 and ω_2 play no role at all. For some other optical phenomena, such as second harmonic generation, the relative phases among the different waves play a very important role. So one has to retain the phase information of the waves in the quantum description for those optical phenomena. This can be done in principle by using so-called coherent quantum states[12][13].

A discussion of susceptibilities in terms of coherent quantum states is very tedious and challenging. Obviously, the difficulty is caused by the wave-particle duality of the photon. It seems that there does not exist such a kind of detailed treatment in the literature yet. The correspondence principle comes to rescue, however. The correspondence principle states that the results from a fully quantum mechanical treatment should be identical with the semiclassical method[11] in the limit of a large average number of photons. We will therefore use the semiclassic approach in this thesis.

Chapter 3
LCAO Method and Bulk ZnO Electronic Band Structure

A medium is a very complicated system which consists of a huge number of nuclei and electrons. By invoking the so-called adiabatic approximation we will ignore the motion of nuclei. We will also ignore the response from those very tightly bound atomic electrons which are often called core electrons. There are two reasons to ignore the core electrons. First, they interact strongly with each other and with the nucleus, and consequently they are perturbed much less by external light than the loosely bound valence electrons. Second, those loosely bound valence electrons adjust their states quickly in response to external light and screen out the light, in some extent, from the core electrons.

Atomic matter can be distinguished into a few categories according to the electronic charge distribution. For some matter, such as ionic and molecular crystals, the charge distribution is determined by the contributions of clearly identifiable units. In such crystals, the loosely-bound electrons are still bound to particular atoms, ions or molecules. In other words, the electrons in such materials are localized. To compute the polarizability of such a system we first apply the formalism given in Chapter 2, compute the polarizability of the identifiable ions, and then do the averaging. In some cases, local field corrections must be included.

For covalent crystals, however, the valence electrons are not bound to a single ion any more. Instead, an appreciable charge density resides between ions. Band theory has to be invoked in calculating optical properties of such covalent crystals. Bulk ZnO is a covalent crystal. So, we have to obtain the electronic band structure of ZnO before we can compute its optical properties.

3.1 The LCAO Method

There are quite a few standard methods for electronic band structure calculations. Some are empirical, some are more or less ab initio. We will use a semiempirical LCAO method[14]. Here, "LCAO" stands for "Linear Combination of Atomic Orbitals".

Suppose we have N atoms, and all the atoms are far away from each other. Then there exists a set of single-electron atomic orbital states for each atom. Those states are denoted by $|n, \vec{R}\rangle$ where $\vec{R}$ represents the position of a particular atom and n represents an orbital for that atom. If all the N atoms are the same, each energy level is N fold degenerate, corresponding to orbitals with wave functions differing from each other only by a shift of their coordinate origin. This degeneracy is removed if the atoms are brought closer together, for the atomic orbital wave functions will overlap and the summation of isolated individual atomic Hamiltonians is replaced by the full crystal Hamiltonian. However, the atomic orbital wave functions can still serve as basis functions for the solutions of the crystal Hamiltonian. In other words, we can expand the eigenfunctions of the crystal Hamiltonian in the space spanned by those atomic orbitals.

3.1.1 Bloch sums

Atomic orbitals are good basis functions for the crystal Hamiltonian, but they have the wrong properties under translations. The crystal has the symmetry of the underlying Bravais lattice, and so does the crystal Hamiltonian. The crystal Hamiltonian for a single electron has the form

$$H = -\frac{\hbar^2}{2m}\nabla^2 + U(\vec{r}) \qquad (3.1)$$

where the effective single electron potential has the periodicity of the lattice:

$$U(\vec{r} + \vec{R}) = U(\vec{r})$$

for all vectors $\vec{R}$ in the Bravais lattice. As a general consequence of this periodicity of $U(\vec{r})$, an eigenfunction $\psi(\vec{r})$ of the crystal Hamiltonian has the property

$$\psi(\vec{r} + \vec{R}) = c\psi(\vec{r}) \qquad (3.2)$$

where c is independent of $\vec{r}$, and $|c| = 1$. We have to choose c as $e^{i\vec{k}\cdot\vec{R}}$ so that equation (3.2) becomes

$$\psi(\vec{r} + \vec{R}) = e^{i\vec{k}\cdot\vec{R}}\psi(\vec{r}) \qquad (3.3)$$

where $\vec{k}$ is called the wave vector. Equation (3.3) is Bloch's theorem[15].

We construct from each atomic orbital a zero-order approximate wave function which satisfies equation (3.3) as follows:

$$\phi_{bn}^{\vec{k}} = \frac{1}{\sqrt{N}}\sum_{\vec{R}} e^{i\vec{k}(\vec{R}+\vec{d}_b)}\left|b,n,\vec{R}\right\rangle \qquad (3.4)$$

where $\left|b,n,\vec{R}\right\rangle$ is the n^{th} atomic orbital of atom b located inside the unit cell at $\vec{R}$. $\vec{d}_b$ is the coordinate vector of atom b in the unit cell relative to the origin of that unit cell. We assume that the total number of unit cells is N. $\vec{k}$ is the wave vector whose value is to be determined. There exist N different $\vec{k}$ values and we can prove that:

$$\left\langle \phi_{bn}^{\vec{k}_2} \middle| H \middle| \phi_{bn}^{\vec{k}_1} \right\rangle = E_{bn}^{\vec{k}_1}\delta_{\vec{k}_1\vec{k}_2}.$$

So, it is much easier if we use $\left\{\phi_{bn}^{\vec{k}}\right\}$ instead of $\left\{\left|b,n,\vec{R}\right\rangle\right\}$ as the first-order approximation to the wave functions.

3.1.2 The Born-Von Karman boundary condition

It can be shown that the wave vector $\vec{k}$ takes exactly N distinguishable values by imposing Born-Von Karman boundary conditions on the wave function. The Born-Von Karman periodic boundary conditions are:

$$\psi_{bn}^{\vec{k}}(\vec{r}+N_i\vec{a}_i)=\psi_{bn}^{\vec{k}}(\vec{r}), \qquad i=1,\ 2,\ 3, \qquad (3.5)$$

where $\vec{a}_i$ $(i=1,2,3)$ stands for the three primitive vectors of the unit cell and N_i are all integers of order $N^{1/3}$. $N=N_1N_2N_3$ is the total number of primitive cells in the crystal.

Combining equation (3.3) and (3.5), $\vec{k}$ is found to be,

$$\vec{k}=\sum_{i=1}^{3}\frac{m_i}{N_i}\vec{b}_i, \qquad m_i \text{ integral.} \qquad (3.6)$$

where $\vec{b}_i$ are the primitive vectors of the reciprocal lattice unit cell[15]. It is straightforward to show that the volume $\Delta\vec{k}$ of k-space per allowed value of $\vec{k}$ is $\frac{(2\pi)^3}{V}$. Therefore, the number of allowed wave vectors in a primitive cell of the reciprocal lattice is equal to the number of unit cells in the crystal because the volume of a reciprocal lattice primitive cell is $\frac{(2\pi)^3}{v}$, where $v=\frac{V}{N}$ is the volume of a direct lattice primitive cell.

3.1.3 The Hamiltonian

The first-order approximation to the wave functions, $\phi_{bn}^{\vec{k}}$, are used as our basis functions for the eigen functions of the crystal Hamiltonian. Due to the periodic symmetry of the Hamiltonian, functions $\phi_{bn}^{\vec{k}}$ with different wave vectors will not mix. However, functions $\phi_{bn}^{\vec{k}}$ with the same $\vec{k}$ but different b or/and n are expected to mix. So, the eigenfunctions of H can be written in the form,

$$\psi_i^{\vec{k}} = \sum_{b,n} a_{bn\vec{k}}^{(i)} \phi_{bn}^{\vec{k}} \qquad (3.7)$$

and the Hamiltonian matrix in terms of the set $\left\{\phi_{bn}^{\vec{k}}\right\}$ is,

$$\begin{aligned} H_{bn,b'n'}^{\vec{k}} &= \left\langle \phi_{bn}^{\vec{k}} \middle| H \middle| \phi_{b'n'}^{\vec{k}} \right\rangle \\ &= \sum_{\vec{R}} e^{i\vec{k}\left(\vec{R}+\vec{d}_{b'}-\vec{d}_b\right)} \left\langle b,n,\vec{0} \middle| H \middle| b',n',\vec{R} \right\rangle \end{aligned} \qquad (3.8)$$

We obtain the eigen energy and the coefficients $a_{bn\vec{k}}^{(i)}$ in equation (3.7) by diagonalizing the matrix (3.8). At this point we still have to determine the value of the crystal Hamiltonian matrix between two atomic orbitals. We will parameterize these Hamiltonian matrices and determine the values by fitting to known band gap values at particular values of the wave vectors. Details will be given when we discuss the Hamiltonian matrix for ZnO.

3.2 Bulk ZnO Electronic Band Structure

3.2.1 ZnO crystal structure

The ZnO crystal consists of two interpenetrating hexagonal closed-packed (hcp) structures as shown in figure (3.1). One of the two hcp lattice contains zinc (Zn) atoms, the other hcp lattice contains oxygen (O) atoms. Oxygen is the anion and zinc is the cation. There is an anion for each cation and it is located directly above the cation along the c-axis of the underlying simple hexagonal Bravais lattice of the zinc oxide crystal. This crystal structure of ZnO is called the wurtzite structure.

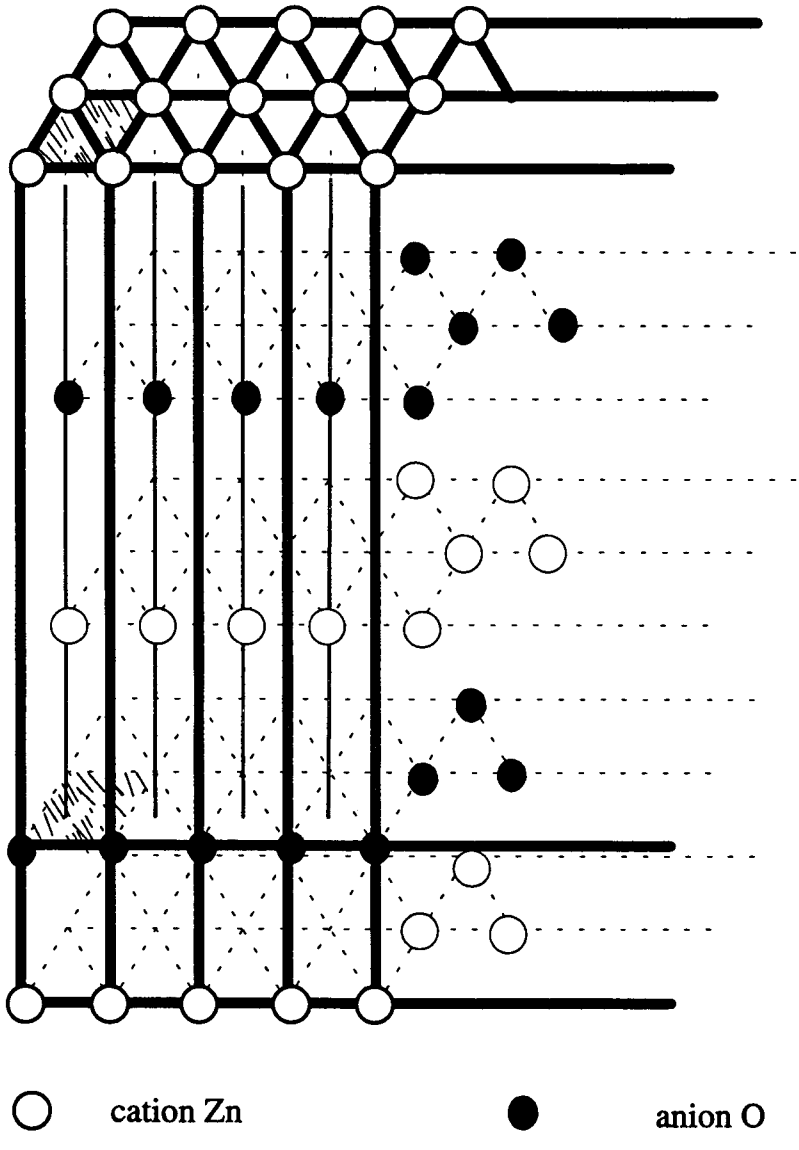

Figure 3.1 The wurtzite crystal structure of ZnO

The hexagonal closed-packed structure is not a Bravais lattice. It consists of two interpenetrating simple hexagonal Bravais lattices. The simple hexagonal Bravais lattice is composed of an infinite number of two-dimensional triangular nets stacked directly above each other. Its three primitive vectors are

$$\vec{a}_1 = a\hat{x},\ \vec{a}_2 = \frac{a}{2}\hat{x} + \frac{\sqrt{3}a}{2}\hat{y},\ \vec{a}_3 = c\hat{z}. \qquad (3.9)$$

where $\hat{x}$, $\hat{y}$,$\hat{z}$ are the unit vectors of the coordinate system, $\hat{z}$ is along the direction of stacking and the $\hat{z}$ axis is called the c-axis, a is the length of a hexagonal side and c is the length of the unit cell along the $\hat{z}$ direction. In the hcp structure, the two interpenetrating simple hexagonal Bravais lattices are displaced from one another by $\frac{\vec{a}_1}{3} + \frac{\vec{a}_2}{3} + \frac{\vec{a}_3}{2}$. The hcp crystal structure is treated as a simple hexagonal Bravais lattice with a basis of two atoms. The wurtzite structure of two interpenetrating hcp structures is therefore treated as a simple hexagonal Bravais lattice with a basis consisting of four atoms. Two are zinc atoms and the other two are oxygen atoms. The anion (O) is displaced by $\frac{3}{8}c$ directly above the cation (Zn). The ideal value of $\frac{c}{a}$ is $\sqrt{\frac{8}{3}}$. For ZnO, $a = 5.52a_0$ and $c = 8.7a_0$ where a_0 is the Bohr radius.

We denote the four basis atoms by a_1, a_2, c_1, c_2 where a_1 and a_2 stand for the two anions and that c_1 and c_2 stand for the two cations. Their coordinate vectors are

$$\vec{d}_{a_1} = \vec{0},\ \vec{d}_{c_1} = \frac{a}{2}\hat{x} + \frac{\sqrt{3}a}{6}\hat{y} + \frac{c}{8}\hat{z},\ \vec{d}_{a_2} = \frac{a}{2}\hat{x} + \frac{\sqrt{3}a}{6}\hat{y} + \frac{c}{2}\hat{z},\ \vec{d}_{c_2} = \frac{5c}{8}\hat{z} \qquad (3.10)$$

Since the direct Bravais lattice is simple hexagonal, the reciprocal lattice is also simple hexagonal. The three primitive vectors of the reciprocal lattice are

$$\vec{b}_1 = \frac{2\pi}{a}\hat{x} - \frac{2\pi}{\sqrt{3}a}\hat{y},\quad \vec{b}_2 = \frac{4\pi}{\sqrt{3}a}\hat{y},\quad \vec{b}_3 = \frac{2\pi}{c}\hat{z}, \qquad (3.11)$$

3.2.2 Hamiltonian of bulk ZnO

For the zinc atom twenty-eight electrons are considered to be core electrons. For the oxygen atom two electrons are considered to be core electrons. All the valence electrons for both Zn and O are in sp^3 orbitals. The principal quantum number is 4 for zinc, but it is 2 for oxygen. We are going to consider mixing of the sp^3 orbitals only. So we have four atomic orbitals with symmetry s, p_x, p_y, p_z for each atom. There are four basis atoms per unit cell, therefore we can construct 16 first-order basis wave functions for each wave vector $\vec{k}$ from equation (3.4) as follows,

$$\left|\phi^{\vec{k}}_{a_1,s}\right\rangle = \frac{1}{\sqrt{N}}\sum_{\vec{R}} e^{i\vec{k}\cdot\left(\vec{R}+\vec{d}_{a_1}\right)}\left|a_1, s\left(\vec{r}-\left(\vec{R}+\vec{d}_{a_1}\right)\right)\right\rangle \tag{3.12}$$

$$\left|\phi^{\vec{k}}_{a_1,p_x}\right\rangle = \frac{1}{\sqrt{N}}\sum_{\vec{R}} e^{i\vec{k}\cdot\left(\vec{R}+\vec{d}_{a_1}\right)}\left|a_1, p_x\left(\vec{r}-\left(\vec{R}+\vec{d}_{a_1}\right)\right)\right\rangle \tag{3.13}$$

$$\left|\phi^{\vec{k}}_{a_1,p_y}\right\rangle = \frac{1}{\sqrt{N}}\sum_{\vec{R}} e^{i\vec{k}\cdot\left(\vec{R}+\vec{d}_{a_1}\right)}\left|a_1, p_y\left(\vec{r}-\left(\vec{R}+\vec{d}_{a_1}\right)\right)\right\rangle \tag{3.14}$$

$$\left|\phi^{\vec{k}}_{a_1,p_z}\right\rangle = \frac{1}{\sqrt{N}}\sum_{\vec{R}} e^{i\vec{k}\cdot\left(\vec{R}+\vec{d}_{a_1}\right)}\left|a_1, p_z\left(\vec{r}-\left(\vec{R}+\vec{d}_{a_1}\right)\right)\right\rangle \tag{3.15}$$

$$\left|\phi^{\vec{k}}_{c_1,s}\right\rangle = \frac{1}{\sqrt{N}}\sum_{\vec{R}} e^{i\vec{k}\cdot\left(\vec{R}+\vec{d}_{c_1}\right)}\left|c_1, s\left(\vec{r}-\left(\vec{R}+\vec{d}_{c_1}\right)\right)\right\rangle \tag{3.16}$$

$$\left|\phi^{\vec{k}}_{c_1,p_x}\right\rangle = \frac{1}{\sqrt{N}}\sum_{\vec{R}} e^{i\vec{k}\cdot\left(\vec{R}+\vec{d}_{c_1}\right)}\left|c_1, p_x\left(\vec{r}-\left(\vec{R}+\vec{d}_{c_1}\right)\right)\right\rangle \tag{3.17}$$

$$\left|\phi^{\vec{k}}_{c_1,p_y}\right\rangle = \frac{1}{\sqrt{N}}\sum_{\vec{R}} e^{i\vec{k}\cdot\left(\vec{R}+\vec{d}_{c_1}\right)}\left|c_1, p_y\left(\vec{r}-\left(\vec{R}+\vec{d}_{c_1}\right)\right)\right\rangle \tag{3.18}$$

$$\left|\phi^{\vec{k}}_{c_1,p_z}\right\rangle = \frac{1}{\sqrt{N}}\sum_{\vec{R}} e^{i\vec{k}\cdot\left(\vec{R}+\vec{d}_{c_1}\right)}\left|c_1, p_z\left(\vec{r}-\left(\vec{R}+\vec{d}_{c_1}\right)\right)\right\rangle \tag{3.19}$$

$$\left|\phi^{\vec{k}}_{a_2,s}\right\rangle = \frac{1}{\sqrt{N}}\sum_{\vec{R}} e^{i\vec{k}\cdot\left(\vec{R}+\vec{d}_{a_2}\right)}\left|a_2, s\left(\vec{r}-\left(\vec{R}+\vec{d}_{a_2}\right)\right)\right\rangle \tag{3.20}$$

$$\left|\phi^{\vec{k}}_{a_2,p_x}\right\rangle = \frac{1}{\sqrt{N}}\sum_{\vec{R}} e^{i\vec{k}\cdot(\vec{R}+\vec{d}_{a_2})}\left|a_2, p_x\left(\vec{r}-\left(\vec{R}+\vec{d}_{a_2}\right)\right)\right\rangle \tag{3.21}$$

$$\left|\phi^{\vec{k}}_{a_2,p_y}\right\rangle = \frac{1}{\sqrt{N}}\sum_{\vec{R}} e^{i\vec{k}\cdot(\vec{R}+\vec{d}_{a_2})}\left|a_2, p_y\left(\vec{r}-\left(\vec{R}+\vec{d}_{a_2}\right)\right)\right\rangle \tag{3.22}$$

$$\left|\phi^{\vec{k}}_{a_2,p_z}\right\rangle = \frac{1}{\sqrt{N}}\sum_{\vec{R}} e^{i\vec{k}\cdot(\vec{R}+\vec{d}_{a_2})}\left|a_2, p_z\left(\vec{r}-\left(\vec{R}+\vec{d}_{a_2}\right)\right)\right\rangle \tag{3.23}$$

$$\left|\phi^{\vec{k}}_{c_2,s}\right\rangle = \frac{1}{\sqrt{N}}\sum_{\vec{R}} e^{i\vec{k}\cdot(\vec{R}+\vec{d}_{c_2})}\left|c_2, s\left(\vec{r}-\left(\vec{R}+\vec{d}_{c_2}\right)\right)\right\rangle \tag{3.24}$$

$$\left|\phi^{\vec{k}}_{c_2,p_x}\right\rangle = \frac{1}{\sqrt{N}}\sum_{\vec{R}} e^{i\vec{k}\cdot(\vec{R}+\vec{d}_{c_2})}\left|c_2, p_x\left(\vec{r}-\left(\vec{R}+\vec{d}_{c_2}\right)\right)\right\rangle \tag{3.25}$$

$$\left|\phi^{\vec{k}}_{c_2,p_y}\right\rangle = \frac{1}{\sqrt{N}}\sum_{\vec{R}} e^{i\vec{k}\cdot(\vec{R}+\vec{d}_{c_2})}\left|c_2, p_y\left(\vec{r}-\left(\vec{R}+\vec{d}_{c_2}\right)\right)\right\rangle \tag{3.26}$$

$$\left|\phi^{\vec{k}}_{c_2,p_z}\right\rangle = \frac{1}{\sqrt{N}}\sum_{\vec{R}} e^{i\vec{k}\cdot(\vec{R}+\vec{d}_{c_2})}\left|c_2, p_z\left(\vec{r}-\left(\vec{R}+\vec{d}_{c_2}\right)\right)\right\rangle \tag{3.27}$$

where $\left|b,\varphi\left(r-\left(\vec{R}+\vec{d}_b\right)\right)\right\rangle$ with $b \equiv \{a_1, c_1, a_2, c_2\}$ and $\varphi \equiv \{s, p_x, p_y, p_z\}$ is the wave function of a localized atomic orbital φ of atom b in unit cell $\vec{R}$.

The Hamiltonian is a 16x16 matrix in the space of the functions $\left|\phi^{\vec{k}}_{b,\varphi}\right\rangle$ for each wave vector $\vec{k}$. We have to diagonalize N 16x16 Hamiltonian matrices because the wave vector $\vec{k}$ can take N different values. The elements of the Hamiltonian are expressed in terms of the Hamiltonian matrix elements $\left\langle b,n,\vec{0}\left|H\right|b',n',\vec{R}\right\rangle$ between the localized atomic orbitals in equation (3.8). Since we do not know the Hamiltonian H, we determine the Hamiltonian matrix element $\left\langle b,n,\vec{0}\left|H\right|b',n',\vec{R}\right\rangle$ empirically through parameterization. We make the following three approximations to simplify our parameterization problem and to reduce the number of parameters.

1. Only on-site integrals and nearest-neighbor integrals are nonzero.
2. We assume that the four nearest neighbor atoms are equivalent.

3. We neglect the small differences between the p_z orbital and the p_x and p_y orbitals due to the crystal field splitting.

With those approximations we can fully parameterize the crystal Hamiltonian by nine independent parameters. This first approximation is called the nearest neighbor approximation. It means that $\langle b,n,\vec{0}|H|b',n',\vec{R}\rangle$ is not equal to zero only if $\{b',\vec{R}\}$ represents an atom that is either the same atom represented by $\{b,\vec{0}\}$ or the nearest neighbor to the atom represented by $\{b,\vec{0}\}$.

When $\{b',\vec{R}\}$ is the same as $\{b,\vec{0}\}$, that is $b=b'$ and $\vec{R}=\vec{0}$, the matrix element becomes $\langle b,n,\vec{0}|H|b,n',\vec{0}\rangle$. We call $\langle b,n,\vec{0}|H|b,n',\vec{0}\rangle$ an on-site integral because both orbitals belong to the same atom. Since Zn is considered to be isotropic in x-y plane, n has to be equal to n' for $\langle b,n,\vec{0}|H|b,n',\vec{0}\rangle$ to be nonzero. Combining the second and third approximations we use four parameters to parameterize the on-site integrals. The four parameters $H(a,s)$, $H(a,p)$, $H(c,s)$ and $H(c,p)$ are defined by

$$H(a,s)\equiv H(a_1,s)\approx H(a_2,s)=\langle\vec{0},s,b_{a_1}|H|b_{a_1},s,\vec{0}\rangle \tag{3.28}$$

$$\begin{aligned}H(a,p)&\equiv H(a_1,p)\approx H(a_2,p)\equiv H(a_2,p_x)=H(a_2,p_y)\approx H(a_2,p_z)\\&=\langle\vec{0},p_x,b_{a_1}|H|b_{a_1},p_x,\vec{0}\rangle\end{aligned} \tag{3.29}$$

$$H(c,s)\equiv H(c_1,s)\approx H(c_2,s)=\langle\vec{0},s,b_{c_1}|H|b_{c_1},s,\vec{0}\rangle \tag{3.30}$$

$$\begin{aligned}H(c,p)&\equiv H(c_1,p)\approx H(c_2,p)\equiv H(c_2,p_x)=H(c_2,p_y)\approx H(c_2,p_z)\\&=\langle\vec{0},p_x,b_{c_1}|H|b_{c_1},p_x,\vec{0}\rangle\end{aligned} \tag{3.31}$$

When $\{b',\vec{R}\}$ denotes a nearest neighbor to the atom denoted by $\{b,\vec{0}\}$, the matrix element $\langle b,n,\vec{0}|H|b',n',\vec{R}\rangle$ is an integral of two orbitals where each belongs to and is

centered on a different atom. We call such an integral the nearest-neighbor integral and such a matrix element is a nearest-neighbor transfer matrix element. Combining our symmetry approximations we can fully parameterize these nearest-neighbor integrals by five numbers $V(ss\sigma), V(sp\sigma), V(ps\sigma), V(pp\sigma)$ and $V(pp\pi)$. These are defined by[14]

$$V(ss\sigma) \equiv \langle \vec{d}, s, b_c | H | b_a, s, \vec{0} \rangle \tag{3.32}$$

$$V(sp\sigma) \equiv \langle \vec{d}, p_x, b_c | H | b_a, s, \vec{0} \rangle \tag{3.33}$$

$$V(ps\sigma) \equiv \langle \vec{d}, s, b_c | H | b_a, p_x, \vec{0} \rangle \tag{3.34}$$

$$V(pp\sigma) \equiv \langle \vec{d}, p_x, b_c | H | b_a, p_x, \vec{0} \rangle \tag{3.35}$$

$$V(pp\pi) \equiv \langle \vec{d}, p_y, b_c | H | b_a, p_y, \vec{0} \rangle = \langle \vec{d}, p_z, b_c | H | b_a, p_z, \vec{0} \rangle \tag{3.36}$$

where $\vec{d}$ is assumed along the $\hat{x}$ direction, $b_c = \{c_1, c_2\}$ and $b_a = \{a_1, a_2\}$. Although the ZnO crystal has C_{3v} symmetry, the local environment can be treated as T_d (tetrahedral) under the approximation of that the four nearest-neighbor atoms are equivalent. The following on-site integrals and nearest-neighbor integrals are zero:

$$\langle \vec{0}, p_z, a_1 | H | a_1, s, \vec{0} \rangle = \langle \vec{0}, p_z, a_2 | H | a_2, s, \vec{0} \rangle = 0 \tag{3.37}$$

$$\langle \vec{0}, p_z, c_1 | H | c_1, s, \vec{0} \rangle = \langle \vec{0}, p_z, c_2 | H | c_2, s, \vec{0} \rangle = 0 \tag{3.38}$$

$$\langle \vec{d}, p_y, c | H | a, p_x, \vec{0} \rangle = \langle \vec{d}, p_z, c | H | a, p_x, \vec{0} \rangle = 0 \tag{3.39}$$

$$\langle \vec{d}, p_y, c | H | a, s, \vec{0} \rangle = \langle \vec{d}, p_z, c | H | a, s, \vec{0} \rangle = 0 \tag{3.40}$$

$$\langle \vec{d}, p_y, c | H | a, p_z, \vec{0} \rangle = \langle \vec{d}, p_z, c | H | a, p_y, \vec{0} \rangle = 0 \tag{3.41}$$

$\langle i \vert H \vert j \rangle$	s^{a1}	p_x^{a1}	p_y^{a1}	p_z^{a1}	s^{c1}	p_x^{c1}	p_y^{c1}	p_z^{c1}	s^{a2}	p_x^{a2}	p_y^{a2}	p_z^{a2}	s^{c2}	p_x^{c2}	p_y^{c2}	p_z^{c2}
s^{a1}	x	0	0	0	x	x	x	x	0	0	0	0	x	0	0	x
p_x^{a1}	0	x	0	0	x	x	x	x	0	0	0	0	0	x	0	0
p_y^{a1}	0	0	x	0	x	x	x	x	0	0	0	0	0	0	x	0
p_z^{a1}	0	0	0	x	x	x	x	x	0	0	0	0	x	0	0	x
s^{c1}	x	x	x	x	x	0	0	0	x	0	0	x	0	0	0	0
p_x^{c1}	x	x	x	x	0	x	0	0	0	x	0	0	0	0	0	0
p_y^{c1}	x	x	x	x	0	0	x	0	0	0	x	0	0	0	0	0
p_z^{c1}	x	x	x	x	0	0	0	x	x	0	0	x	0	0	0	0
s^{a2}	0	0	0	0	x	0	0	x	x	0	0	0	x	x	x	x
p_x^{a2}	0	0	0	0	0	x	0	0	0	x	0	0	x	x	x	x
p_y^{a2}	0	0	0	0	0	0	x	0	0	0	x	0	x	x	x	x
p_z^{a2}	0	0	0	0	x	0	0	x	0	0	0	x	x	x	x	x
s^{c2}	x	0	0	x	0	0	0	0	x	x	x	x	x	0	0	0
p_x^{c2}	0	x	0	0	0	0	0	0	x	x	x	x	0	x	0	0
p_y^{c2}	0	0	x	0	0	0	0	0	x	x	x	x	0	0	x	0
p_z^{c2}	x	0	0	x	0	0	0	0	x	x	x	x	0	0	0	x

Figure 3.2 The zero and nonzero elements of ZnO crystal Hamiltonian

Finally, the Hamiltonian matrix in the space of the functions $\left|\phi_{b,\varphi}^{\vec{k}}\right\rangle$ can be written as

$$
\begin{array}{c|cccc}
b \setminus b' & a_1 & c_1 & a_2 & c_2 \\
a_1 & H_a & H_{a_1,c_1} & 0 & H_{a_1,c_2} \\
c_1 & H_{a_1,c_1}^{+} & H_c & H_{c_1,a_2} & 0 \\
a_2 & 0 & H_{c_1,a_2}^{+} & H_a & H_{a_2,c_2} \\
c_2 & H_{a_1,c_2}^{+} & 0 & H_{a_2,c_2}^{+} & H_c
\end{array}
$$

Each element of this matrix is a 4X4 matrix. When it is expanded, the Hamiltonian matrix is a 16X16 matrix as shown in figure (3.2). In figure (3.2) we use the symbol x to represent nonzero elements. The detailed expression for those nonzero elements can be found in appendix A.

3.2.3 Parameters of the ZnO Hamiltonian

Now that we have the Hamiltonian matrix expressed in terms of the nine parameters for every wave vector $\vec{k}$, we have to determine the values of these parameters. We can do this by fitting the energy eigenvalues to the known band structure at particular $\vec{k}$ points. An efficient fitting method was used[16] as given by Donald W. Marquardt[17].

John D. Dow and co-workers[18] have performed such a fit. They used the band structure at the Γ point ($\vec{k} = \vec{0}$) in addition to some rules which were deduced by Vogl et al[19] for chemical trends. In our calculation, we will use their values for the

nine parameters. The following table 3.1 lists the nine parameter values calculated from their results for five wurtzite crystals,

Table 3.1 Parameter values for five wurtzite crystals (eV)

Parameters	ZnO	AlN	CdS	CdSe	ZnS
$H(a,s)$	-19.046	-12.104	-11.133	-10.782	-10.634
$H(c,s)$	1.666	-0.096	2.243	1.682	2.134
$H(a,p)$	4.142	3.581	1.327	1.309	1.574
$H(c,p)$	12.368	9.419	6.673	6.091	6.626
$V(ss\sigma)$	-1.511	-2.684	-0.554	-0.504	-1.226
$V(pp\sigma)$	7.078	5.695	3.000	2.868	3.391
$V(pp\pi)$	-0.855	-0.670	-0.384	-0.375	-0.485
$V(sp\sigma)$	2.036	3.504	0.405	0.477	0.155
$V(ps\sigma)$	3.739	4.224	1.955	1.727	2.702

3.2.4 The band structure

Using the parameter values listed in the table above we are able to evaluate the Hamiltonian for each wave vector $\vec{k}$. After diagonalizing the Hamiltonian, we obtain the band structure at each wave vector. Figure 3.3 shows the band structure for the ZnO crystal. The points denoted by Γ, K, M, A, H, L are high symmetry points in the Brillouin zone and their coordinates are:

$$\Gamma = (0,\ 0,\ 0),\quad A = \left(0,\ 0,\ \frac{1}{2}\right)\frac{2\pi}{c},\quad M = \left(\frac{1}{2},\ \frac{\sqrt{3}}{6},\ 0\right)\frac{2\pi}{a}$$

$$K = \left(\frac{1}{3}, \frac{\sqrt{3}}{3}, 0\right)\frac{2\pi}{a}, \quad L = \left(\frac{2\pi}{a}\frac{1}{2}, \frac{2\pi}{a}\frac{\sqrt{3}}{6}, \frac{2\pi}{c}\frac{1}{2}\right)$$

$$H = \left(\frac{2\pi}{a}\frac{1}{3}, \frac{2\pi}{a}\frac{\sqrt{3}}{3}, \frac{2\pi}{c}\frac{1}{2}\right)$$

The wave vectors used to calculate the band structure shown in figure 3.3 are $\bar{k}$ vectors along the line segments $A \rightarrow L \rightarrow M \rightarrow \Gamma \rightarrow A \rightarrow H \rightarrow K \rightarrow \Gamma$ in the Brillouin zone. The narrow lowest valence band near -20eV corresponds to an atomic-like oxygen 2s state, the upper valence bands are mainly derived from the oxygen 2p state with a sizable mixture of Zn 4s and 4p states. The lowest conduction band is composed primarily of Zn 4s states. These bands reproduce those of Reference [18] quite accurately.

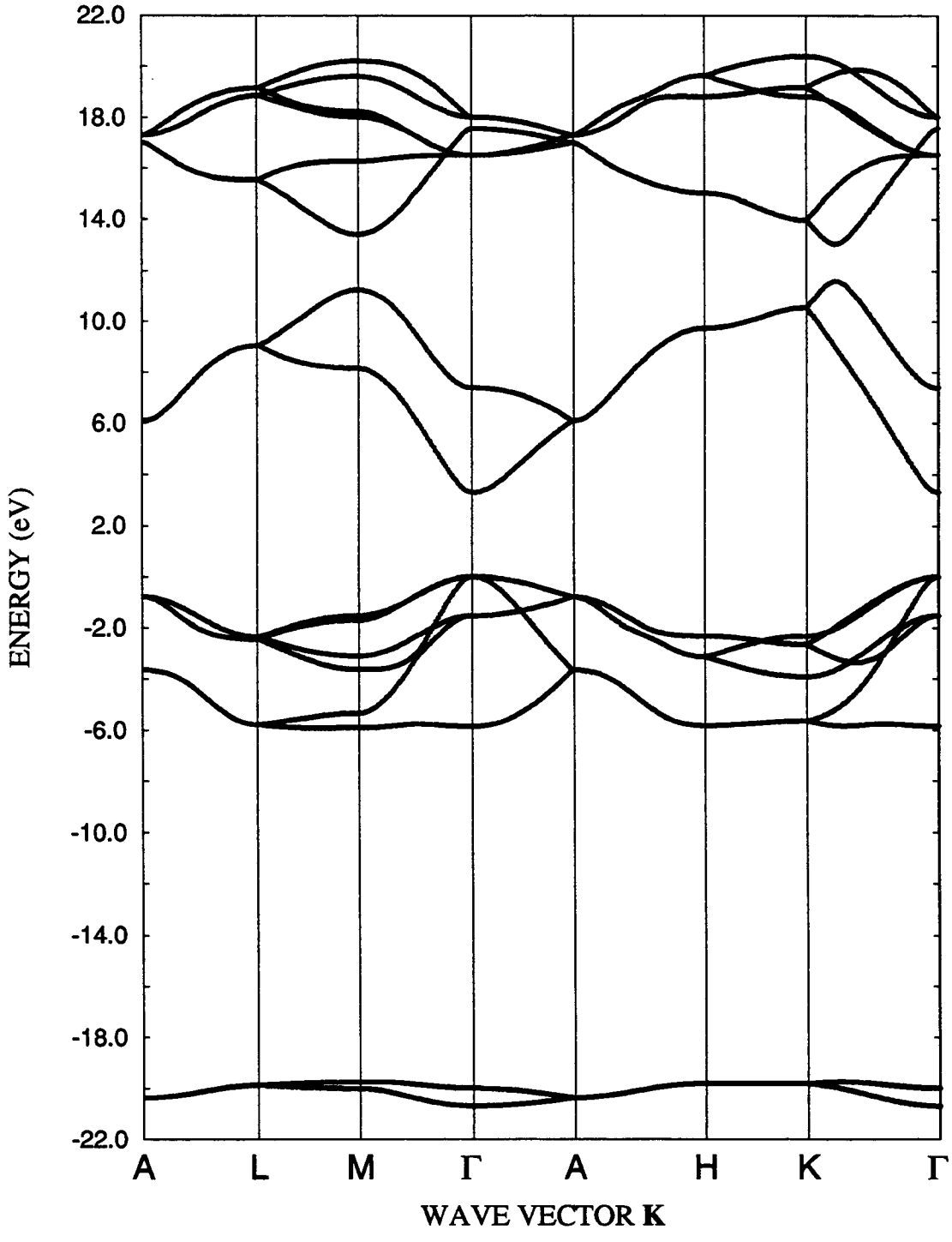

Figure 3.3 The Bulk band structure of the ZnO crystal.

Chapter 4
A Simple Model for Surface

The surface of dielectric materials is of major interest in our research. We investigate simple one-dimensional models in this chapter before we attack the real two-dimensional surface. How the intrinsic atomic properties and the structures beneath the surface determine the surface behavior is easier to understand using these simple models as a guideline. Also these simple models show some generic features of surfaces. Furthermore, the discussion of these models tells us about the convergence properties of the calculations for our ZnO surface model.

4.1 The One-Dimensional Model

Suppose that N objects are located in one-dimensional chain as shown in the following figure.

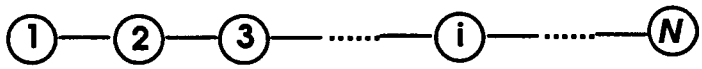

Although each object may have many single-object eigenstates, we assume that only one particular eigenstate for each object is coupled to its nearest neighbor after an interaction is turned on between the nearest neighbors. To simplify our description, we assume each object has only one eigenstate. We use ϕ_i to denote the eigenfunction of the i^{th} object. The energy spectrum of this chain is simply composed of single-object energy levels before we turn on the interactions, and it consists of only one N-fold degenerate level if all the objects are the same. The degeneracy will decrease and the spectrum will change after the interactions are turned on. The coupled chain system has a new set of

eigenstates with eigenfunctions $\{\Phi^i \quad i=1,\cdots,N\}$. Each eigenfunction Φ^i is a superposition of the single-object eigenfunctions as in equation (4.1):

$$\Phi^j = \sum_{i=1}^{N} a_{ji}\phi_i \quad j=1,\cdots,N \tag{4.1}$$

where $|a_{ji}|^2$ indicates the weight of ϕ_i in Φ^j. If the Hamiltonian of the coupled chain is denoted as H, the Schrödinger equation is,

$$H\Phi^j = E^j\Phi^j \quad j=1,\cdots,N \tag{4.2}$$

where E^j is the energy of the eigenstate with eigenfunction Φ^i.

In the space of $\{\phi_i \quad i=1,\cdots,N\}$, the Hamiltonian of the coupled one-dimensional chain system looks like the following tridiagonal matrix:

$$H=[H_{i,j}]=[\langle\phi_j|H|\phi_i\rangle]=\begin{bmatrix} x & x & 0 & 0 & 0 & 0 \\ x & x & x & 0 & 0 & 0 \\ & \ddots & \ddots & \ddots & & \\ & & \ddots & \ddots & \ddots & \\ 0 & 0 & 0 & x & x & x \\ 0 & 0 & 0 & 0 & x & x \end{bmatrix} \tag{4.3}$$

In this Hamiltonian matrix of equation (4.3), only those elements marked x are possible nonzero elements. The dimensionality of this matrix is equal to the number of objects of the chain N.

By diagonalizing the Hamiltonian matrix (4.3) we obtain the energy spectrum $\{E^j\}$, with $j=1,\cdots,N$. At the same time, we obtain the coefficients $\{a_{ji}\}$ in equation (4.1) as the eigenfunction for the j^{th} eigenstate. In the rest of this chapter, we will study several one-dimensional models.

4.2 Identical Objects in a Chain

4.2.1 Case one

The simplest case of our one-dimensional model is when all the objects are the same. First we ignore the boundary effects or the terminal effects. Hence, the diagonal elements of the Hamiltonian matrix take the same values and we set them equal to zero. The nonzero off-diagonal elements represents the coupling strength between nearest neighbors, and we assign the value of one to all of them since they are equal to each other in this case. We studied this model with various values of N, and we draw the following three major conclusions:

1. The distribution of the ordered eigenvalues is smooth. There are no sharp jumps.
2. The single-object eigenfunctions are mixed "evenly". There are no localized states. The mixing of the basis functions creates standing waves.
3. The upper and lower bounds of the energy spectrum will increase as we increase the number of objects on the chain. However, they will quickly reach certain limits (see figure 4.1).

Figure 4.1 shows seven sets of spectra corresponding to seven different values of the total number of objects in the chain. As we can see from this figure, the upper (lower) bound of the spectrum is equal to 1.00(-1.00) when N is 2, but the bound becomes very close to the limit 2.0(-2.0) when N is 20. Figure 4.1 also shows spectra for N=40 and N=80, and the corresponding bounds are almost equal to the limit.

Next, we study the effects of terminating the chain differently. We will vary the value of the first diagonal element of the Hamiltonian matrix or the coupling strength between the first and the second object to study the surface effects.

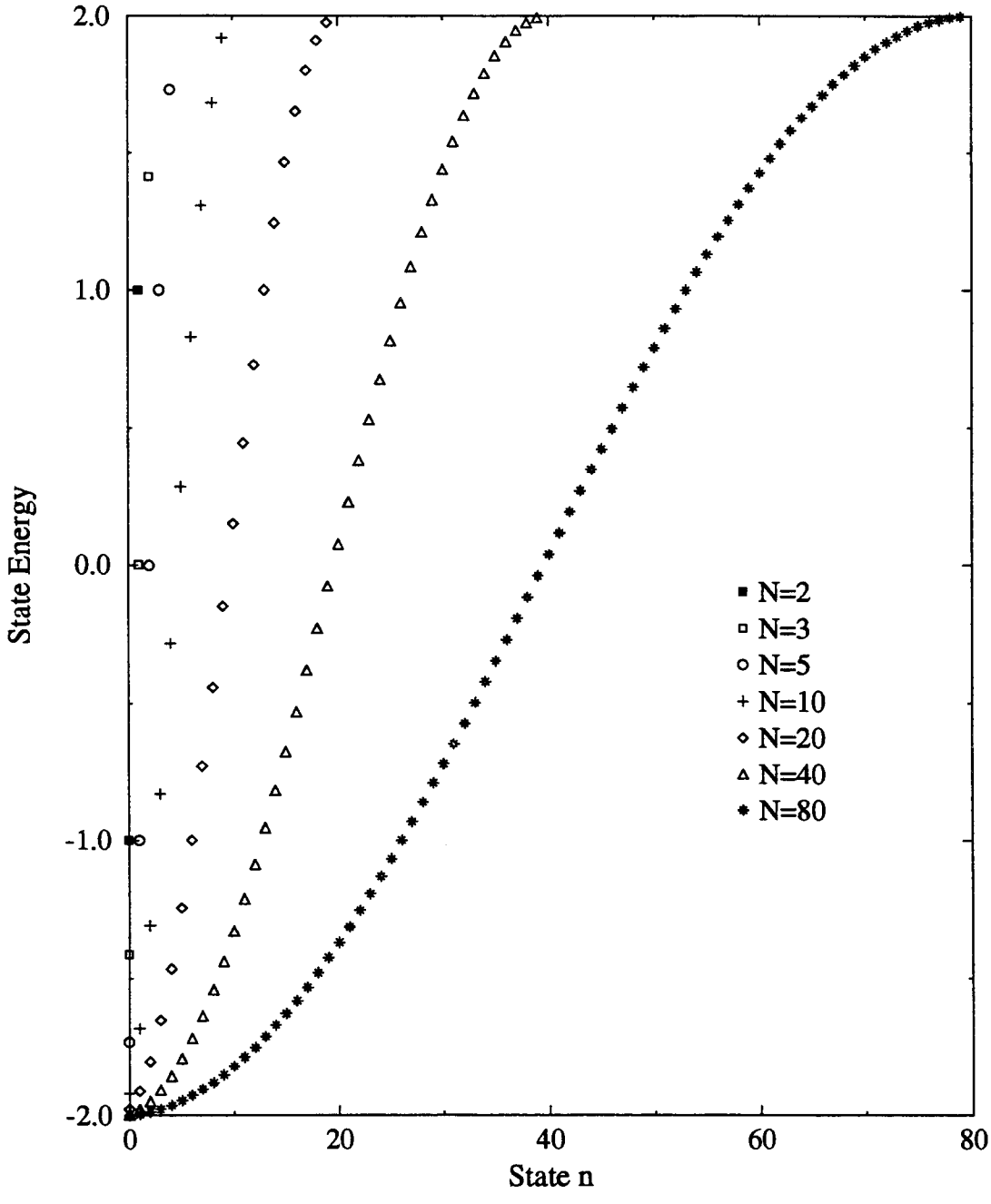

Figure 4.1 Energy spectra corresponding to different numbers (N) of objects in the 1D model.

4.2.2 Case two

The environment of the terminal object is different from other objects on the chain. As a result of this environmental difference, the first order correction to the eigenvalue of the terminal object is different from the first order corrections to the eigenvalues of the other objects. That is:

$$H_{1,1} \neq H_{i,i} \quad \text{for } i = 2, \cdots, N.$$

As this shows, we do not make $H_{N,N}$ different from others in this model in order to simulate a semi-infinite chain. In this case we still assume that all $H_{i,i\pm1}$ values are equal. To be specific, we consider $H_{1,1} \neq 0$ and take $H_{i,i} = 0$ for $i = 2, \cdots, N$. After varying $H_{1,1}$, we found that:

1. There is no localized end state if $H_{1,1}$ is small comparing to the coupling strength (or the off-diagonal elements). There may exist a few states that have a larger weight of the end object than others, but the eigenfunctions of these states do not decay exponentially from the end into the chain. The eigenvalues are still confined between the upper and lower limits when $H_{1,1}$ is smaller than the value of the coupling strength. See figure 4.2.
2. One localized end state will appear when $H_{1,1}$ is larger than the value of the coupling strength. In this case, the eigenvalue of the localized end state is above the upper limit in the spectrum if $H_{1,1}$ is positive (see figure 4.3); it is below the lower limit if $H_{1,1}$ is negative. The eigenfunction of this end state decays exponentially as it goes into the chain (see figure 4.4). The exponent is related to the gap that is defined as the difference between the eigenvalue of the end state and the upper bound. See figure 4.5.

Figure 4.2 shows the energy spectra corresponding to values of 0.25, 0.50, 0.75 and 1.00 respectively for $H_{1,1}$. We can see that the spectrum is not significantly changed

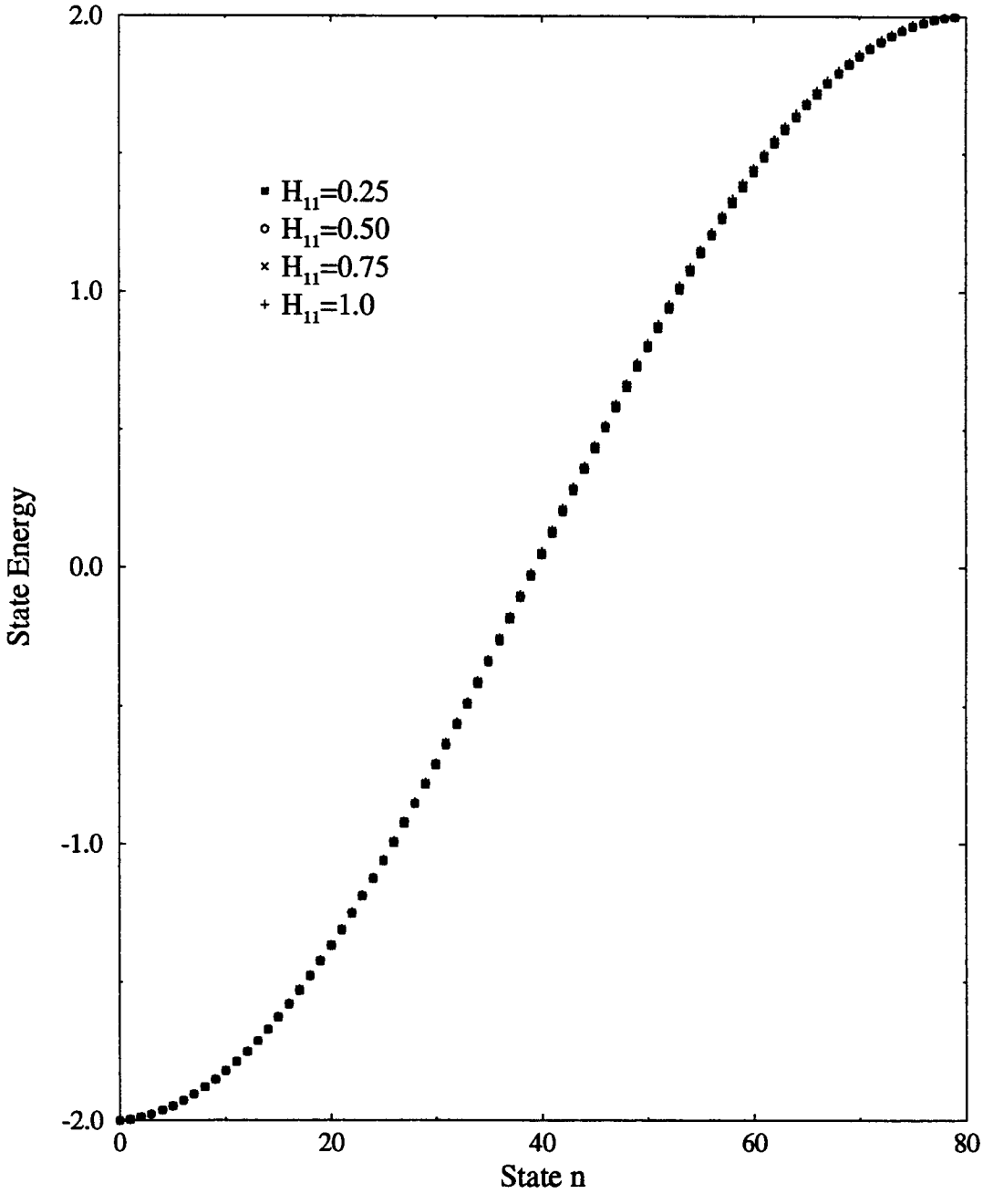

Figure 4.2 Energy spectra of the 1D model with a small difference between the eigenvalues of the terminal object and the others.

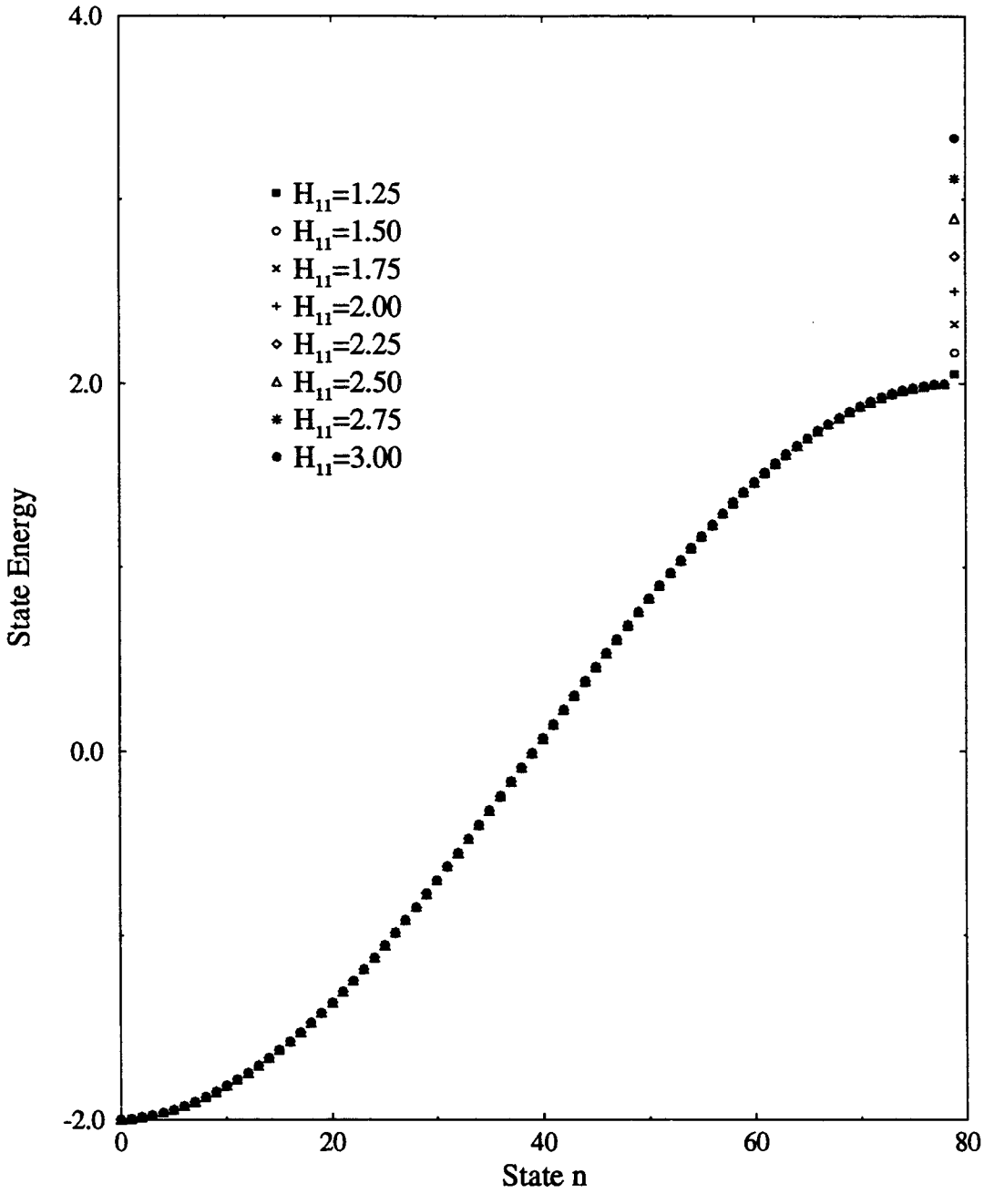

Figure 4.3 Energy spectra of the 1D model with a large difference between the eigenvalues of the terminal object and the others.

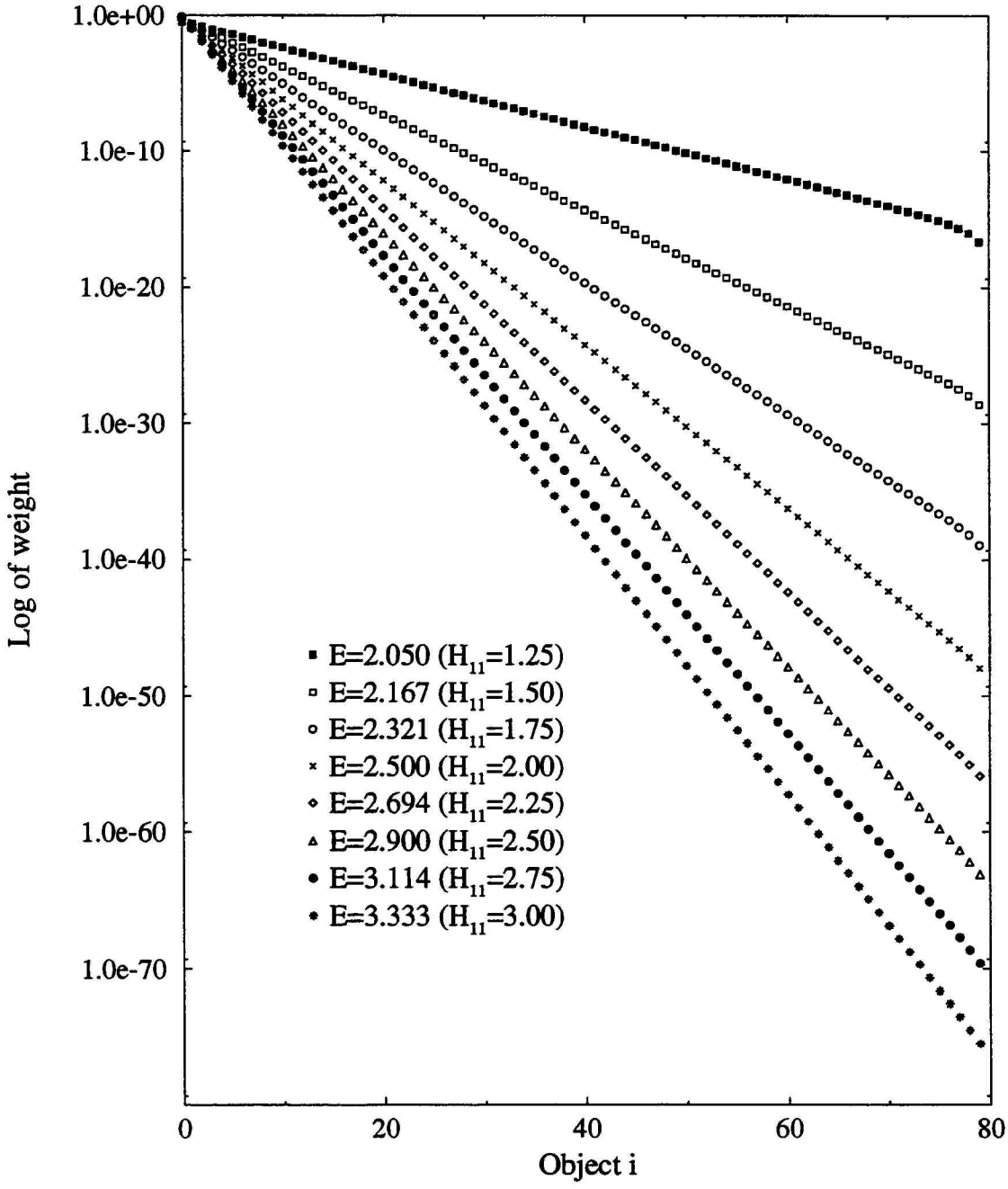

Figure 4.4 Localized end state eigenfunction for different H_{11} values of the 1D model.

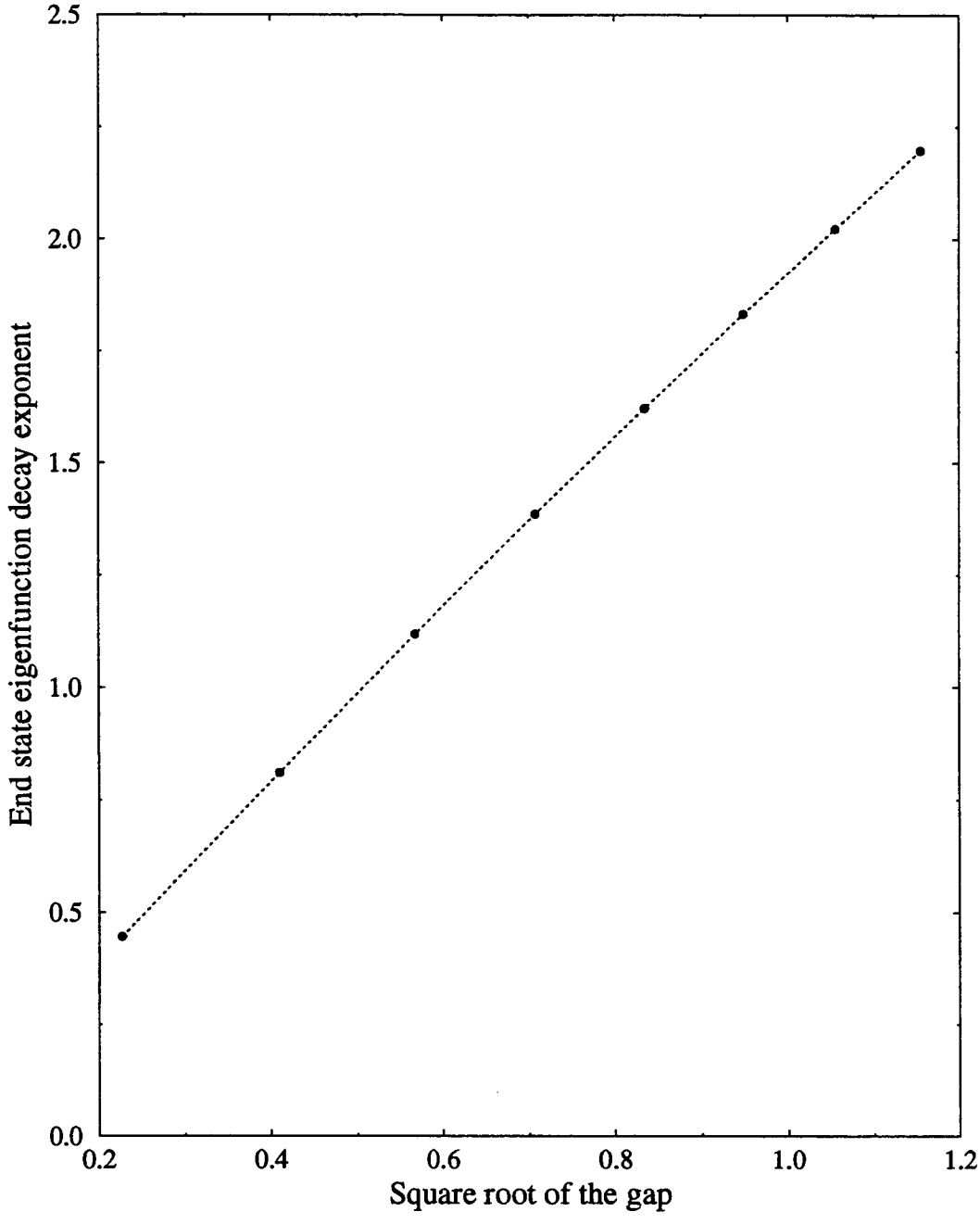

Figure 4.5 Relationship between the end state eigenfunction decay exponent and the relative end state eigenvalue of the 1D model with different H_{11} values.

even when $H_{1,1}$ is set equal to as large as 1.00. There is, however, one eigenvalue that is above the upper limit in the spectrum when $H_{1,1}$ is larger than 1.00. That is the energy of the localized end state. Figure 4.3 shows the spectra for eight different $H_{1,1}$ values of 1.25, 1.50, 1.75, 2.00, 2.25, 2.50, 2.75 and 3.00. The eigenfunction Φ^N of the end state has a much larger weight for ϕ_1 than the others, and $|a_{Ni}|^2 \propto e^{-wi}$. The values of $H_{1,1}$, and corresponding eigenvalues of the end states, as well as its eigenfunction decay exponents, are listed in the following table 4.1.

Table 4.1 Eigenenergy and eigenfunction behavior of end states corresponding to seven different $H_{1,1}$ values of the 1D single-type object model

$H_{1,1}$	1.25	1.50	1.75	2.00	2.25	2.50	3.00
Eigenvalue	2.05	2.167	2.321	2.500	2.694	2.900	3.333
Bound	1.9983	1.9983	1.9984	1.9984	1.9984	1.9984	1.9984
Gap	0.0517	0.1682	0.3230	0.5015	0.6960	0.9015	1.3348
Decay exponent w	0.4462	0.8109	1.1192	1.3862	1.6218	1.8325	2.1972

There is a relationship between the "gap" and eigenfunction decay exponent w, and it is approximately $w \propto \sqrt{gap} \propto \sqrt{E^{(N)} - limit}$. Figure 4.5 shows this relationship graphically. Figure 4.4 shows eigenfunctions of the end states corresponding to different $H_{1,1}$ values.

4.2.3 Case three

Another result of the environmental difference for the terminal atom is a change in the coupling strength between the terminal object and its neighbor; it may be different from the coupling strengths among other objects. To discuss this case, we make the

value of the first off-diagonal element of the tridiagonal Hamiltonian matrix different from the other off-diagonal values but keep all the diagonal elements equal to zero. That means:

$$H_{1,2} = H_{2,1} \neq 1.00 \text{ and } H_{i,i+1} = H_{i+1,i} = 1.00 \quad for \quad i = 2, \cdots, N-1$$

$$\text{but } H_{ii} = 0.0 \quad for \quad i = 1, \cdots, N.$$

Localized end states may or may not appear depending on how large $H_{1,2}$ is. We varied $H_{1,2}$, and we observed phenomena similar to those in case two.

1. If $H_{1,2}$ is smaller than the other coupling strength or slightly greater, there is no localized end state (see figure 4.6).
2. If $|H_{1,2}|$ is made large enough, there are two localized end states. One has an eigenvalue larger than the upper limit; another has eigenvalue smaller than the lower limit (see figure 4.7).

Figure 4.6 shows the spectra for small $H_{1,2}$ values of 0.25, 0.50, 0.75, 1.00 and 1.25. Figure 4.7 shows the spectra exhibiting localized end states for large $H_{1,2}$ values of 1.50, 1.75, 2.00, 2.25, 2.50 and 2.75. The energies of these localized end states corresponding to six different $H_{1,2}$ values are listed in table 4.2 below. Also listed are those corresponding eigenfunction decay exponents.

Table 4.2 Eigenenergy and eigenfunction behavior of end states corresponding to six different $H_{1,2}$ values of the 1D single-type object model

$H_{1,2}$	1.50	1.75	2.00	2.25	2.50	2.75
energy	±2.012	±2.132	±2.309	±2.512	±2.728	±2.952
Decay exponent	0.142	0.612	0.960	1.240	1.475	1.679

Figure 4.8 shows the localized end state eigenfunctions vs the distance from that end. Figure 4.9 shows table 4.2 graphically. We can see from figure 4.9 that again there exists a square root relation between the "gap" and eigenfunction decay exponent.

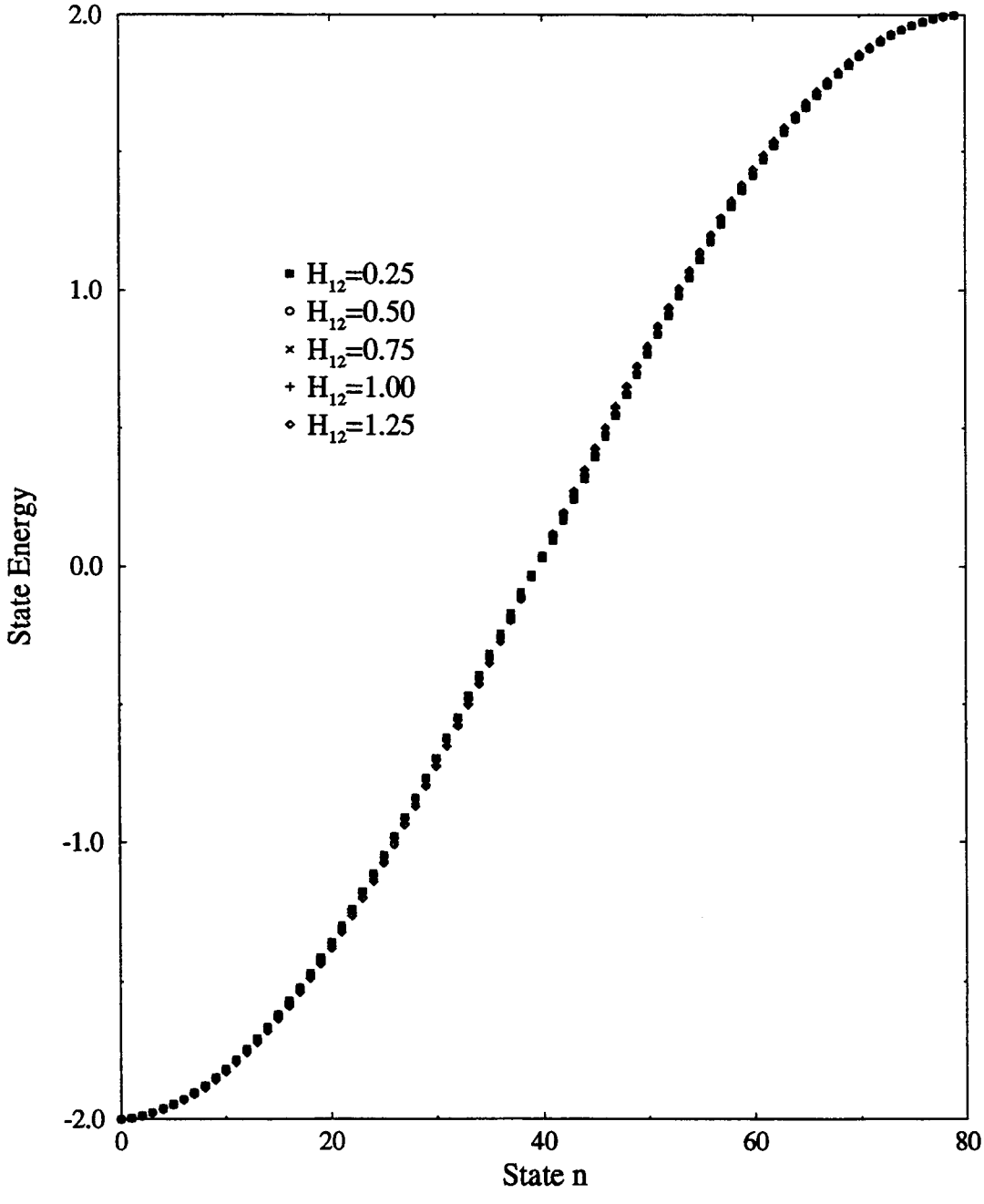

Figure 4.6 The 1D model energy spectra for small H_{12} values.

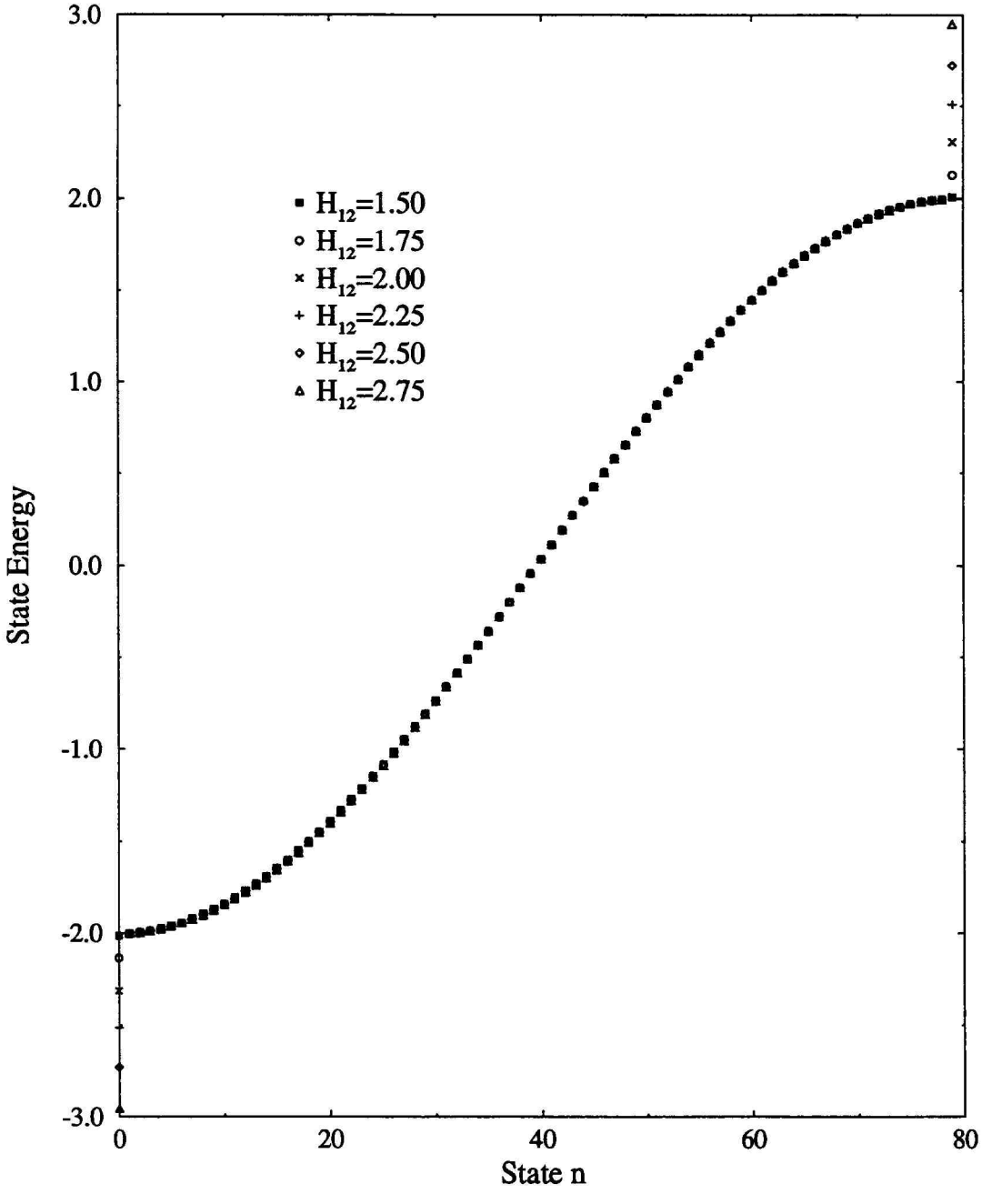

Figure 4.7 The 1D model energy spectra for large H_{12} values.

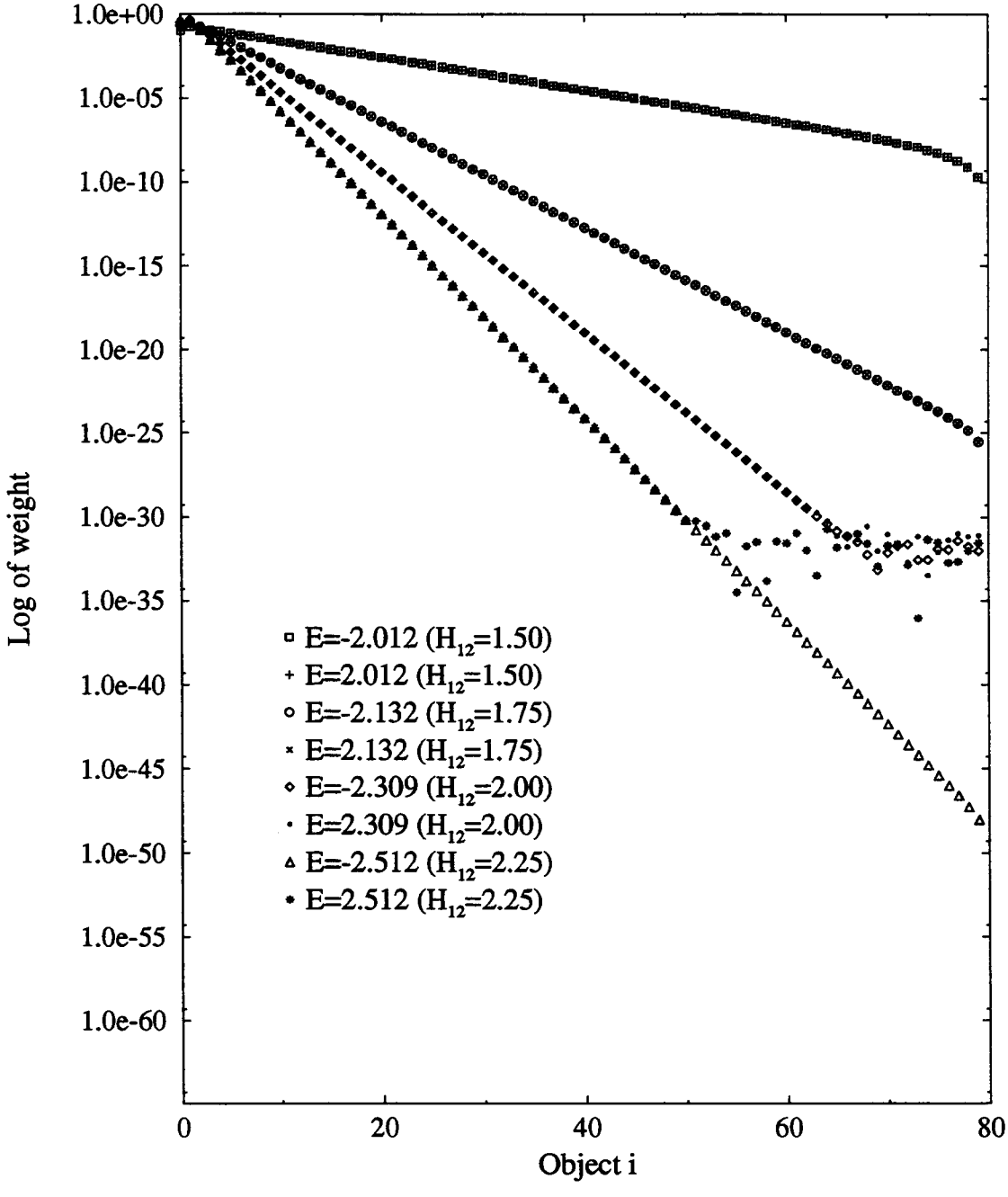

Figure 4.8 The localized end state eigenfunctions for different H_{12} values. For each H_{12} value, the model has two localized end states.

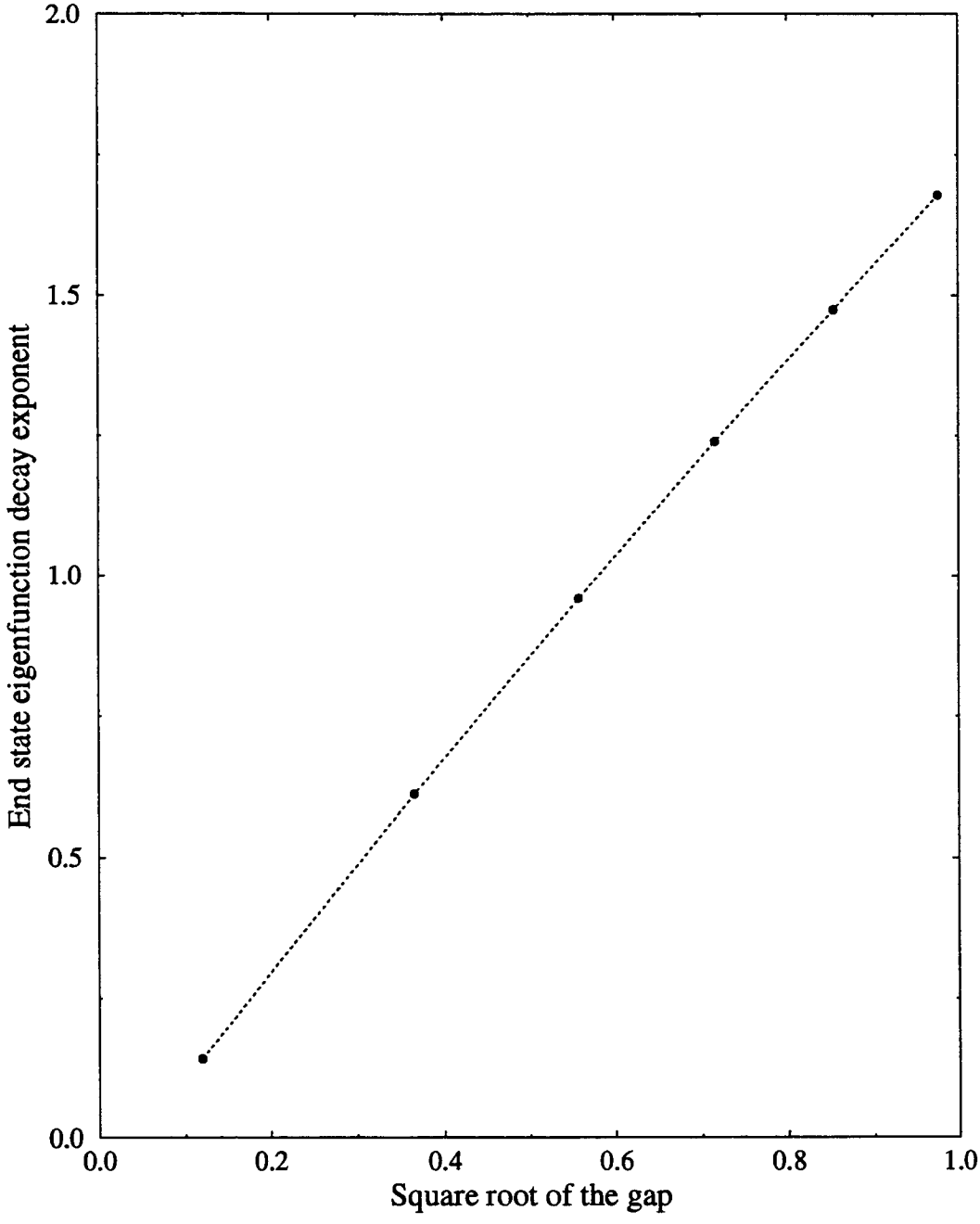

Figure 4.9 Relationship between the end state eigenfunction decay exponent and the relative end state eigenvalue of the 1D model with different H_{12} values.

4.3 A Chain with Alternate Objects

In order to make the model a little more complex, we suppose that there are two different types of objects on the chain and that they take alternate positions as shown in the following figure:

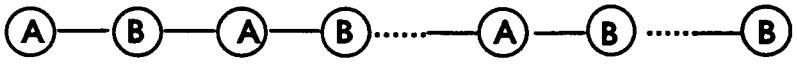

The Hamiltonian matrix of this system is still tridiagonal because only nearest-neighbor coupling is considered. However, there are two different values for the diagonal elements of the Hamiltonian matrix with one value for A objects and another for B objects. We call this model a (H_{even}, H_{odd}) or (2, 0) chain model. We investigate this model in the following subsections.

4.3.1 Case one

We set the energy of sets B equal to zero and investigate the model for various values of A. We make the nonzero off-diagonal elements all equal to 1.00. Hence the Hamiltonian matrix is

$$H_{2i+1,2i+1} \equiv H_{odd} \neq 0.0 \text{ and } H_{2i.2i} = 0.0; \quad H_{i,i+1} = H_{i+1,i} = 1.0$$

Notice that the nonzero value on the diagonal of the matrix is actually the difference between these two different objects' energies.

We vary this value of the energy difference from small to large and observe the following:

The spectrum is split into two parts. The gap between the two parts increases as we increase H_{odd}. There are no localized end states.

Figure 4.10 shows the spectra for various H_{odd} values.

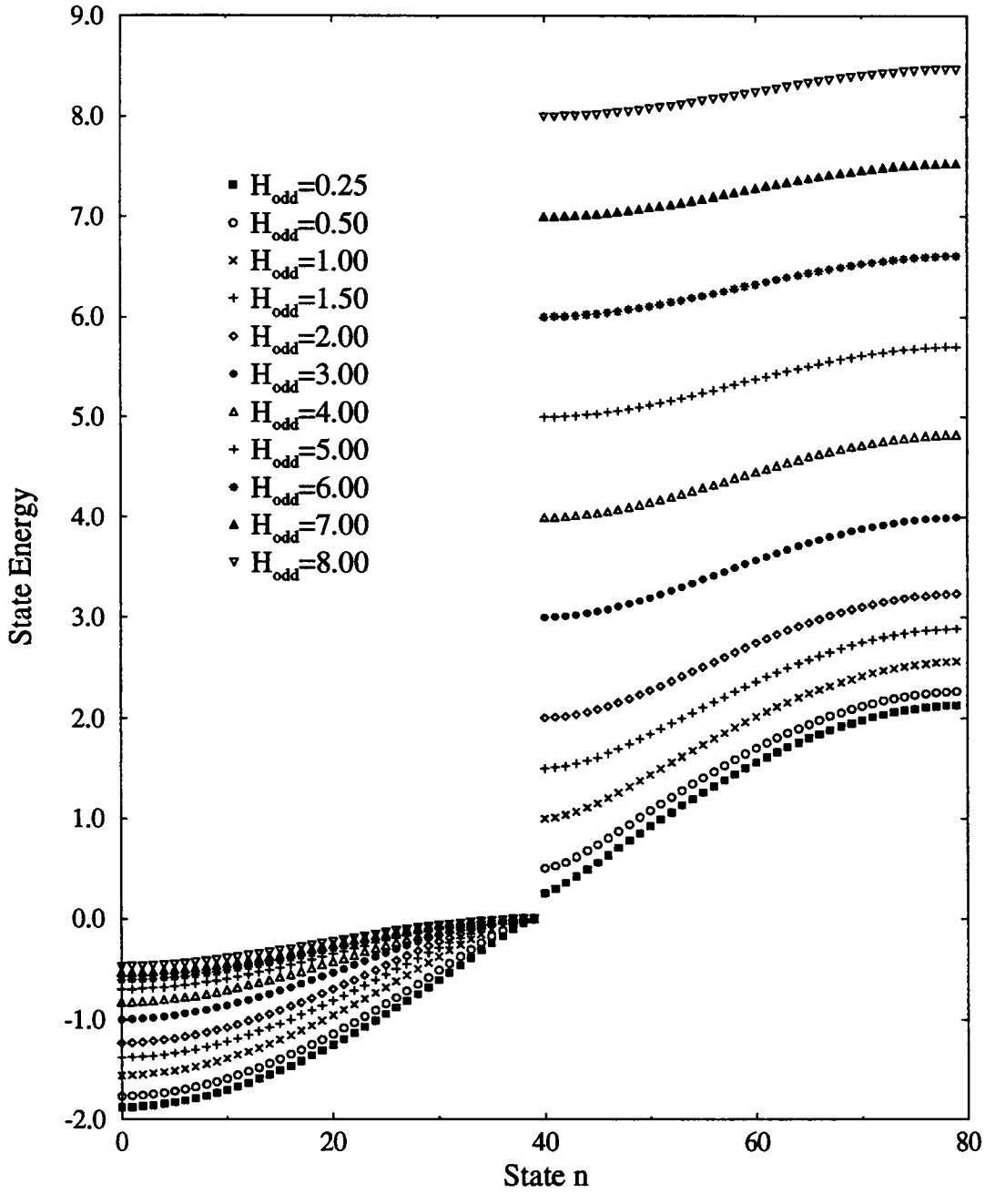

Figure 4.10 Energy spectra for various H_{odd} values of the (H_{even}, H_{odd}) chain model.

4.3.2 Case two

In order to study the effects of terminating the chain differently, we fix all H_{odd}, except $H_{1,1}$, at 2.0 and vary the value of $H_{1,1}$. Figure 4.11 shows the spectra for nine different values of $H_{1,1}$. In table 4.3, we list the end state eigenvalues for each $H_{1,1}$ value. If $H_{1,1}$ is close or in the lower part of the spectrum, we get two localized end states. One is below the lower part of the spectrum; the another is below the upper part of the spectrum but above the lower part. As $H_{1,1}$ increases away from the lower part towards

Table 4.3 End state eigenvalues of the (2, 0) chain model when varying the value of $H_{1,1}$

$H_{1,1}$	-1.0	-0.5	0.0	1.0	1.75	2.0	2.75	3.25	4.0
E_1	0.387	0.551	0.781	1.414	1.919	X	3.267	3.606	4.266
E_2	-1.721	-1.451	-1.281	X	X	X	X	X	X

X stands for nonlocalized end state.

the upper part, we get only one localized end state in the gap between these two parts of the spectrum. The localized end state disappears when $H_{1,1} > H_{odd}$ but close to H_{odd} of value 2.0. The localized end state appears again with its eigen energy bigger than the upper part. Figure 4.12 shows eigenfunctions of the localized end states.

Figure 4.13 shows the relation between the decay exponent of the localized end state eigenfunction and square root of the difference between the eigen energy of the localized end state and the bound value of the corresponding part of the spectrum. There are three groups of data. One is for localized end states with energies below the lower part marked as lower; one is for localized end states with energies in the gap

between the two parts marked as middle, and the third one is for localized end states with energies above the upper part marked as higher. The lower and higher groups show the square root relationship on the same straight line, but the middle group shows a little more complicated relation. This is because the eigenvalues of both the lower and higher group end states are pushed in the same direction by all the other states, but for the middle group, the end state eigenvalues are pushed in one direction by the eigenstates with eigenvalues in the upper part of the spectrum and are pushed in the opposite direction by the eigenstates with eigenvalues in the lower part of the spectrum.

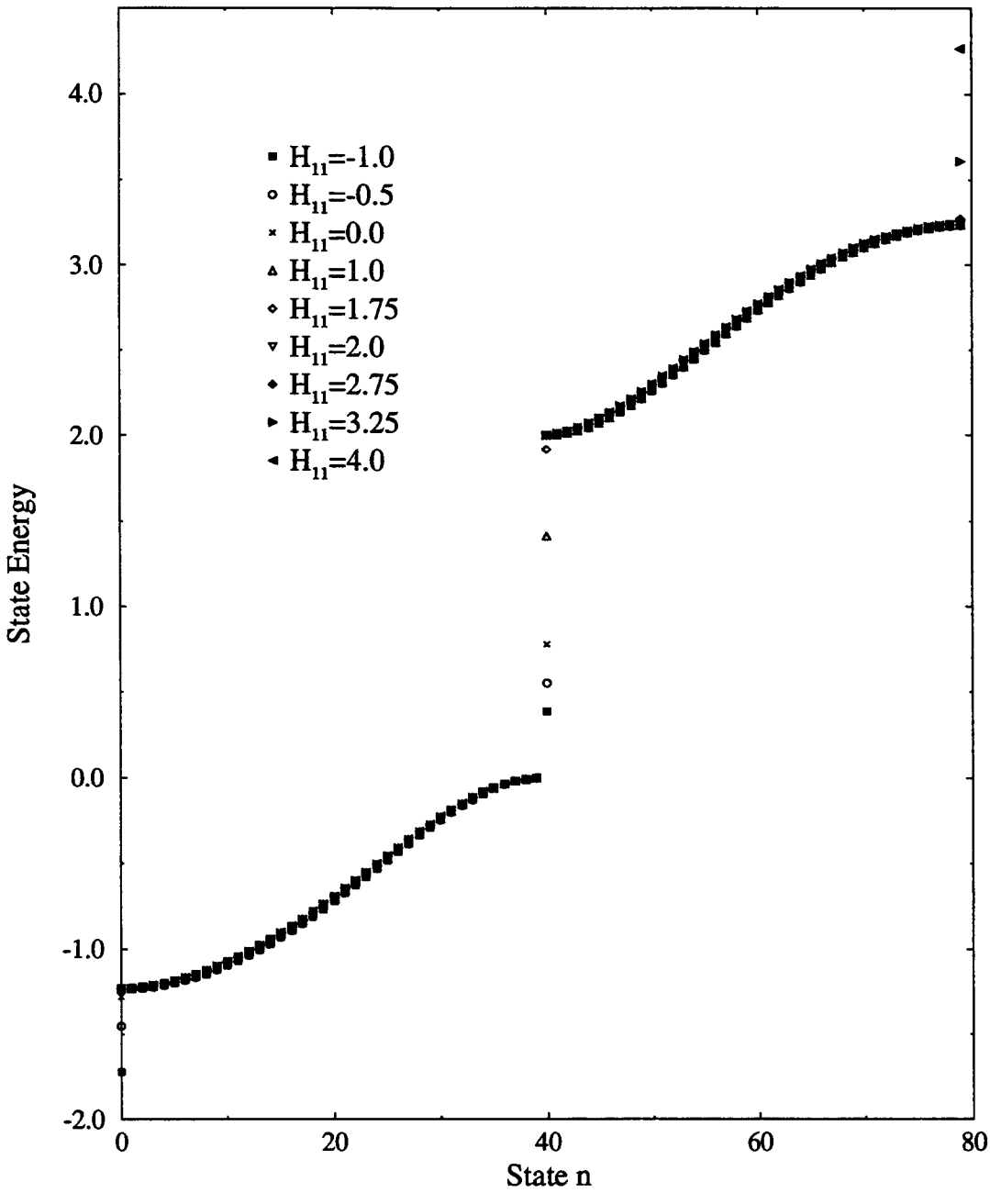

Figure 4.11 Energy spectra for different H_{11} values in the (2, 0) chain model.

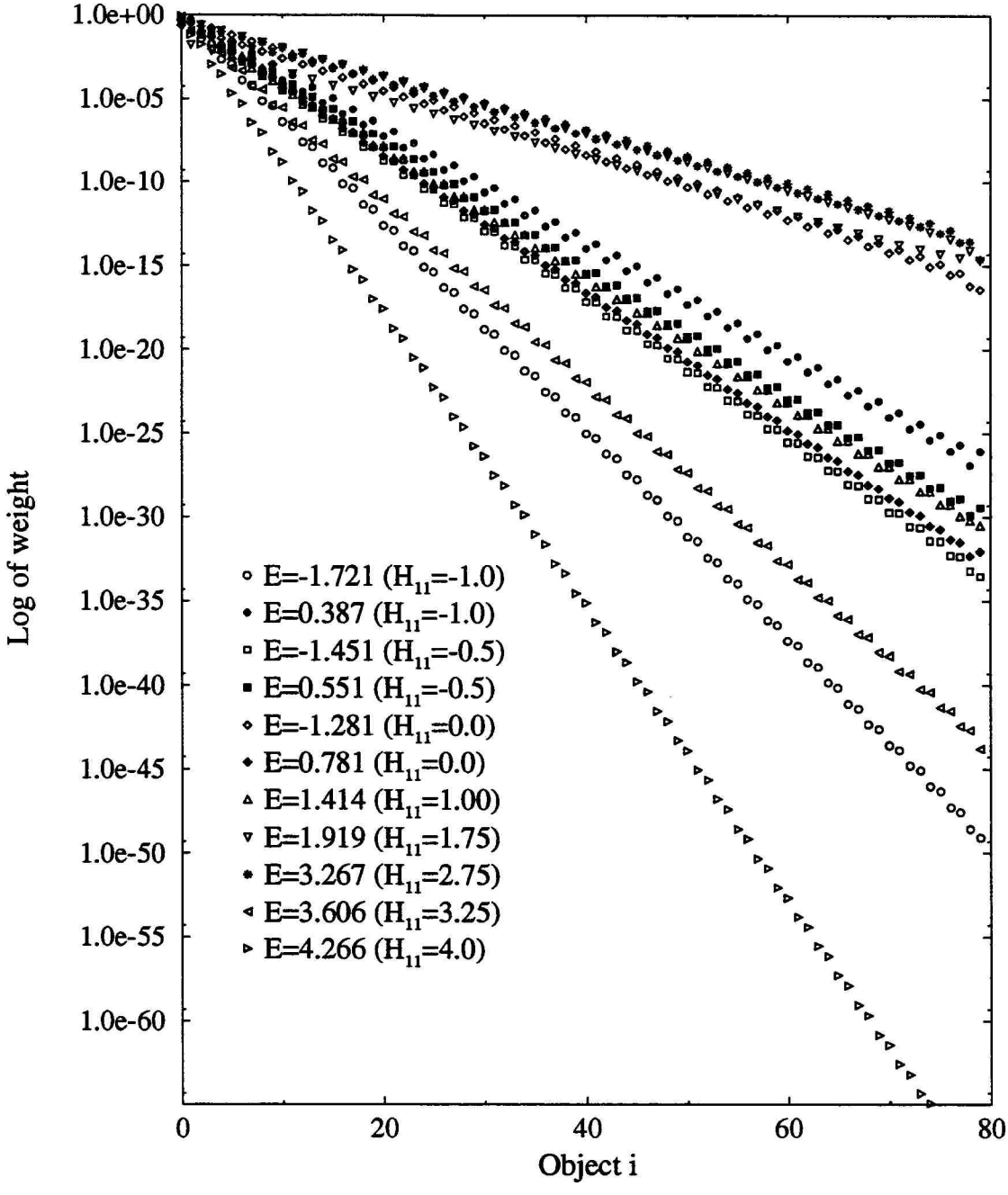

Figure 4.12 The end state eigenfunctions for different H_{11} values in the (2, 0) chain model.

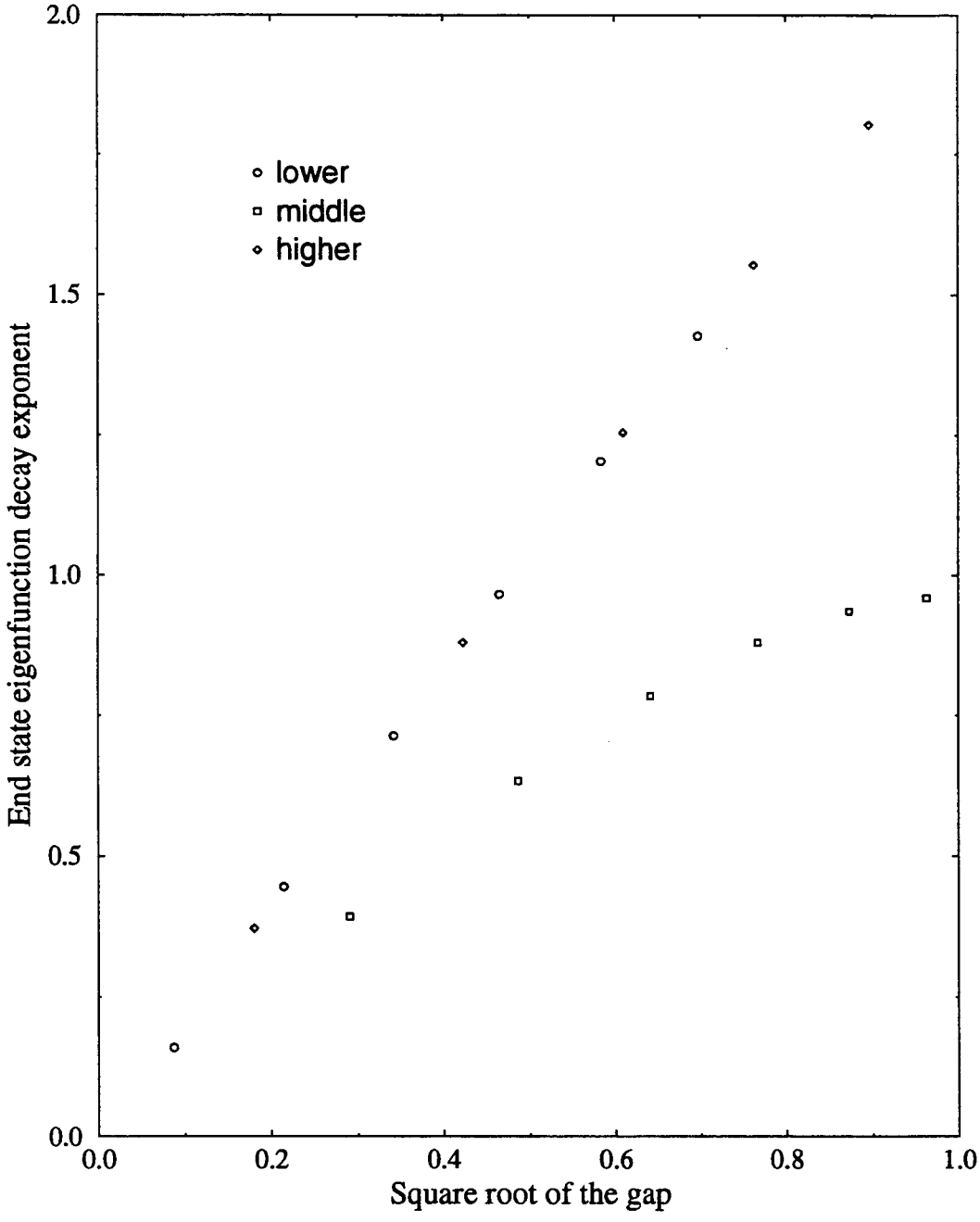

Figure 4.13 Relationship between the end state eigenfunction decay exponent and the relative end state eigenvalue of the (2, 0) chain model with different H_{11} values.

4.3.3 Case three

In this case we study the effects of changing the coupling near the surface. We vary the first off-diagonal element $H_{1,2}$ while keeping all other $H_{i,i\pm1} = 1.0$ and $H_{2i+1,2i+1} = 2.0$ and $H_{2i,2i} = 0.0$. we found that:

1. If $H_{1,2}$ is smaller or slightly larger than 1.0 by <0.5, there is no localized end state.
2. If $H_{1,2}$ is large enough (> 1.5), there are two localized end states. One has an energy above the upper part of the spectrum, and the another has an energy below the lower part of the spectrum.

Figure 4.14 shows the spectra for various values of $H_{1,2}$. Figure 4.15 shows the eigenfunctions of the localized end states. In table 4.4, we list the end state eigenvalues

Table 4.4 End state eigenvalues of the (2, 0) chain model when varying the value of $H_{1,2}$

$H_{1,2}$	0.75	1.25	1.50	1.75	2.00	2.25	2.50
E_1	X	X	-1.247	-1.355	-1.516	-1.703	-1.905
E_2	X	X	3.247	3.355	3.516	3.703	3.905

X stands for nonlocalized end state.

for different $H_{1,2}$ values of the model. Figure 4.16 shows the relationship between the decay exponent and the square root of eigen energies relative to the bound of the spectrum.

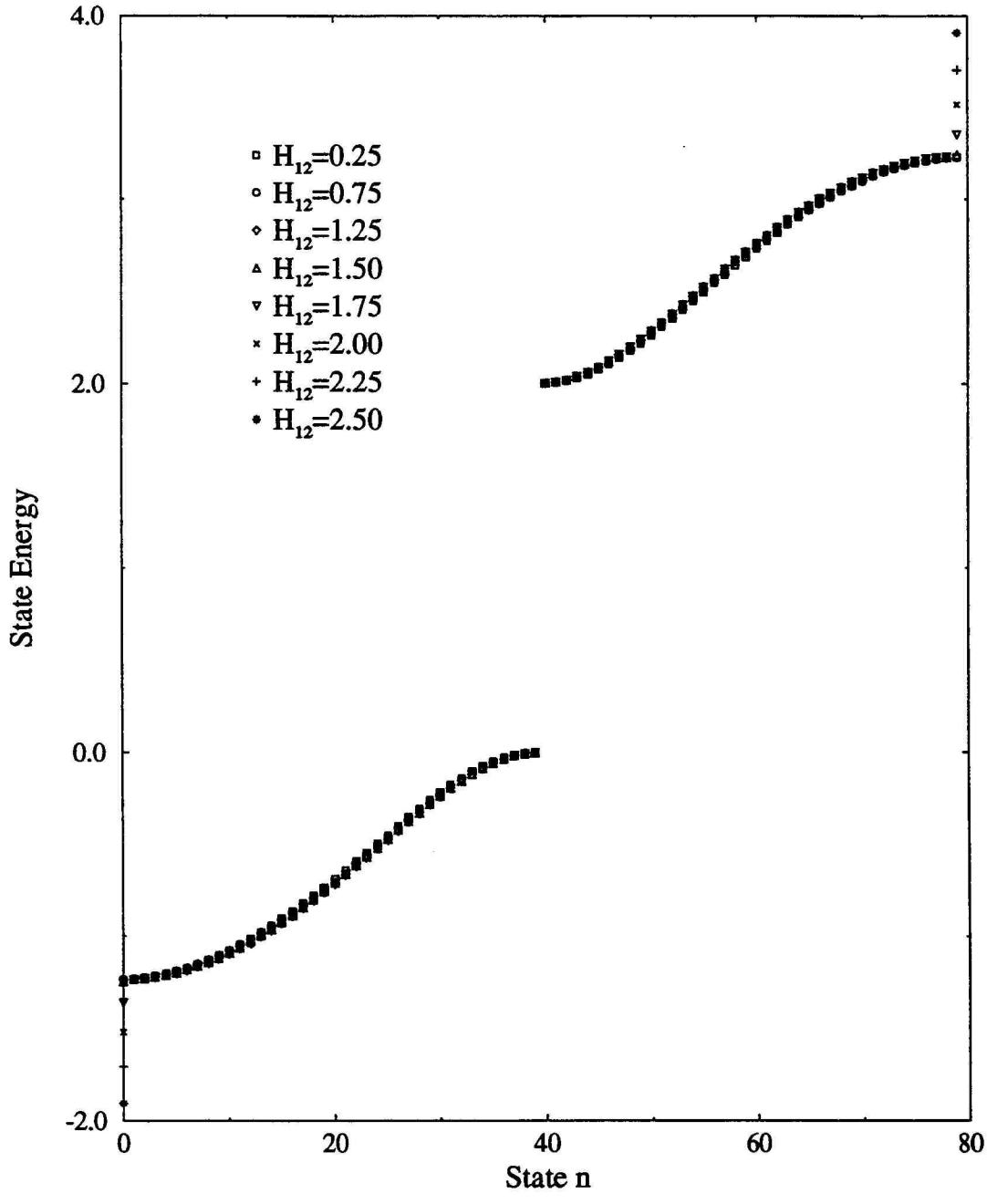

Figure 4.14 The energy spectra for different H_{12} values in the (2, 0) chain model.

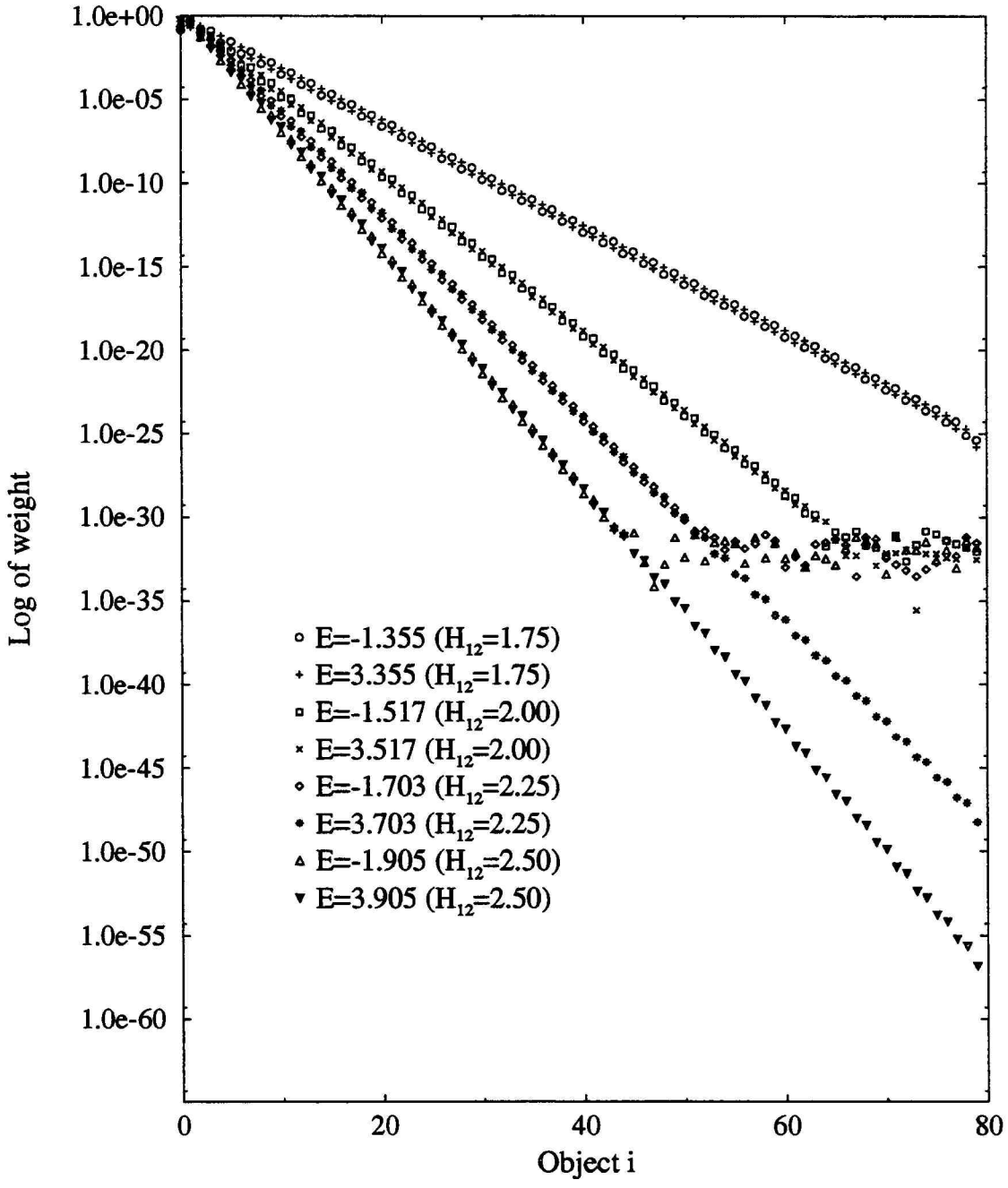

Figure 4.15 The end state eigenfunction for different H_{12} values in the (2, 0) chain model.

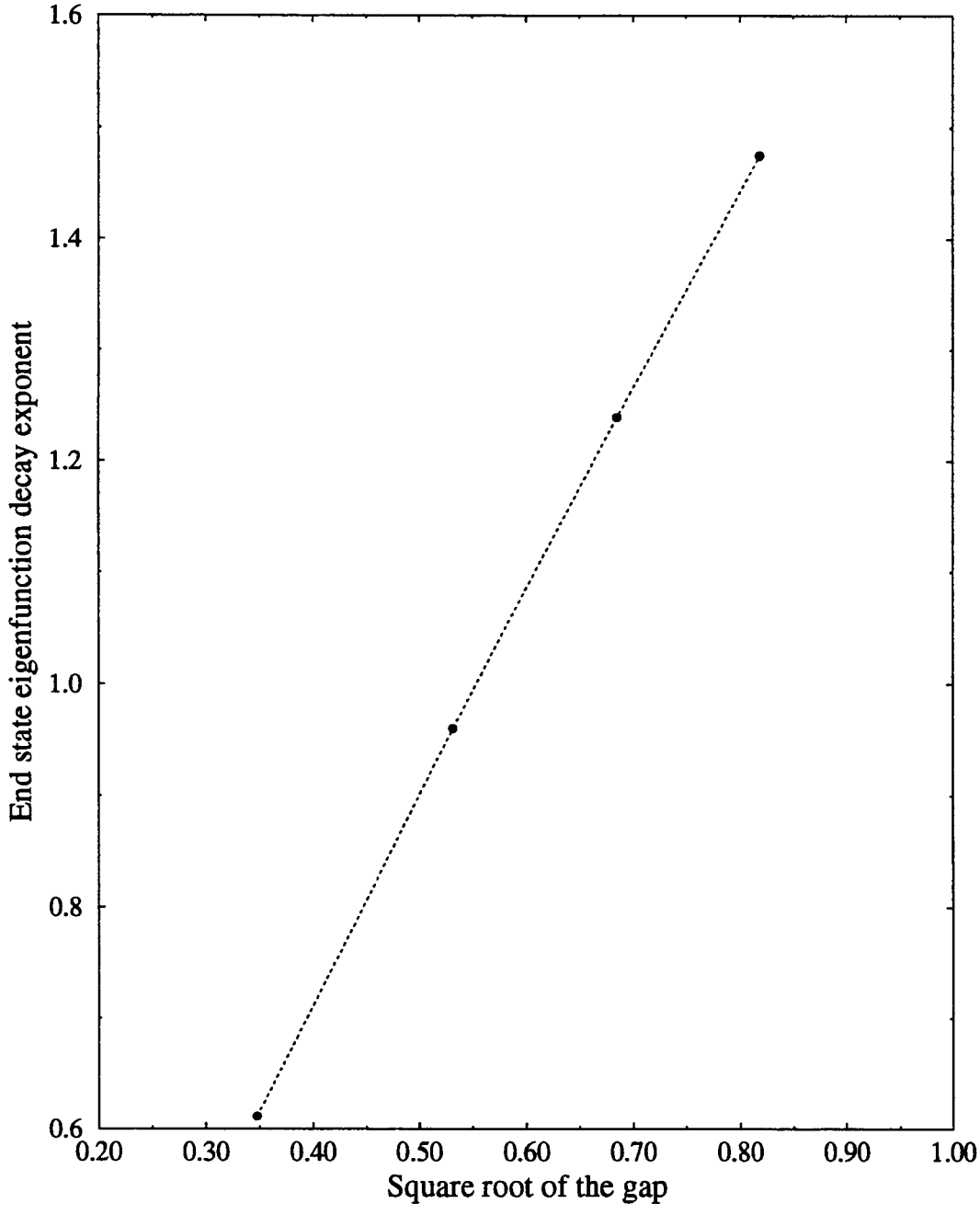

Figure 4.16 Relationship between the end state eigenfunction decay exponent and the relative end state eigenvalues of the (2, 0) chain model with different H_{12} values.

Using the results of this one-dimensional model to guide us, we are in a better position to understand the surface of a real material like ZnO. In the next chapter, we will look into the localized "surface" states and surface resonant states in ZnO. Many phenomena will be similar to those found in our one-dimensional model.

Chapter 5
Surface Electronic Structure of ZnO

5.1 The "Layered" Model for Surface

Actual crystals are finite. The infinite system of a Bravais lattice is an idealization. It is a very good and useful idealization when the vast majority of atoms concerned are far from the surface. However, when the surface atoms are of interest we have to consider new models.

The periodic crystal structure of a solid can be viewed as a layered structure. The layers are parallel to each other. In chapter 3, where we were interested in bulk properties, we assumed not only that each layer is infinitely large but also that the total number of layers is infinite. Consequently, the properties of the surface were ignored. In this chapter, we intend to retain the properties of the surface by considering a finite number of layers. It would be ideal if we could include every layer of a given solid sample in our model.

In reality, it is not possible to include a realistic number of layers characteristic for a solid sample because the number is too large. A computer can handle only a small number of layers. So, in our "layered model" the real sample of a huge number of layers is replaced by a small number of layers, and each layer is supposed to be so large that it can be idealized to be a two-dimensional Bravais lattice.

An important question addresses the sensitivity of the properties of the surface layer to the number of layers beneath it. It seems that the properties of the surface should be different when there are 10 layers of atoms beneath it or when there are 100 layers of atoms beneath it. If these differences are so significant that we have to take

care of them, we run into trouble since we are forced to include a large number of layers like a realistic sample contains. We are unable to do that. Fortunately, convergence of electronic structure properties occurs within only tens of layers.

5.2 Structure of the Model for a ZnO Surface

For crystalline ZnO, we concentrate on the surface that is perpendicular to the c-axis in the wurtzite ZnO crystal. Hence, each layer contains either all Zn or all O atoms and every layer of Zn is sandwiched between two layers of O and vice versa. The layers are stacked along the $\hat{z}$ direction. If the number of layers is infinite and the surface properties are ignored, we recover the bulk case discussed in Chapter 3.

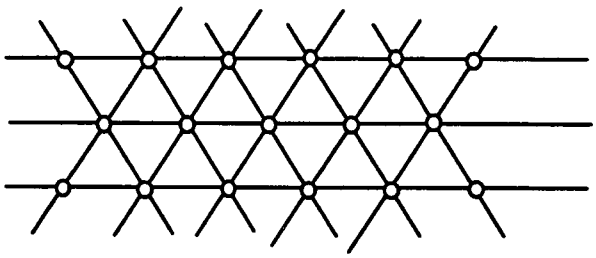

Figure 5.1 The triangular net structure of ZnO layers

Figure 5.1 above shows the structure of each layer in ZnO. It is a two-dimensional Bravais lattice: a triangular net. In the coordinate system that we chose the two primitive vectors of the Bravais lattice are

$$\vec{a}_1 = a\hat{x},\ \vec{a}_2 = \frac{a}{2}\hat{x} + \frac{\sqrt{3}a}{2}\hat{y}. \qquad (5.1)$$

The two-dimensional reciprocal lattice of a triangular net is also a triangular net and the two primitive vectors of the two-dimensional reciprocal lattice are

$$\vec{b}_1 = \frac{2\pi}{a}\hat{x} - \frac{2\pi}{\sqrt{3}a}\hat{y},\quad \vec{b}_2 = \frac{4\pi}{\sqrt{3}a}\hat{y} \qquad (5.2)$$

Equations (5.1) and (5.2) are equations (3.9) and (3.11) without the third component.

5.3 Hamiltonian of the ZnO Model Surface System

5.3.1 The basis wave functions

The atomic orbitals will hybridize when we put the atoms into a triangular net. We will treat only mixtures of sp^3 orbitals, and we will apply the LCAO method discussed in Chapter 3. Although it loses the periodicity along the c-axis, the Hamiltonian still has the periodicity of the two-dimensional Bravais lattice. Therefore, we should take advantage of the symmetry and work with the right zero-order basis wave functions or Bloch wave functions instead of atomic orbitals. For each two-dimensional wave vector and each layer, we construct four basis wave functions corresponding to four atomic orbitals. If the layer contains oxygen atoms, the four basis wave functions are:

$$\left|\phi^{\vec{k}}_{a,l,s}\right\rangle = \frac{1}{\sqrt{N}}\sum_{\vec{R}} e^{i\vec{k}\cdot\vec{R}}\left|a,s\left(\vec{r}-\left(\vec{d}_l+\vec{R}\right)\right)\right\rangle \tag{5.3}$$

$$\left|\phi^{\vec{k}}_{a,l,p_x}\right\rangle = \frac{1}{\sqrt{N}}\sum_{\vec{R}} e^{i\vec{k}\cdot\vec{R}}\left|a,p_x\left(\vec{r}-\left(\vec{d}_l+\vec{R}\right)\right)\right\rangle \tag{5.4}$$

$$\left|\phi^{\vec{k}}_{a,l,p_y}\right\rangle = \frac{1}{\sqrt{N}}\sum_{\vec{R}} e^{i\vec{k}\cdot\vec{R}}\left|a,p_y\left(\vec{r}-\left(\vec{d}_l+\vec{R}\right)\right)\right\rangle \tag{5.5}$$

$$\left|\phi^{\vec{k}}_{a,l,p_z}\right\rangle = \frac{1}{\sqrt{N}}\sum_{\vec{R}} e^{i\vec{k}\cdot\vec{R}}\left|a,p_z\left(\vec{r}-\left(\vec{d}_l+\vec{R}\right)\right)\right\rangle \tag{5.6}$$

where a represents anion of oxygen, N is the total number of atoms contained in each layer, l is the layer index, $\vec{d}_l$ is a vector leading toward layer l from the origin of the coordinate system, $\vec{k}$ is a two-dimensional wave vector and $\vec{R}$ is a two-dimensional Bravais lattice vector. If the layer contains zinc atoms, the four basis wave functions are:

$$\left|\phi^{\vec{k}}_{c,l,s}\right\rangle = \frac{1}{\sqrt{N}}\sum_{\vec{R}} e^{i\vec{k}\cdot\vec{R}}\left|c,s\left(\vec{r}-\left(\vec{d}_l+\vec{R}\right)\right)\right\rangle \tag{5.7}$$

$$\left|\phi^{\vec{k}}_{c,l,p_x}\right\rangle = \frac{1}{\sqrt{N}}\sum_{\vec{R}} e^{i\vec{k}\cdot\vec{R}}\left|c, p_x\left(\vec{r}-\left(\vec{d}_l+\vec{R}\right)\right)\right\rangle \tag{5.8}$$

$$\left|\phi^{\vec{k}}_{c,l,p_y}\right\rangle = \frac{1}{\sqrt{N}}\sum_{\vec{R}} e^{i\vec{k}\cdot\vec{R}}\left|c, p_y\left(\vec{r}-\left(\vec{d}_l+\vec{R}\right)\right)\right\rangle \tag{5.9}$$

$$\left|\phi^{\vec{k}}_{c,l,p_z}\right\rangle = \frac{1}{\sqrt{N}}\sum_{\vec{R}} e^{i\vec{k}\cdot\vec{R}}\left|c, p_z\left(\vec{r}-\left(\vec{d}_l+\vec{R}\right)\right)\right\rangle \tag{5.10}$$

where c represents the zinc cation.

These basis wave functions follow Bloch's theorem. That means they satisfy the following equation:

$$\phi^{\vec{k}}_{b,l,n}\left(\vec{r}+\vec{R}\right) = e^{i\vec{k}\cdot\vec{R}}\phi^{\vec{k}}_{b,l,n}\left(\vec{r}\right) \tag{5.11}$$

where b, n are the labels for atom and atomic orbital respectively, $\vec{k}$ and $\vec{R}$ are respectively a two-dimensional wave vector and a Bravais lattice vector. $\vec{k}$ is found to take N distinguishable values if Born-Von Karman boundary conditions are applied:

$$\vec{k} = \sum_{i=1}^{2}\frac{m_i}{N_i}\vec{b}_i, \qquad m_i \text{ integer.} \tag{5.12}$$

where $\vec{b}_1$ and $\vec{b}_2$ are defined in equation (5.2), $N_1N_2 = N$ is the total number of atoms in each layer, and is equal to the number of unit cells of the two-dimensional Bravais lattice. It can be easily shown that the area $\Delta\vec{k}$ of the two-dimensional k-space per allowed value of $\vec{k}$ is $\frac{(2\pi)^2}{A}$. So, the number of allowed wave vectors in a primitive cell of the two-dimensional reciprocal lattice is equal to N. If our model consists of L layers, we have a total of $4LN$ basis wave functions.

5.3.2 The Hamiltonian matrix

In the space spanned by the total $4LN$ basis wave functions of our "layered" model of L layers the Hamiltonian is a $4LN \times 4LN$ matrix. A matrix with size of $4LN \times 4LN$ is too large to handle.

We can prove, however, that only those basis wave functions with the same wave vector $\vec{k}$ will mix because the Hamiltonian has the periodicity of the two-dimensional Bravais lattice. We know that the system is invariant under a translation by any two-dimensional Bravais lattice vector $\vec{R}$. So, if we denote the translational operation of any given Bravais lattice vector $\vec{R}$ by the operator T_R, the invariance property of the system is expressed as,

$$T_R H T_R^{-1} = H \qquad (5.13)$$

where H is the Hamiltonian of the system. Following Bloch's theorem of equation 5.11, any wave function of equations 5.3 to 5.10 $\left|\phi_l\left(\vec{k}_l\right)\right\rangle$ satisfies,

$$T_R\left|\phi_l\left(\vec{k}_l\right)\right\rangle = e^{i\vec{k}_l\cdot\vec{R}}\left|\phi_l\left(\vec{k}_l\right)\right\rangle \qquad (5.14)$$

Hence,

$$\begin{aligned}\left\langle\phi_{l_1}\left(\vec{k}'_{l_1}\right)\middle|H\middle|\phi_{l_2}\left(\vec{k}''_{l_2}\right)\right\rangle &= \left\langle\phi_{l_1}\left(\vec{k}'_{l_1}\right)\middle|T_R^{-1}T_R H T_R^{-1}T_R\middle|\phi_{l_2}\left(\vec{k}''_{l_2}\right)\right\rangle \\ &= e^{i\left(\vec{k}_{l_2}-\vec{k}_{l_1}\right)\cdot\vec{R}}\left\langle\phi_{l_1}\left(\vec{k}'_{l_1}\right)\middle|H\middle|\phi_{l_2}\left(\vec{k}''_{l_2}\right)\right\rangle\end{aligned} \qquad (5.15)$$

and thus,

$$\left(1-e^{i\left(\vec{k}_{l_2}-\vec{k}_{l_1}\right)\cdot\vec{R}}\right)\left\langle\phi_{l_1}\left(\vec{k}'_{l_1}\right)\middle|H\middle|\phi_{l_2}\left(\vec{k}''_{l_2}\right)\right\rangle = 0 \qquad (5.16)$$

Since equation (5.16) has to hold for an arbitrary two-dimensional Bravais lattice vector $\vec{R}$, we arrive at:

$$\left\langle\phi_{l_1}\left(\vec{k}'_{l_1}\right)\middle|H\middle|\phi_{l_2}\left(\vec{k}''_{l_2}\right)\right\rangle \propto \delta\left(\vec{k}'_{l_1}-\vec{k}''_{l_2}\right) \qquad (5.17)$$

Equation (5.17) states that two basis wave functions of two different wave vectors do not couple to each other. Therefore, the huge Hamiltonian matrix of $4LN_l$ by $4LN_l$ is reduced to N_l smaller matrices; each has the size of $4L$ by $4L$. It is feasible to diagonalize the Hamiltonian matrix of size $4L$ by $4L$ if L is not too large.

For a given wave vector $\vec{k}$, the $4L$ basis wave functions are

$$\left|\phi_{l,n}^{\vec{k}}(\vec{r})\right\rangle = \frac{1}{\sqrt{N}}\sum_{\vec{R}} e^{i\vec{k}\cdot\vec{R}}\left|l,n\left(\vec{r}-\vec{d}_l-\vec{R}\right)\right\rangle \qquad (5.18)$$

where $\left|l,n\left(\vec{r}-\vec{d}_l-\vec{R}\right)\right\rangle$ is the atomic wave function of the atom at site $\vec{d}_l+\vec{R}$ in layer l where l runs over the layers starting from the top ($l=1$) to the bottom ($l=L$); n runs over the orbitals s, p_x, p_y, and p_z. We assume that every layer has the same number of atoms N. The Hamiltonian matrix elements $H_{l,n;l',n'}$ can be written as,

$$\begin{aligned} H_{l,n;l',n'}(\vec{k}) &\equiv \left\langle \phi_{l,n}^{\vec{k}}(\vec{r})\middle|H\middle|\phi_{l',n'}^{\vec{k}}(\vec{r})\right\rangle \\ &= \frac{1}{N}\sum_{\vec{R},\vec{R}'} e^{i\vec{k}\cdot\left(\vec{R}'-\vec{R}+\vec{d}_{l'}-\vec{d}_l\right)}\left\langle l,n\left(\vec{r}-\vec{d}_l-\vec{R}\right)\middle|H\middle|l',n'\left(\vec{r}-\vec{d}_{l'}-\vec{R}'\right)\right\rangle \end{aligned} \qquad (5.19)$$

In equation (5.19), $\left\langle l,n\left(\vec{r}-\vec{d}_l-\vec{R}\right)\middle|H\middle|l',n'\left(\vec{r}-\vec{d}_{l'}-\vec{R}'\right)\right\rangle$ is the Hamiltonian matrix element between the atomic orbital n of the atom located at $\vec{d}_l+\vec{R}$ in layer l and the atomic orbital n' of the atom located at $\vec{d}_{l'}+\vec{R}$ in layer l'. Under the nearest neighbor approximation, $\left\langle l,n\left(\vec{r}-\vec{d}_l-\vec{R}\right)\middle|H\middle|l',n'\left(\vec{r}-\vec{d}_{l'}-\vec{R}'\right)\right\rangle$ is equal to zero unless both $l'=l$ and $\vec{R}=\vec{R}'$ in the on-site case, or, $l'-l=\pm 1$ for the nearest neighbor case. Hence, equation (5.19) is reduced to

$$H_{l,n;l',n'}(\vec{k}) = \sum_{\vec{d}_{l,l'}} e^{i\vec{k}\cdot\vec{d}_{l,l'}}\left\langle l,n(\vec{r})\middle|H\middle|l',n'\left(\vec{r}-\vec{d}_{l,l'}\right)\right\rangle \qquad (5.20)$$

where, for a given atom in layer l, $\vec{d}_{l,l'}$ runs over the nearest neighbor atoms in layer l' if $l'-l=\pm 1$. If $l'=l$, $\vec{d}_{l,l'}$ is zero and the summation in (5.20) is removed. When $l'=l$, we assume that $\left\langle l,n(\vec{r})\middle|H\middle|l',n'(\vec{r})\right\rangle$ is not zero only if $n=n'$, as in Chapter 3. When

$l'-l=\pm 1$, $\vec{d}_{l,l'}$ may take one vector value or three vector values depending on what kind of atoms are in layer l and whether $l'-l$ is positive or negative.

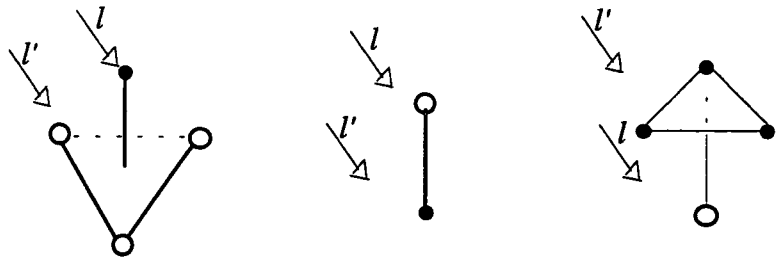

● cation of zinc ○ anion of oxygen

Figure 5.2 The possible nearest neighbor relations

Figure 5.2 above shows in the middle that an anion can be directly on top of a cation along the c-axis. This is because an anion is always sitting directly above each cation along the c-axis in the wurtzite crystal structure. However, when we view a layer of cations as sitting on top of an anion layer we get two cases. These two cases are represented by the left and right sides in figure 5.2.

The nonzero Hamiltonian matrix elements $\langle l,n(\vec{r})|H|l',n'(\vec{r}-\vec{d}_{l,l'})\rangle$ between atomic orbitals are parameterized in the way discussed in Chapter 3. The Hamiltonian matrix is obtained in terms of these parameters. After diagonalizing the Hamiltonian matrix we obtain the electronic structure of our layered surface model.

5.4 ZnO Surface Electronic Structure

In this section, we discuss the results for the unrelaxed surface first. Then, we will follow Harrison's d^{-2} rule[14] to modify that part of the Hamiltonian matrix that is related to the top layers of our layered model. Harrison's d^{-2} rule states that the

interatomic matrix elements scale from material to material quite accurately as the inverse square of the interatomic distance between atoms. We will apply this d^{-2} rule to discuss the effects of possible surface relaxation in our layered model.

5.4.1 Unrelaxed ZnO surface electronic structure

We use the same parameter values as for the bulk electronic structure in chapter three. Figure 5.3 shows the unrelaxed surface electronic band structure calculated using the layered model with 48 layers. The surface electronic structure has two parts. One part consists of surface states and surface resonances, and the other part consists of the bulk band structure. Figure 5.4 shows the electronic band structure obtained from the bulk band structure calculation described in chapter three. In order to compare with the "layered" model calculation, we calculated the energy spectra at points that project to the lines from Γ to M to K, and back to Γ when $\bar{k}_z$ is taken to be zero. For each $(\bar{k}_x, \bar{k}_y)$ on the lines from Γ to M to K, and back to Γ, we calculated the energy spectra for $\frac{L}{4}$ different $\bar{k}_z$ values evenly distributed from $-\frac{1}{2}\frac{2\pi}{c}$ to $\frac{1}{2}\frac{2\pi}{c}$. Comparing figure 5.3 with figure 5.4, we found that the bulk band structure is very well reproduced by the layered model.

Surface states and surface resonances are identified by calculating the charge density. The charge density is localized within the top layers for both surface states and surface resonances. The density decays exponentially into the bulk for surface states while for surface resonances the density does not decay exponentially. As demonstrated in chapter four, an eigenstate corresponds to a surface resonance if the

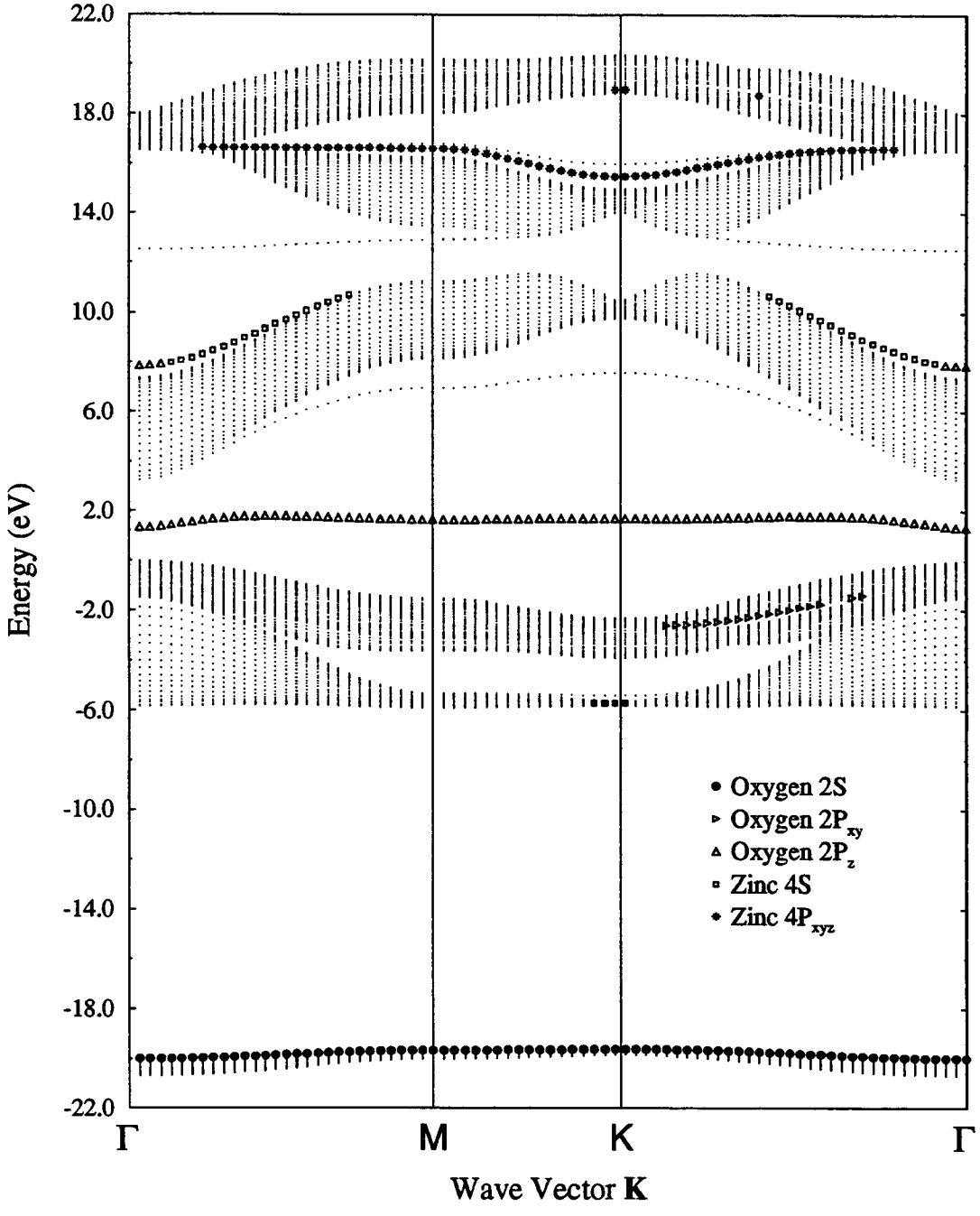

Figure 5.3 The 48 layers electronic structure of ZnO layered model without relaxation.

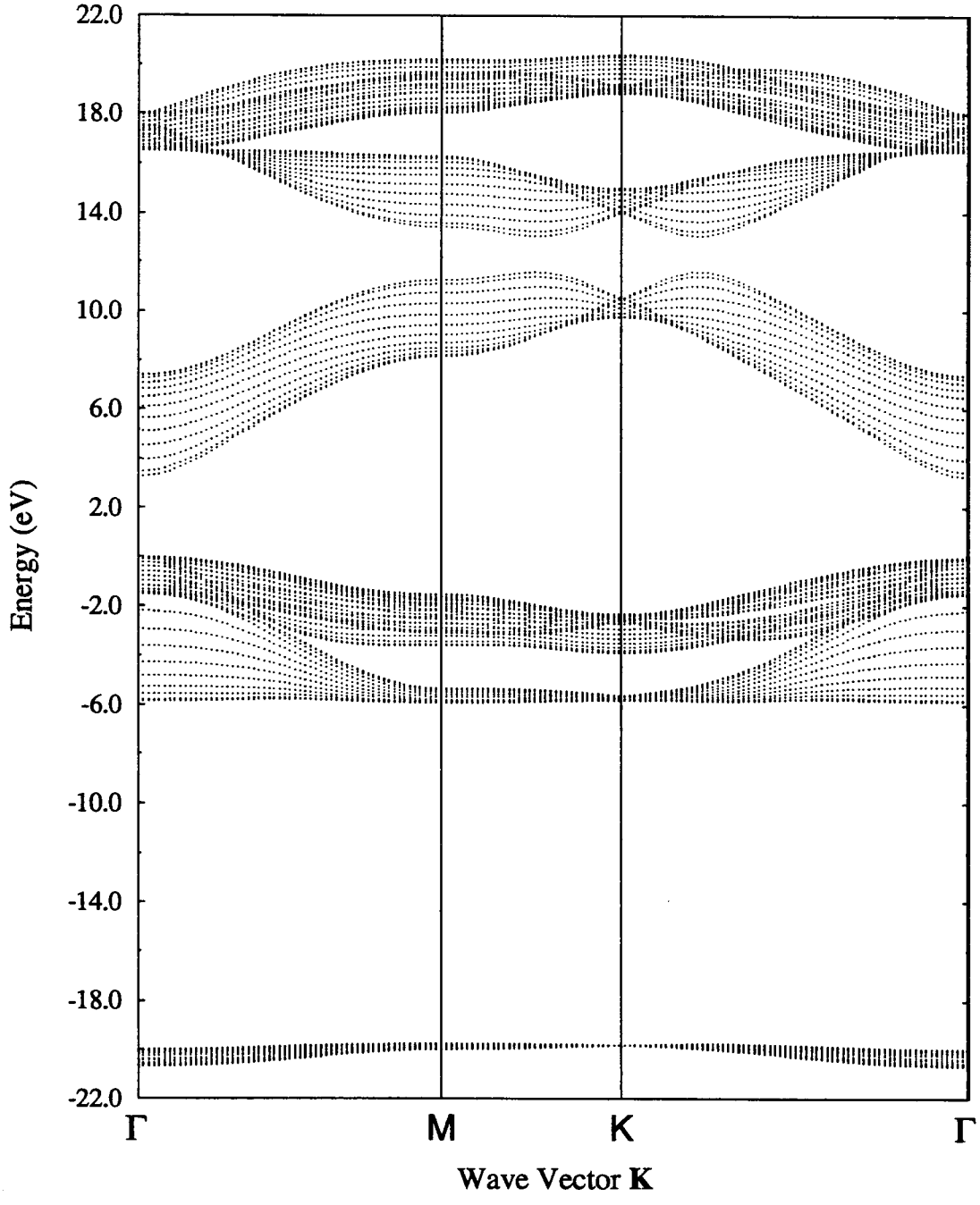

Figure 5.4 The bulk band structure of ZnO crystal with multifold $\mathbf{K}_z$ values for each two-dimensional wave vector.

eigen energy is within the bulk spectrum. It is a surface state if the eigen energy of the state is in the energy gap, larger than the upper bound, or smaller than the lower bound of the spectra at the particular $\bar{k}$ point.

The surface states near the top of the narrow, lowest valence band around -20 eV correspond to oxygen 2s states in the top oxygen layer. Above the upper valence bands but below the lowest conduction band one finds surface states mainly derived from oxygen $2p_z$ states in the top oxygen layer; these are coupled slightly to the Zn 4s and $4p$ states in the layer underneath. The surface states whose eigen energies fall between the middle and uppermost conduction bands have Zn character. These surface states, derived mainly from the states of Zn 4s character in the second layer, have a sizable admixture of top oxygen $2p_z$ and Zn $4p_z$, and small amount of top oxygen $2p_{x,y}$ and oxygen $2p_z$ in the third layer. Finally, Zn $4p_{x,y}$ derived surface states and surface resonance have a sizable mixture of top oxygen $2p$ (see figure 5.3).

5.4.2 Consequences of relaxation of the top layer

We will discuss two possible ways to relax the position of the top oxygen layer: pushing it outward or pulling it inward. The result of our calculations show that the electronic structure favors pulling it inward.

If the top layer is pushed outward about ten percent, the coupling strength between the top two layers reduces to about eighty percent using Harrison's d^{-2} rule[14]. Figure 5.5 shows the surface electronic structure when the top layer is pushed outward about ten percent. Although we find surface states of Zn $4p$ character at lower energies, they are above the lowest conduction bands. Those surface states have higher energy eigenvalues than the corresponding states in the unrelaxed structure. We can see that the surface states corresponding to the top oxygen 2s and $2p_z$ states are higher than those in the surface electronic structure of the unrelaxed case. In addition,

eigenvalues pertaining to the top oxygen $2p_{x,y}$ states jump up from the upper valence bands. Hence, the total electronic ground state energy of the system increases if the top layer is placed farther away from the Zn layer underneath.

Figure 5.6 shows the surface electronic structure when the top layer is pulled inwards about ten percent. We see that the eigenvalues of occupied surface states are pulled down when the distance between the top oxygen layer and the zinc layer underneath it decreases. Also, the eigenvalues of the top layer oxygen 2s atomiclike surface states are moved down from above the narrow lowest valence bands around -20 eV to below those bands. In addition to the lowering of the energy of the oxygen $2P_z$ surface states, oxygen $2p_{x,y}$ surface states appear, with eigenvalues in the lower part of the upper valence bands, and occupied 4s surface states appear with eigenvalues below the upper valence band.

Those zinc 4s surface states show a mixture of top layer oxygen $2p$, third layer oxygen $2P_z$ and the second layer zinc $4P_z$ states. The top layer of oxygen $2p_{x,y}$ surface states have a sizable mixture of second layer zinc $4p_{x,y}$. Relaxing the top oxygen layer closer to the zinc layer underneath is favored from an electronic energy point of view, since it results in a lower total ground state energy of the system.

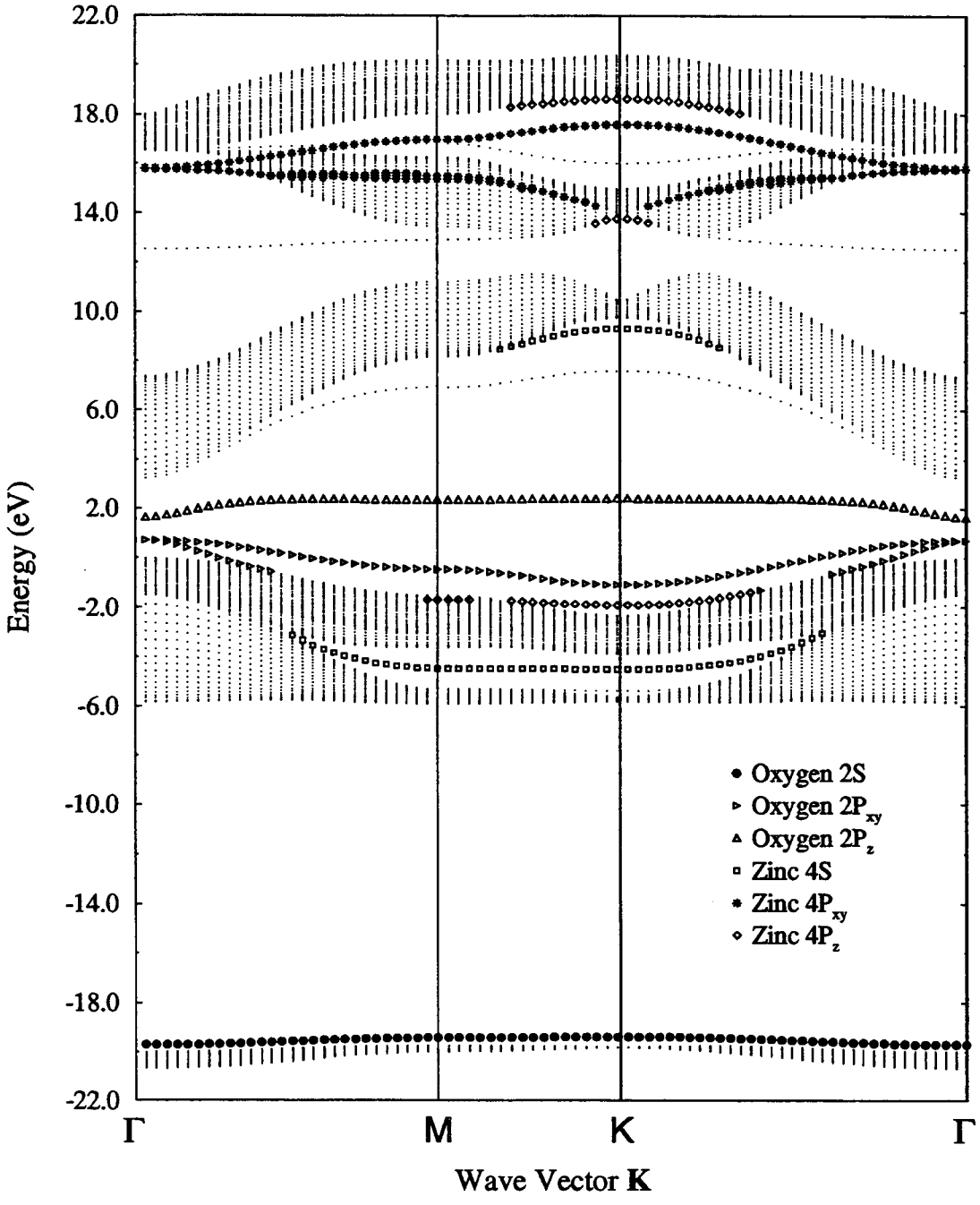

Figure 5.5 The 48 layers electronic structure of ZnO layered model with the top oxygen layer relaxed outward by 10%.

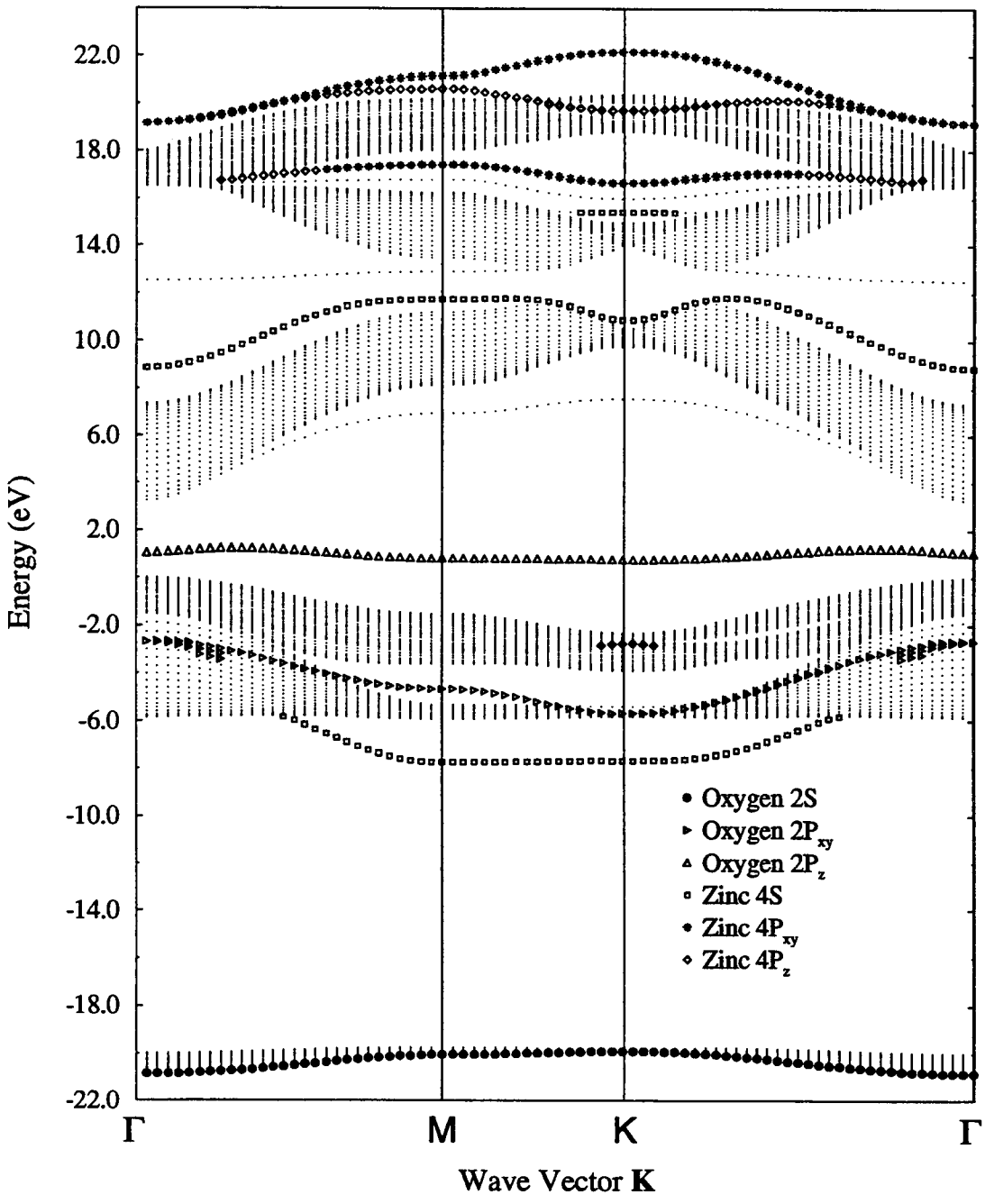

Figure 5.6 The 48 layers electronic structure of ZnO layered model with the top oxygen layer relaxed inward by 10%.

Chapter 6

Linear Optical Properties of ZnO Bulk and ZnO Surface

The linear optical property of a system is characterized by its first order susceptibility tensor $\bar{\bar{\chi}}^{(1)}$ according to the semiclassical theory of interactions between the electromagnetic fields and atomic matter. This susceptibility tensor $\bar{\bar{\chi}}^{(1)}$ of rank two is a macroscopic quantity. We obtained the formula for $\bar{\bar{\chi}}^{(1)}$ in terms of eigen energies and wave functions of the system by using the density matrix formalism in Chapter 2. We also calculated the electronic structure and wavefunctions for bulk ZnO in Chapter 3 and for the layered model of ZnO in Chapter 5 respectively. In this chapter, we present the results of our calculations for the density of states(DOS), the joint density of states(JDOS), and the susceptibility tensor $\bar{\bar{\chi}}^{(1)}$ for both bulk and surface of ZnO.

6.1 The Susceptibility Tensor $\bar{\bar{\chi}}^{(1)}$

$\bar{\bar{\chi}}^{(1)}$ has complex values. Its real part is related to its imaginary part by the Kramers-Kronig relation:

$$\mathrm{Re}\,\bar{\bar{\chi}}^{(1)}(\omega) = \frac{2}{\pi} P \int_0^{\infty} \frac{\omega' \,\mathrm{Im}\,\bar{\bar{\chi}}^{(1)}(\omega')}{\omega'^{2} - \omega^{2}} d\omega' \qquad (6.1)$$

where P means principal value, Re means real part, and Im means imaginary part. We calculate the imaginary part of $\bar{\bar{\chi}}^{(1)}$ and obtain the real part of $\bar{\bar{\chi}}^{(1)}$ from the imaginary part using the Kramers-Kronig relation (6.1).

6.1.1 The imaginary parts of $\bar{\bar{\chi}}^{(1)}$

From Chapter 2, we know that the linear polarization is

$$\vec{P}_a^{(1)}(t) = \sum_{b,\alpha} \bar{\bar{\chi}}_{ab}^{(1)}(\omega_\alpha)\vec{E}_b^{\alpha} e^{-i\omega_\alpha t} \tag{6.2}$$

where the susceptibility tensor $\bar{\bar{\chi}}_{ab}^{(1)}(\omega_\alpha)$ is written from equations (2.72) and (2.65) as

$$\bar{\bar{\chi}}_{ab}^{(1)}(\omega_\alpha) = -\sum_{i,j}\left[\frac{e}{m\omega_\alpha}\right]^2 \frac{f_{ij}^{(0)}}{\hbar(\omega_\alpha - \omega_{ji})} p_{ij}^a p_{ji}^b \tag{6.3}$$

The notation is the same as explained in Chapter 2. If we introduce the perturbation adiabatically, we can write $\bar{\bar{\chi}}_{ab}^{(1)}(\omega)$ as

$$\bar{\bar{\chi}}_{ab}^{(1)}(\omega) = -\sum_{i,j}\left[\frac{e}{m\omega}\right]^2 \frac{f_{ij}^{(0)}}{\hbar\omega - E_{ji} + i\varepsilon} p_{ij}^a p_{ji}^b \tag{6.4}$$

where $E_{ji} = \hbar\omega_{ji}$. Substituting $p = -i\hbar\nabla$ and the following identity,

$$\lim_{\varepsilon\to 0}\frac{1}{x + i\varepsilon} = P\left(\frac{1}{x}\right) - i\pi\delta(x) \tag{6.5}$$

where P indicates principle value, into equation (6.4) and writing $\bar{\bar{\chi}}_{ab}^{(1)}(\omega)$ as

$$\bar{\bar{\chi}}_{ab}^{(1)}(\omega) = \bar{\bar{\chi}}_{ab}^{(1)'}(\omega) + i\bar{\bar{\chi}}_{ab}^{(1)''}(\omega), \tag{6.6}$$

we obtain the imaginary part $\bar{\bar{\chi}}_{ab}^{(1)''}(\omega)$

$$\bar{\bar{\chi}}_{ab}^{(1)''}(\omega) = -\pi\sum_{i,j}\left[\frac{e\hbar}{m\omega}\right]^2 \mathrm{Re}\left[\nabla_{ij}^a \nabla_{ji}^b\right] f_{ij}^{(0)}\delta(\hbar\omega - E_{ji}) \tag{6.7}$$

where Re means the real part; i and j run over all single-particle electronic states. In our band structure calculation, i(and j) is replaced by n and $\vec{k}$; n is the band index, $\vec{k}$ is a reciprocal wave vector. When i runs over all the single-particle states, its corresponding n and $\vec{k}$ will run over every band and every possible wave vector. Therefore, we obtain from equation (6.7) the following:

$$\bar{\bar{\chi}}_{ab}^{(1)''}(\omega) = -\pi\sum_{n\vec{k};n'\vec{k}'}\left[\frac{e\hbar}{m\omega}\right]^2 \mathrm{Re}\left[\nabla_{n\vec{k};n'\vec{k}'}^a \nabla_{n'\vec{k}';n\vec{k}}^b\right] f_{n\vec{k};n'\vec{k}'}^{(0)}\delta(\hbar\omega - E_{n'\vec{k}';n\vec{k}}) \tag{6.8}$$

In section 6.1.3, we will derive the following important relation:

$$\nabla^{b}_{n\vec{k},n'\vec{k}'} \propto \delta_{\vec{k}\vec{k}'} \tag{6.9}$$

If we put relation (6.9) in equation (6.8) we obtain

$$\bar{\bar{\chi}}^{(1)}_{ab}(\omega) = \sum_{nn'\vec{k}} F_{nn'}(\vec{k}) f^{(0)}_{nn'} \delta(\hbar\omega - E_{n'n}) \tag{6.10}$$

where

$$F_{nn'}(\vec{k}) = -\pi\left[\frac{e\hbar}{m\omega}\right]^2 \mathrm{Re}\left[\nabla^{a}_{n\vec{k};n'\vec{k}} \nabla^{b}_{n'\vec{k};n\vec{k}}\right]. \tag{6.11}$$

6.1.2 From summation to integration

The summation over all allowed values of $\vec{k}$ in equation (6.10) is carried out as follows:

$$\sum_{\vec{k}} \Rightarrow \frac{V}{(2\pi)^3} \sum_{\Delta\vec{k}} \Delta\vec{k} \tag{6.12}$$

In the limit $V \to \infty$, we have $\Delta\vec{k} \to 0$ and the summation approaches an integration. For the bulk calculation, $\vec{k}$ space is three dimensional and we write

$$\bar{\bar{\chi}}^{(1)}_{ab}(\omega) = 2 \cdot \frac{V}{(2\pi)^3} \int d^3\vec{k} \sum_{nn'} F_{nn'}(\vec{k}) f^{(0)}_{nn'} \delta(\hbar\omega - E_{n'n}) \tag{6.13}$$

where V is the volume of the ZnO crystal and the integral is over any primitive cell of the three dimensional reciprocal space. For our layered model, the $\vec{k}$ space is two dimensional and we write

$$\bar{\bar{\chi}}^{(1)}_{ab}(\omega) = 2 \cdot \frac{A}{(2\pi)^2} \int d^2\vec{k} \sum_{nn'} F_{nn'}(\vec{k}) f^{(0)}_{nn'} \delta(\hbar\omega - E_{n'n}) \tag{6.14}$$

where A is the area of one layer and the integral is over a primitive cell of the two dimensional reciprocal space. If we assume that the layered model contains L layers,

then its volume is $V = \frac{L}{4} c \times A$, where c is the height of a ZnO crystal unit cell. So, equation (6.14) can be written:

$$\bar{\bar{\chi}}^{(1)\prime\prime}_{ab}(\omega) = 8 \cdot \frac{V}{(2\pi)^2 Lc} \int d^2\bar{k} \sum_{nn'} F_{nn'}(\bar{k}) f^{(0)}_{nn'} \delta(\hbar\omega - E_{n'n}) \qquad (6.15)$$

In the rest of this thesis, we calculate the susceptibility per unit volume.

6.1.3 The matrix element $\nabla^b_{n\bar{k},n'\bar{k}'}$

The matrix element $\nabla^b_{n\bar{k},n'\bar{k}'}$ in equation (6.11) is defined as

$$\nabla^b_{n\bar{k},n'\bar{k}'} = \left\langle \Psi^n_{\bar{k}} \middle| \nabla^b \middle| \Psi^{n'}_{\bar{k}'} \right\rangle \qquad (6.16)$$

where $\left|\Psi^n_{\bar{k}}\right\rangle$ is a single-particle wavefunction with band index n and wave vector $\bar{k}$. From equations (3.4) and (3.7), we write $\left|\Psi^n_{\bar{k}}\right\rangle$ as follows:

$$\left|\Psi^n_{\bar{k}}\right\rangle = \sum_{a,o} c^n_{a,o} \left|\phi^{\bar{k}}_{a,o}\right\rangle$$

$$= \frac{1}{\sqrt{N}} \sum_{a,o} c^n_{a,o} \sum_{\bar{R}} e^{i\bar{k}\cdot(\bar{R}+\bar{d}_a)} \left| a, o\left(\bar{r} - \left(\bar{R} + \bar{d}_a\right)\right)\right\rangle \qquad (6.17)$$

where $\left|a, o\left(\bar{r} - \left(\bar{R} + \bar{d}_a\right)\right)\right\rangle$ is the wavefunction of the atomic orbital, $\bar{R}$ runs over all the lattice vectors in the direct Bravais lattice. The direct Bravais lattice is simple hexagonal for our bulk calculation and it is a triangular net for our layered model calculation. N is the total number of unit cells in the bulk case while it is the total number of atoms in a single layer in the layered model case. $c^n_{a,o}$ is the admixture coefficient and it is also a function of the wave vector $\bar{k}$. The index a of $c^n_{a,o}$ represents one of the four basis atoms in a unit cell for the bulk case, and for the layered model case it represents the atom in a specific layer.

Substituting equation (6.17) into equation (6.16) we obtain

$$\nabla^{b}_{n\vec{k},n'\vec{k}'} = \frac{1}{N}\sum_{a,o}\sum_{a',o'} c^{n}_{a,o}{}^{*} c^{n'}_{a',o'} \sum_{\vec{R},\vec{R}'} e^{i\vec{k}\cdot(\vec{R}+\vec{d}_a)-i\vec{k}'\cdot(\vec{R}'+\vec{d}_{a'})} \left\langle a,o\left(\vec{r}-\left(\vec{R}+\vec{d}_a\right)\right)\middle|\nabla^{b}\middle|a',o'\left(\vec{r}-\left(\vec{R}'+\vec{d}_{a'}\right)\right)\right\rangle \tag{6.18}$$

In our calculation, we make the on site approximation. That is to assume

$$\left\langle a,o\left(\vec{r}-\left(\vec{R}+\vec{d}_a\right)\right)\middle|\nabla^{b}\middle|a',o'\left(\vec{r}-\left(\vec{R}'+\vec{d}_{a'}\right)\right)\right\rangle = \langle a,o(\vec{r})|\nabla^{b}|a',o'\rangle\delta_{aa'}\delta_{\vec{R}\vec{R}'} \tag{6.19}$$

After substituting (6.19) in (6.18) and summing over a', $\vec{R}$, and $\vec{R}'$, we obtain

$$\nabla^{b}_{n\vec{k},n'\vec{k}'} = \sum_{a,o,o'} c^{n}_{a,o}{}^{*} c^{n'}_{a,o'} \langle a,o(\vec{r})|\nabla^{b}|a,o'(\vec{r})\rangle\delta_{\vec{k}\vec{k}'} \tag{6.20}$$

The integral of $\langle a,o(\vec{r})|\nabla^{b}|a,o'(\vec{r})\rangle$ in equation (6.20) is nozero only if one of o and o' is the s-orbital while the other is p_b orbital; b can be x, y, and z. We use a program written by Dr. Jansen to obtain the wave functions of the atomic orbitals. Then, the integral of $\langle a,o(\vec{r})|\nabla^{b}|a,o'(\vec{r})\rangle$ is performed for atom Zn and atom O and the results are:

$$\langle Zn,p_x(\vec{r})|\frac{\partial}{\partial x}|Zn,s(\vec{r})\rangle = -1.04$$

$$\langle O,p_x(\vec{r})|\frac{\partial}{\partial x}|O,s(\vec{r})\rangle = -1.001$$

Combining equation (6.20) with either equation (6.13) or equation (6.15), we can calculate the imaginary parts of the first order susceptibility for the bulk and layered model respectively.

6.2 DOS, JDOS, and $\bar{\bar{\chi}}^{(1)}$ of ZnO Bulk

The imaginary part of the first order ZnO bulk susceptibility is given by equations (6.13), (6.11), and (6.20),

$$\bar{\bar{\chi}}^{(1),\prime\prime}_{ab}(\omega) = -V\int d^3\vec{k}\sum_{nn'}\left(\frac{e\hbar^2}{2\pi m\hbar\omega}\right)^2 \mathrm{Re}\left[\nabla^{a}_{nn'}\nabla^{b}_{n'n}\right]\delta(\hbar\omega - E_{n'n}) \tag{6.21}$$

where n' runs over the unoccupied conduction bands and n runs over the occupied valence bands. Here, we assume zero temperature. To facilitate the computation we use the symmetry in the x-y plane of ZnO to convert the integral in (6.21) to one over only an irreducible segment of the Brillouin zone(BZ).

We use the linear analytic tetrahedron method[21] to evaluate the integral

$$\bar{\bar{\chi}}^{(1),\prime\prime}_{ab}(\omega) = -\int_{IBZ} d^3\vec{k} \sum_{nn'} \left(\frac{e\hbar^2}{2\pi m\hbar\omega}\right)^2 \mathrm{Re}\left[\nabla^a_{nn'}\nabla^b_{n'n}\right]\delta(\hbar\omega - E_{n'n}) \qquad (6.22)$$

where IBZ stands for an irreducible segment of the BZ. To illustrate the method, we explain how the density of states and joint density of states are calculated.

6.2.1 Density of states and joint density of states

The density of states per unit volume $g_n(\varepsilon)$ for band n is defined as:

$$g_n(\varepsilon) = \frac{2}{(2\pi)^3}\int d^3\vec{k}\,\delta\left(\varepsilon - \varepsilon_n(\vec{k})\right) \qquad (6.23)$$

where $\varepsilon_n(\vec{k})$ is the band energy function and the integral is over a primitive cell in $\vec{k}$ space. Since $\varepsilon = \varepsilon_n(\vec{k})$ represents a surface $S_n(\varepsilon)$, we convert the integral of equation (6.23) to an integral of

$$g_n(\varepsilon) = \frac{2}{(2\pi)^3}\int_{S_n(\varepsilon)} \frac{ds}{\left|\nabla\varepsilon_n(\vec{k})\right|} \qquad (6.24)$$

where the integral is over a $\vec{k}$ space surface inside a primitive cell on which the band energies are the same for every wave vector $\vec{k}$. $\left|\nabla\varepsilon_n(\vec{k})\right|$ is the absolute value of the band energy gradient. The key to doing the integral numerically is to break the surface $S_n(\varepsilon)$ into many small pieces, with each small piece treated as a plane approximately. This is done by dividing the primitive cell into many tetrahedrons. The contributions $\Delta g_n(\varepsilon)$ from each tetrahedron are calculated and added to give $g_n(\varepsilon)$.

Each tetrahedron has four vertices. We calculate the $\varepsilon_n(\vec{k})$ values at these four vertices and we obtain $\varepsilon_n(\vec{k})$ values anywhere else inside the tetrahedron by interpolating linearly using the values obtained at the vertices. We find that if a tetrahedron contains a piece of the $\varepsilon = \varepsilon_n(\vec{k})$ surface, it may be either a triangle or a quadrilateral.

We denote values of the $\varepsilon_n(\vec{k})$ at four vertices by ε_1, ε_2, ε_3, ε_4 and assume that:

$$\varepsilon_1 \geq \varepsilon_2 \geq \varepsilon_3 \geq \varepsilon_4 .$$

Then, the contribution $\Delta g_n(\varepsilon)$ from the tetrahedron is as follows:

$$\Delta g_n(\varepsilon) = \begin{cases} \frac{1}{2} v f_0 & \varepsilon_4 \leq \varepsilon < \varepsilon_3 \\ \frac{1}{2} v f_1 & \varepsilon_3 \leq \varepsilon < \varepsilon_2 \\ \frac{1}{2} v f_2 & \varepsilon_2 \leq \varepsilon < \varepsilon_1 \\ 0 & \varepsilon < \varepsilon_4, \ or \ \varepsilon \geq \varepsilon_1 \end{cases}$$

where v is the volume of the tetrahedron multiplied by six, and

$$f_0 = \frac{(\varepsilon - \varepsilon_4)^2}{(\varepsilon_1 - \varepsilon_4)(\varepsilon_2 - \varepsilon_4)(\varepsilon_3 - \varepsilon_4)}$$

$$f_1 = \left(\frac{(\varepsilon - \varepsilon_3)(\varepsilon_1 - \varepsilon)}{(\varepsilon_1 - \varepsilon_3)(\varepsilon_2 - \varepsilon_3)} + \frac{(\varepsilon_2 - \varepsilon)(\varepsilon - \varepsilon_4)}{(\varepsilon_2 - \varepsilon_3)(\varepsilon_2 - \varepsilon_4)} \right) \frac{1}{(\varepsilon_1 - \varepsilon_4)}$$

$$f_2 = \frac{(\varepsilon - \varepsilon_1)^2}{(\varepsilon_1 - \varepsilon_4)(\varepsilon_1 - \varepsilon_3)(\varepsilon_1 - \varepsilon_2)}$$

Figure (6.1) shows the density of states for zinc oxide bulk. The joint density of states $G_{n'n}(\varepsilon)$ is defined as $G_{n'n}(\varepsilon) = \frac{2}{(2\pi)^3} \int d^3\vec{k} \delta\left(\varepsilon - \varepsilon_{n'n}(\vec{k})\right)$ where n' and n represent conduction bands and valence bands respectively, $\varepsilon_{n'n}(\vec{k})$ is the eigen energy difference

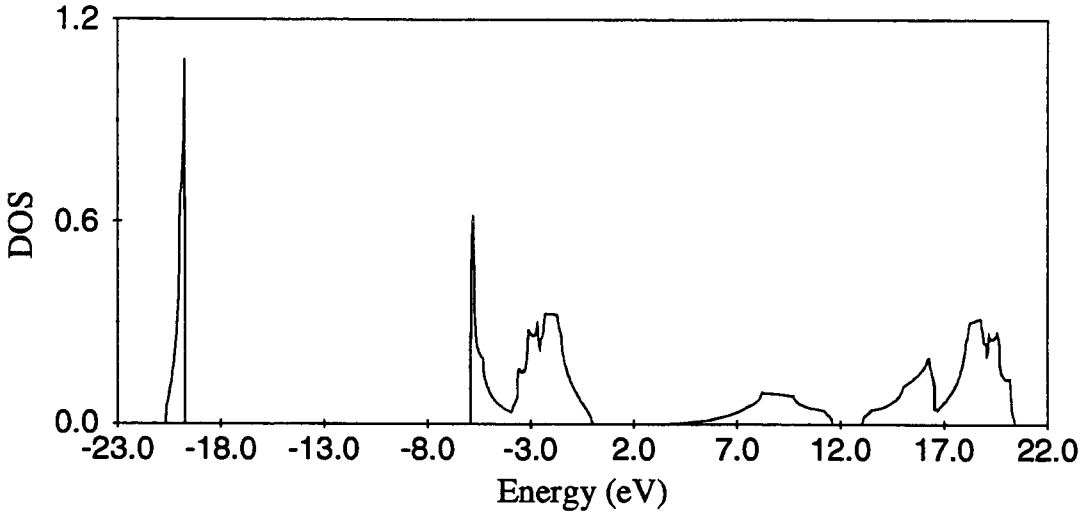

Figure 6.1 Density of states for ZnO bulk.

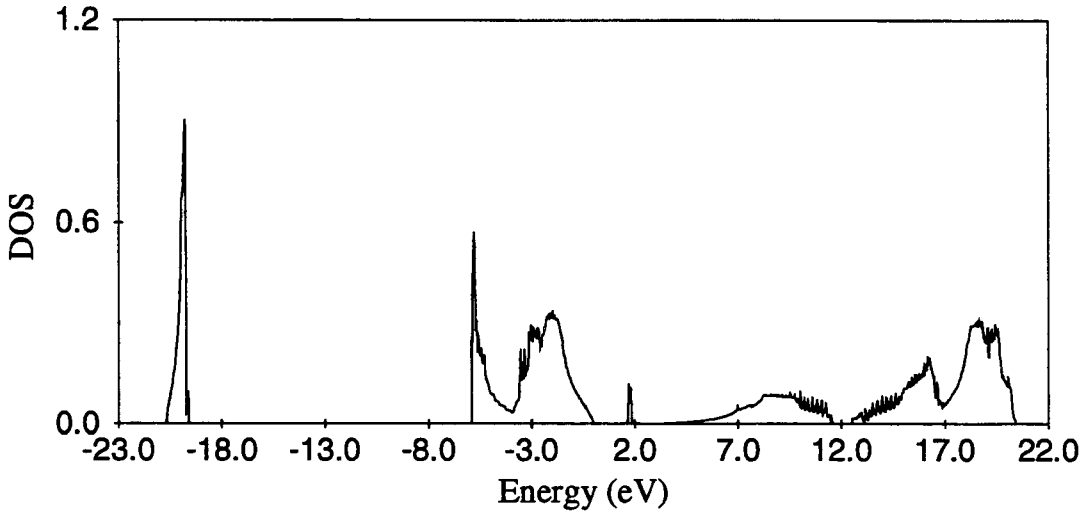

Figure 6.2 Density of states for ZnO layered model of 48 layers.

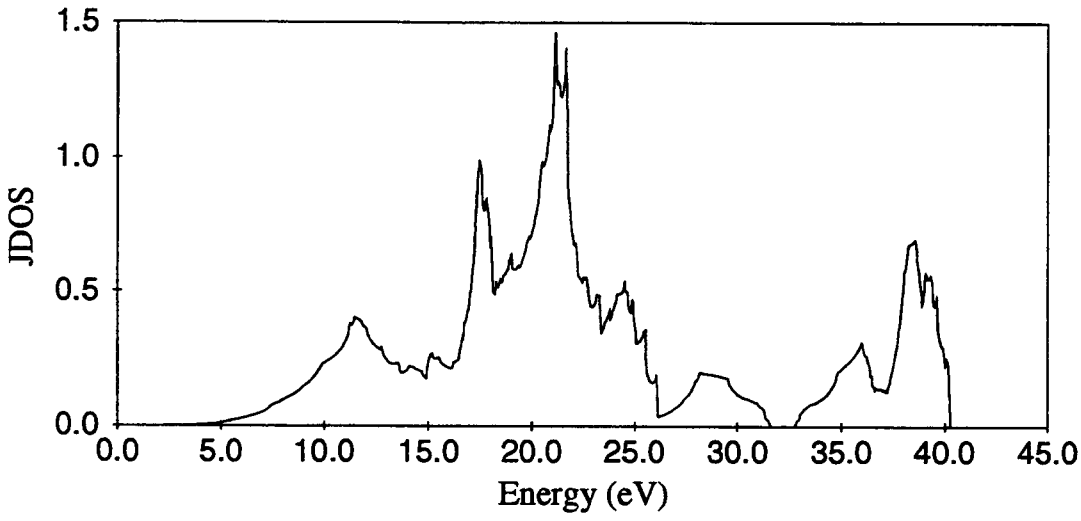

Figure 6.3 Joint density of states for ZnO bulk.

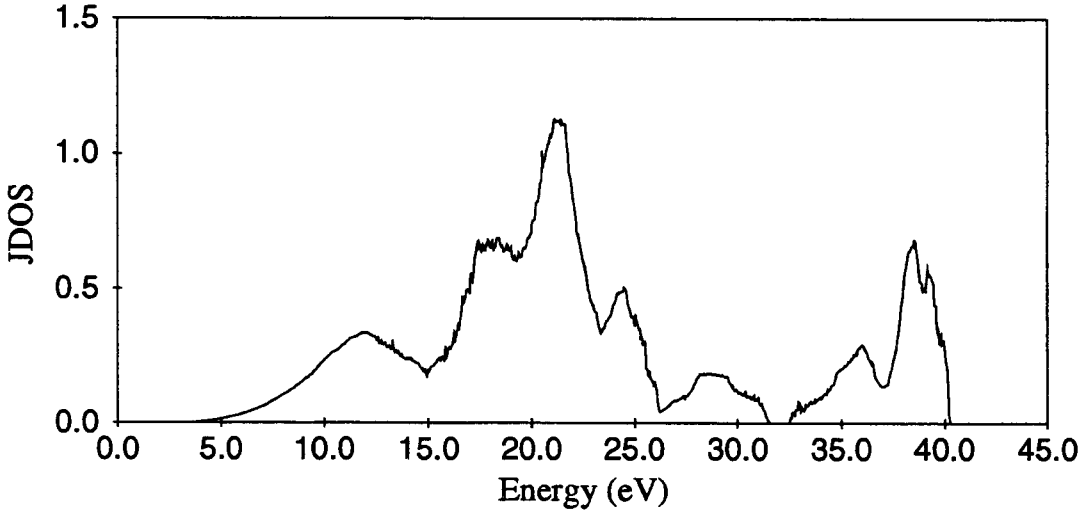

Figure 6.4 Joint density of states for ZnO layered model of 48 layers.

between the conduction band n' and the valence band n at wave vector $\vec{k}$. The joint density of states of the bulk ZnO crystal is shown in figure (6.3).

6.2.2 The first order susceptibility of ZnO bulk

The integral for $\bar{\bar{\chi}}^{(1)''}_{ab}(\omega)$ in equation (6.22) differs from equation (6.23) by an additional function. We treat the additional function $\mathrm{Re}\left[\nabla^{a}_{nn'}\nabla^{b}_{n'n}\right]$ as constant on the surface found inside each tetrahedron. The constant value is obtained by evaluating the function at an arbitrary wave vector inside the tetrahedron.

We divide the IBZ into 400,000 tetrahedrons. The imaginary part $\bar{\bar{\chi}}^{(1)''}_{ab}(\omega)$ of the first order susceptibility is shown in figure (6.5). For our first order susceptibility calculation, the energy resolution is $0.04\ eV$. The real parts are obtained using the Kramers-Kronig relation and are presented in figure (6.6). Notice that there are only two components shown in figures (6.5) and (6.6). This is because $\bar{\bar{\chi}}^{(1)}$ of ZnO has only two independent nonzero elements: $\bar{\bar{\chi}}^{(1)}_{zz}$ and $\bar{\bar{\chi}}^{(1)}_{xx} = \bar{\bar{\chi}}^{(1)}_{yy}$ on the diagonal. We calculated the off-diagonal components and they were found to be zero as they should due to the symmetry of ZnO. From $\bar{\bar{\chi}}^{(1)}$ we calculated the energy loss function and the results are shown in figure (6.7).

6.3 DOS, JDOS, and $\bar{\bar{\chi}}^{(1)}$ of Layered Model ZnO

Similar to the ZnO bulk, the imaginary part of the first order layered model ZnO susceptibility is given by equations (6.15), (6.11), and (6.20):

$$\bar{\bar{\chi}}^{(1)''}_{ab}(\omega) = -\frac{8\pi}{Lc}\int d^2\vec{k}\sum_{nn'}\left(\frac{e\hbar^2}{2\pi m\hbar\omega}\right)^2 \mathrm{Re}\left[\nabla^{a}_{nn'}\nabla^{b}_{n'n}\right]\delta(\hbar\omega - E_{n'n}) \qquad (6.25)$$

where n' runs over the unoccupied surface states, surface resonances, and conduction

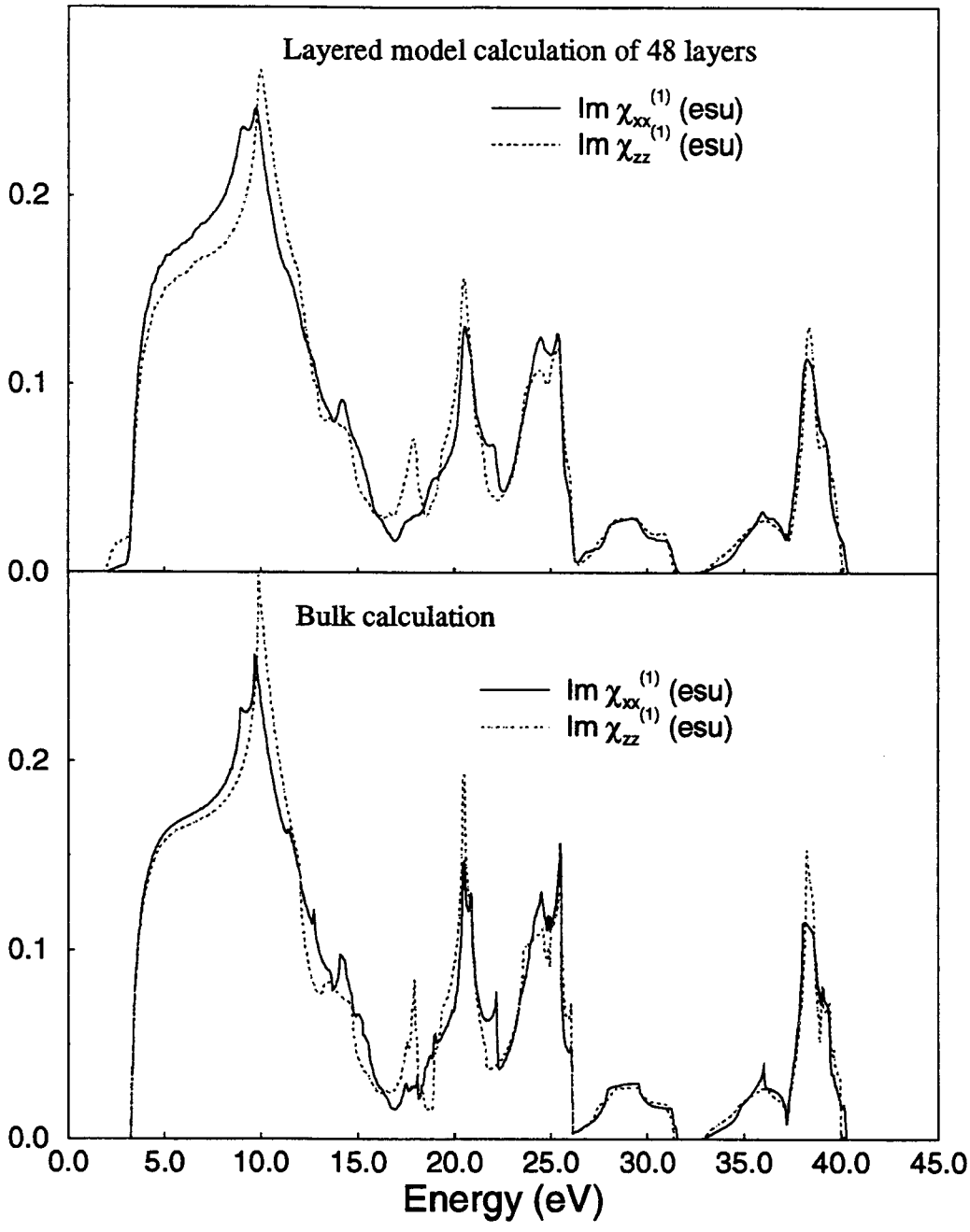

Figure 6.5 Imaginary part of the 1st order susceptibilities.

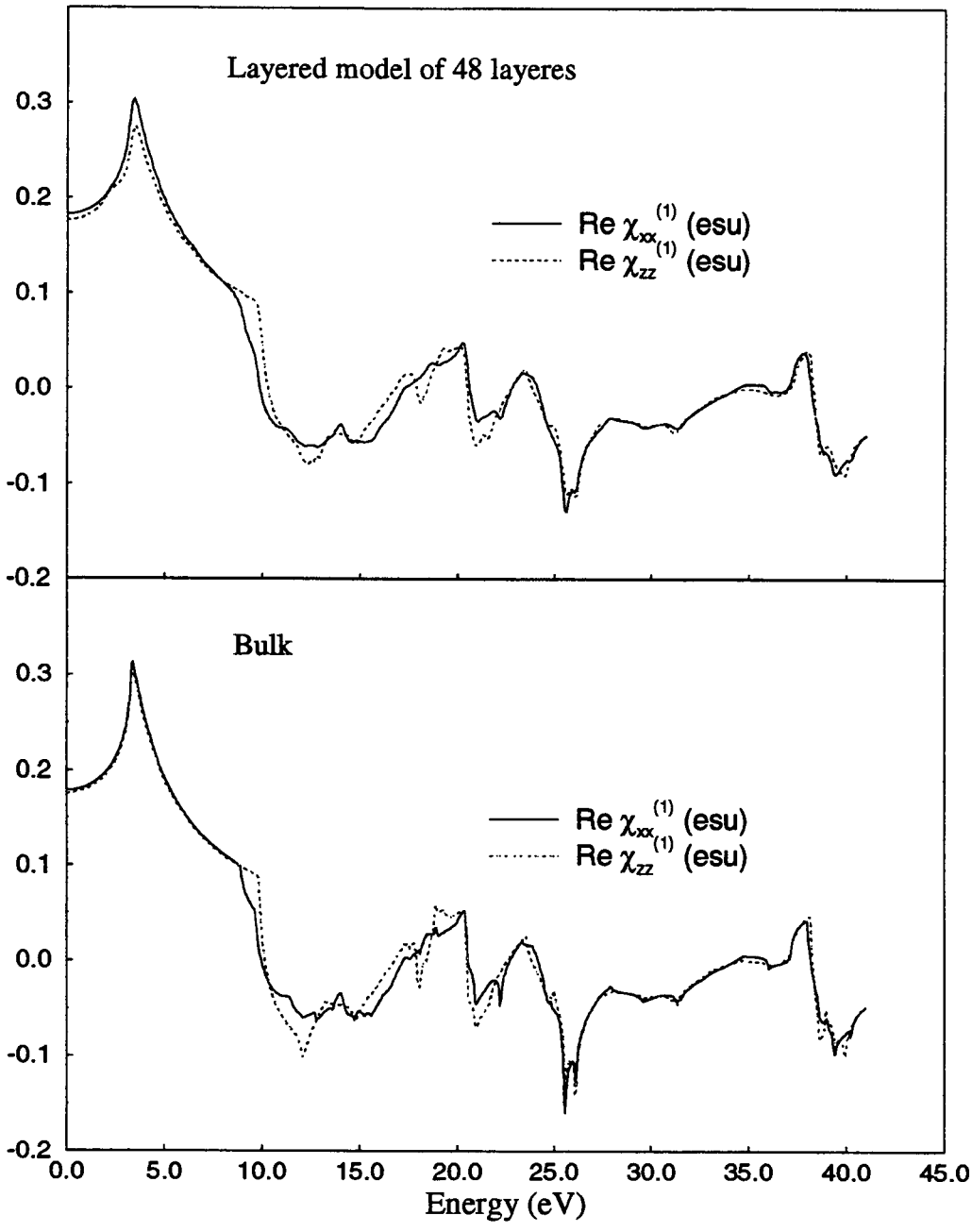

Figure 6.6 Real part of the 1st order susceptibilities.

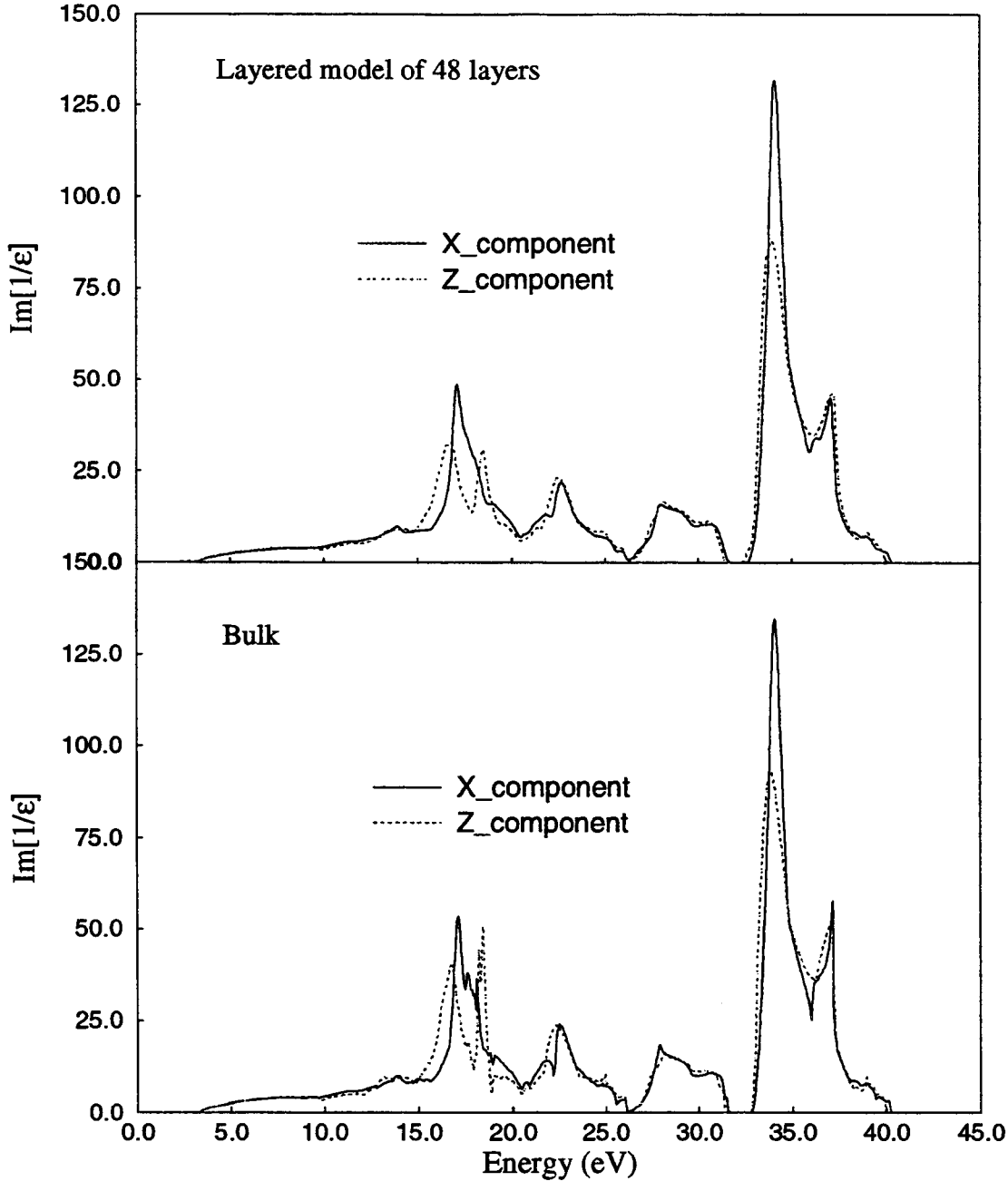

Figure 6.7 The energy loss functions Im[1/ε].

bands; n runs over the occupied surface states, surface resonances, and valence bands. The integral in equation (6.25) is over a primitive cell in two dimensional $\vec{k}$ space.

In analogy to the linear analytic tetrahedron method in the 3D integration, we use the linear analytic triangle method to perform the integration in equation (6.25). To illustrate the linear analytic triangle method, we describe how the density of states is calculated.

6.3.1 The density of states and joint density of states

In 2D $\vec{k}$ space, the density of states is defined as

$$g_n(\varepsilon) = \frac{2}{(2\pi)^2} \int d^2\vec{k}\,\delta\left(\varepsilon - \varepsilon_n(\vec{k})\right) \qquad (6.26)$$

where $\varepsilon_n(\vec{k})$ is the band energy function and the integral is over a primitive cell in 2D $\vec{k}$ space. Since $\varepsilon = \varepsilon_n(\vec{k})$ represents a curve $\ell_n(\varepsilon)$ in the 2D $\vec{k}$ space, we convert the integral of equation (6.23) to an integral of the form:

$$g_n(\varepsilon) = \frac{2}{(2\pi)^2} \int_{\ell_n(\varepsilon)} \frac{dl}{\left|\nabla\varepsilon_n(\vec{k})\right|} \qquad (6.27)$$

where the integral is over a curve which is inside the primitive cell and on which the band energies are the same for every wave vector $\vec{k}$. $\left|\nabla\varepsilon_n(\vec{k})\right|$ is the absolute value of the band energy gradient. The integral is calculated numerically by breaking the curve $\ell_n(\varepsilon)$ into many small segments, with each small segment approximately treated as a straight line. This is done by dividing the primitive cell into many triangles. The contribution $\Delta g_n(\varepsilon)$ from each triangle is calculated and added to give $g_n(\varepsilon)$.

Each triangle has three vertices. We calculate $\varepsilon_n(\vec{k})$ values at these three vertices and we obtain the values of $\varepsilon_n(\vec{k})$ anywhere else inside the triangle by

interpolating linearly using the values at the vertices. So, if a triangle contains a segment of the curve $\varepsilon = \varepsilon_n(\bar{k})$ this segment will be a straight line.

Let's denote the values of $\varepsilon_n(\bar{k})$ at the three vertices by ε_1, ε_2, ε_3 respectively and assume that:

$$\varepsilon_1 \le \varepsilon_2 \le \varepsilon_3 \ .$$

Then, the contribution $\Delta g_n(\varepsilon)$ from the triangle is found to be:

$$\Delta g_n(\varepsilon) = \begin{cases} \dfrac{2(\varepsilon - \varepsilon_1)}{(\varepsilon_3 - \varepsilon_1)(\varepsilon_2 - \varepsilon_1)} S_{\bar{k}_1\bar{k}_2\bar{k}_3} & \varepsilon_1 < \varepsilon \le \varepsilon_2 \\ \dfrac{2(\varepsilon_3 - \varepsilon)}{(\varepsilon_3 - \varepsilon_1)(\varepsilon_3 - \varepsilon_2)} S_{\bar{k}_1\bar{k}_2\bar{k}_3} & \varepsilon_2 < \varepsilon \le \varepsilon_3 \\ 0 & \varepsilon \le \varepsilon_1 \quad \text{or} \quad \varepsilon \ge \varepsilon_3 \end{cases}$$

where $S_{\bar{k}_1\bar{k}_2\bar{k}_3}$ is the area of the triangle in the 2D $\bar{k}$ space.

We calculated the density of states for our ZnO layered model with 48 layers. The results are shown in figure (6.2). Comparing the DOS of ZnO bulk in figure (6.1) with the DOS of the ZnO layered model in figure (6.2), we find that they are very similar. This similarity is expected since the electronic structure of the layered model consists of the electronic structure of the bulk and the surface states, and the number of surface states is much smaller than the number of bulk-like states. The number of surface states do not change when we increase the number of layers in our layered model. Figure (6.4) shows the joint density of states for our ZnO layered model. Again, it is very similar to the joint density of states in figure (6.3).

6.3.2 The first order susceptibility of ZnO layered model

The integral for $\bar{\bar{\chi}}^{(1)''}_{ab}(\omega)$ in equation (6.25) differs from equation (6.26) by an additional function. We treat the additional function as constant on the line segment inside each triangle in the 2D $\vec{k}$ space. The constant value is obtained by evaluating and averaging the function values at the three vertices of the triangle.

We divide the IBZ into 3,000 triangles and the calculated imaginary parts $\bar{\bar{\chi}}^{(1)''}_{ab}(\omega)$ of the first order susceptibility for our layered model of 48 layers are shown together with the bulk results in figure (6.5). The real parts and the energy loss functions are calculated from the imaginary parts. They are also presented together with the bulk results in figures (6.6) and (6.7).

6.4 Results and Discussion

We plot $\bar{\bar{\chi}}^{(1)}_{xx}$ and $\bar{\bar{\chi}}^{(1)}_{zz}$ on the same graph in figures (6.5) and (6.6) so that the polarization dependence is clearly shown. In figures (6.8) and (6.9), we compare the results of the ZnO bulk calculation with the layered model calculation. As one can see from the figures, there are small differences between the crystal bulk calculation and the layered model calculation. This tells us that the linear response of ZnO to electronmagnetic fields is a bulk feature and the surface effects can be safely ignored. We will see in next chapter, however, that the surface plays a significant role in the second harmonic response of zinc oxide.

For the first order susceptibility, the main difference between the bulk and the layered model lies from 2 eV to 3.3 eV in the photon energy. The nonzero values of the imaginary parts of both $\bar{\bar{\chi}}^{(1)}_{xx}$ and $\bar{\bar{\chi}}^{(1)}_{zz}$ for the layered model in this range are pure surface features. However, this pure surface feature is insignificant because the values

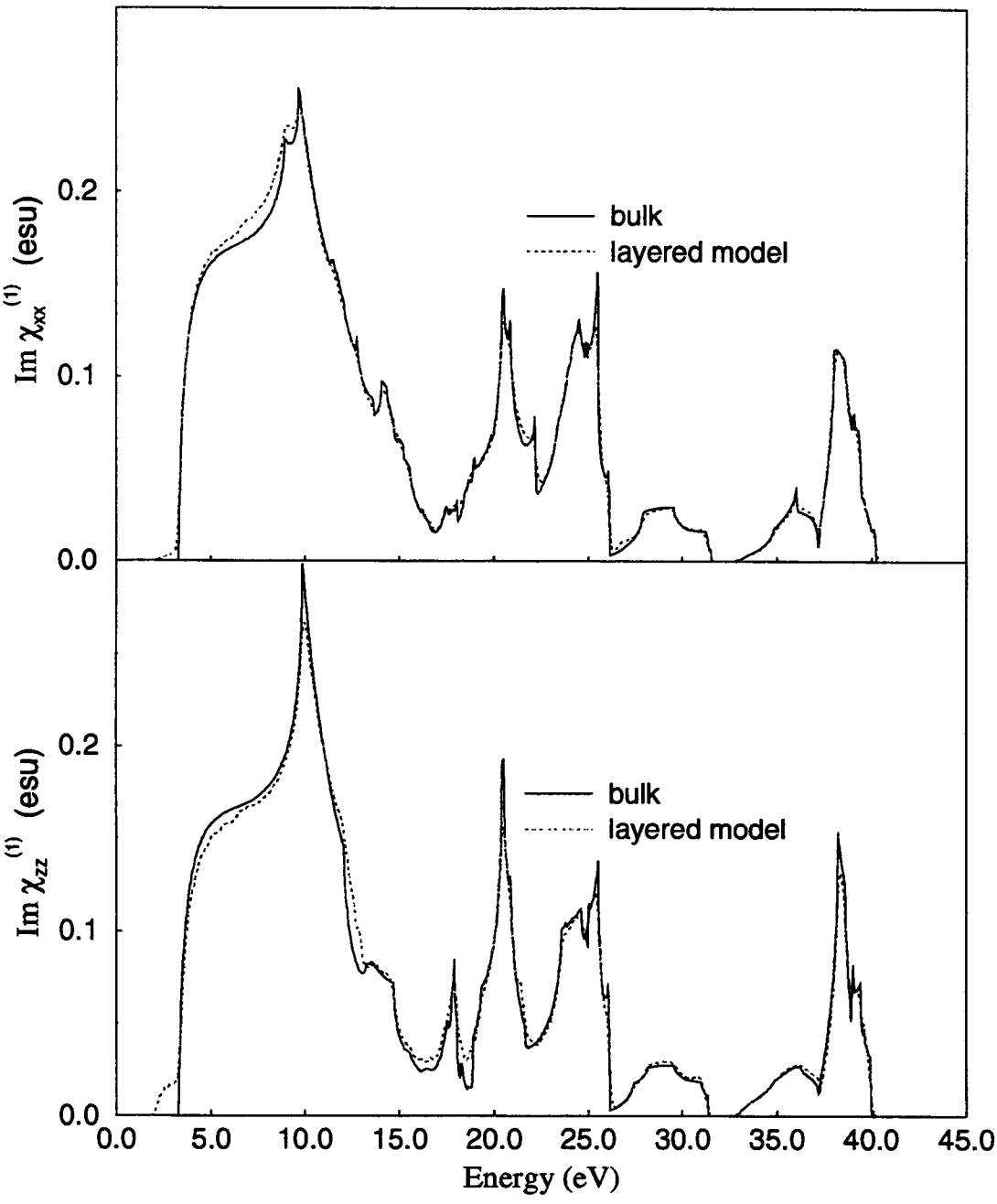

Figure 6.8 Comparison of the imaginary part of the 1st order susceptibilities for the bulk and the layered model of 48 layers.

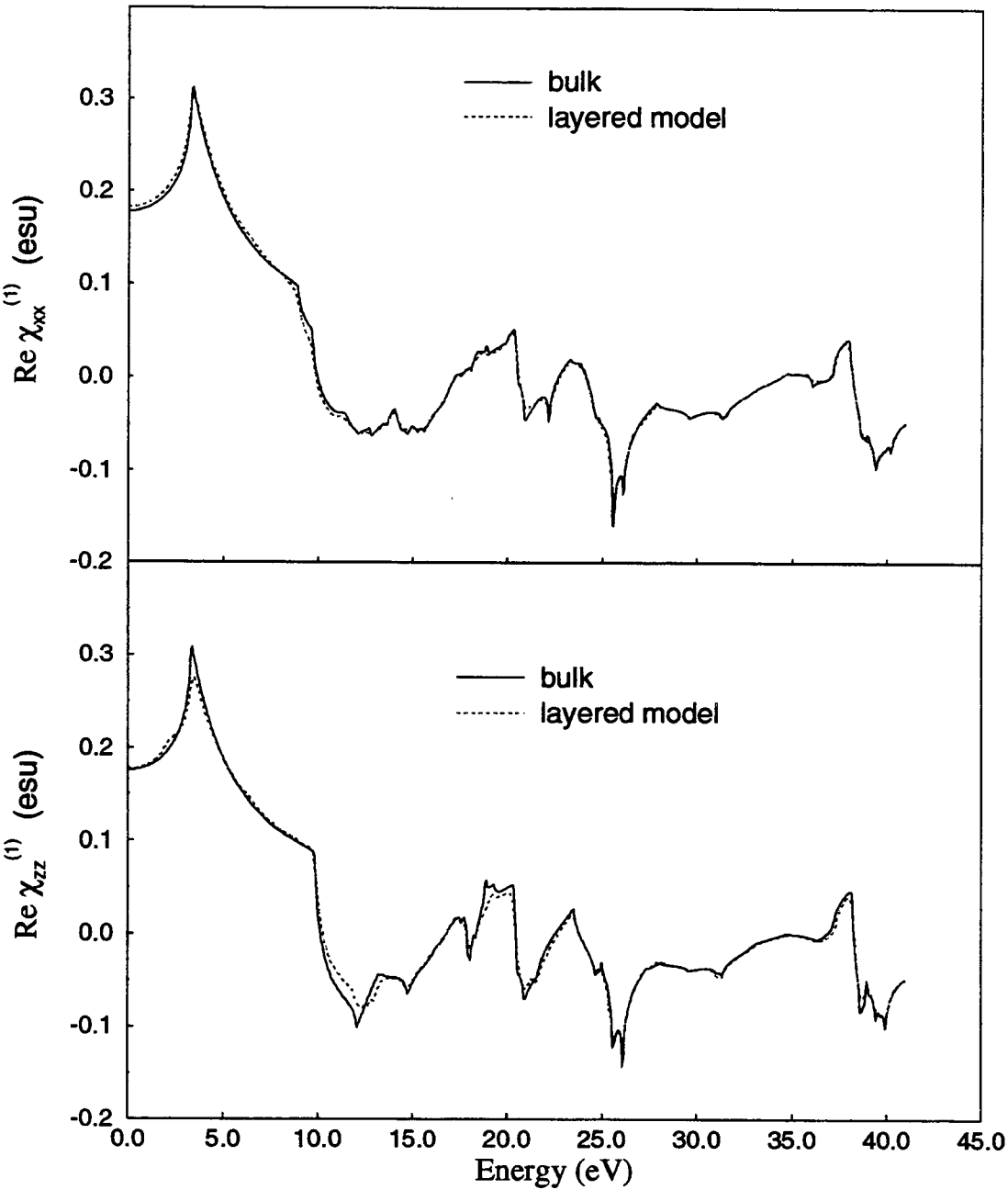

Figure 6.9 Comparison of the real part of the 1st order susceptibilities for the bulk and the layered model of 48 layers.

are small and they decrease as we increase the number of layers in our layered model.

We calculated the normal-incidence reflectivities from vacuum using the following formula:

$$R = \frac{(n_2 - 1)^2 + \kappa_2^{\,2}}{(n_2 + 1)^2 + \kappa_2^{\,2}}$$

where n_2 and κ_2 are respectively refractive index and absorption coefficient, which are defined in equations (2.30a) and (2.30b) based on the first order susceptibilities. The results are shown in figure (6.10). Figure (6.11) shows the reflectance spectra of ZnO measured by R. Klucker et al[22]. The experimental measurements made by J.L. Freeouf[23] are shown in figure (6.12). Above the band-gap exciton around 3.3 eV, the first structure observed by J.L.Freeouf is at about 8.7 eV. He did not find the small structure reported by R.Klucker et al at about 7 eV. At higher energies above 10 eV, although these two experimental results give similar spectral shape and polarization dependence, their magnitudes are different.

Table 6.1 Energies (in eV) of prominent features in the reflectance spectra of ZnO

$\vec{E}\perp\vec{c}^{(1)}$	3.3	7.00		9.2		12.6	14.0	15.2		17.1	19.3	20.8
$\vec{E}\parallel\vec{c}^{(1)}$	3.3	7.05	8.95				13.8	14.7	15.6		18.9	
$\vec{E}\parallel\vec{c}^{(2)}$	3.4			9.76		12.7	13.0	14.9		17.7	19.3	20.2
$\vec{E}\perp\vec{c}^{(2)}$	3.4		8.68	9.52	11.5		13.4	14.6	15.7		18.7	20.3
$\vec{E}\perp\vec{c}^{(3)}$	3.3		8.6		11.0	12.5	13.8	15.2		17	20.5	23
$\vec{E}\parallel\vec{c}^{(3)}$	3.3		8.8	10.2	11.1		13.8	15.2	16.2		21	23.5

(1) experimental results by R.Klucker et al[22].
(2) our calculated results.
(3) experimental results by J.L.Freeouf[23].

In order to compare our results to those experimental results, we plot the reflectivities calculated using our layered model in figure (6.13) for photon energies ranging from 0 to 25 eV. The peak positions in the reflectivity spectra of experimental results from R.Klucker et al[22] and J.L. Freeouf[23] as well as our calculation are listed in Table (6.1).

The small structure at about 7 eV reported by R.Klucker et al does not show up in our calculation. This might explain why J.L.Freeouf did not see such peak around 7 eV even although he carefully studied this region of the spectrum and searched for the peak. There are no agreement as of the reflectance magnitude among the experimental results and our calculated results. However, there are quite good agreements as of the spectral shape among them.

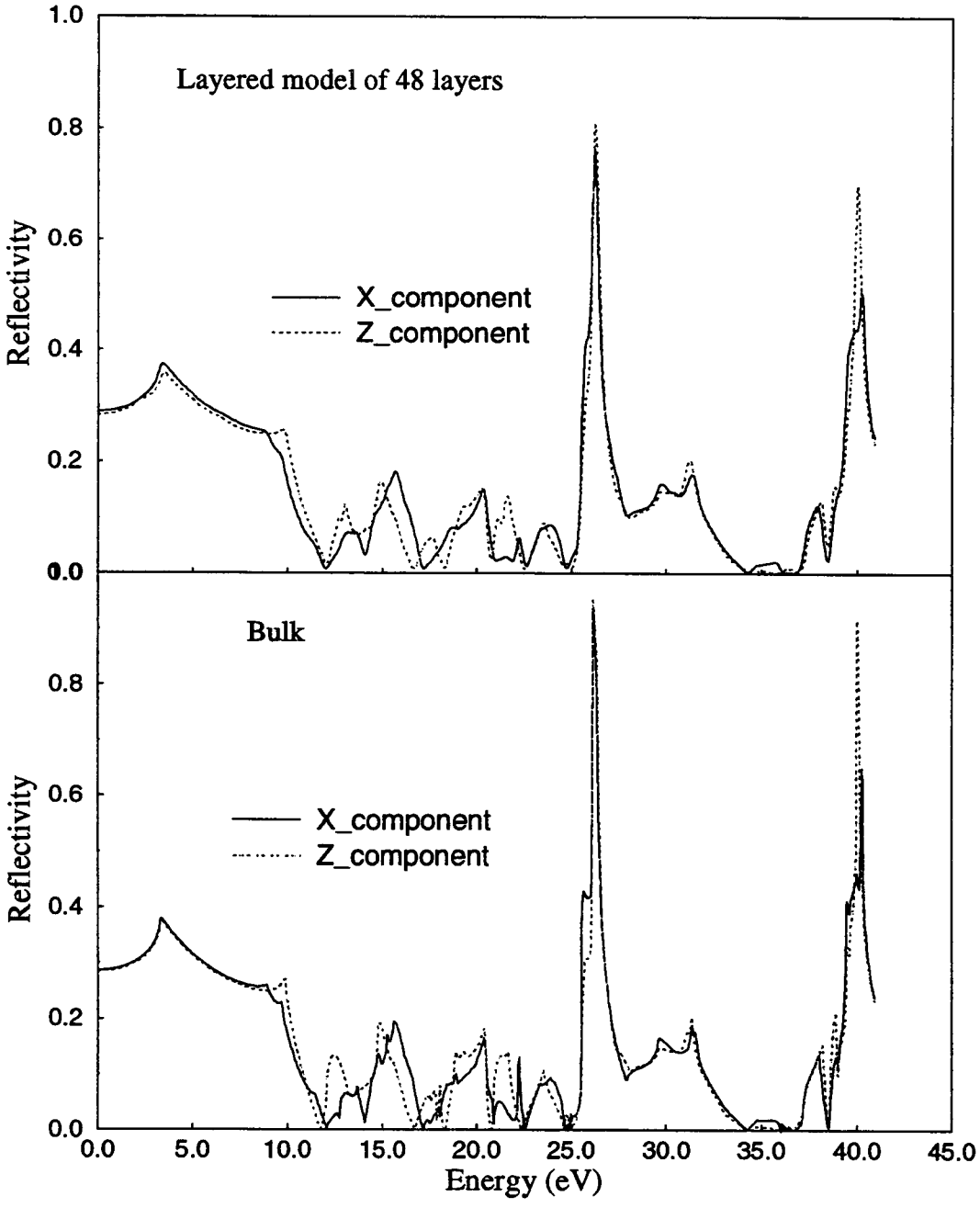

Figure 6.10 Normal-incidence reflectivities calculated from the first order susceptibilities.

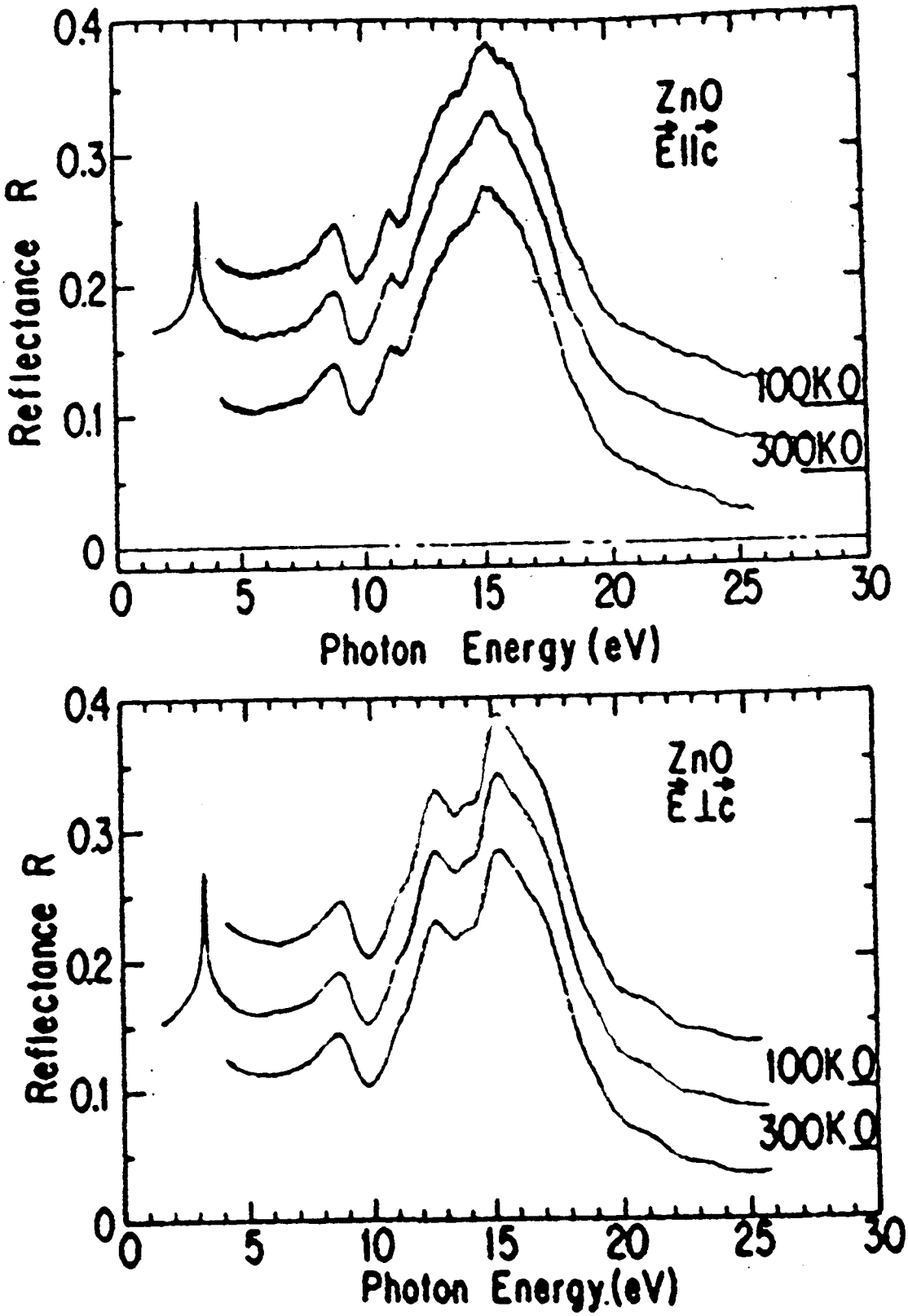

Figure 6.11 Reflectance spectra of ZnO measured by J.L.Freeouf[23].

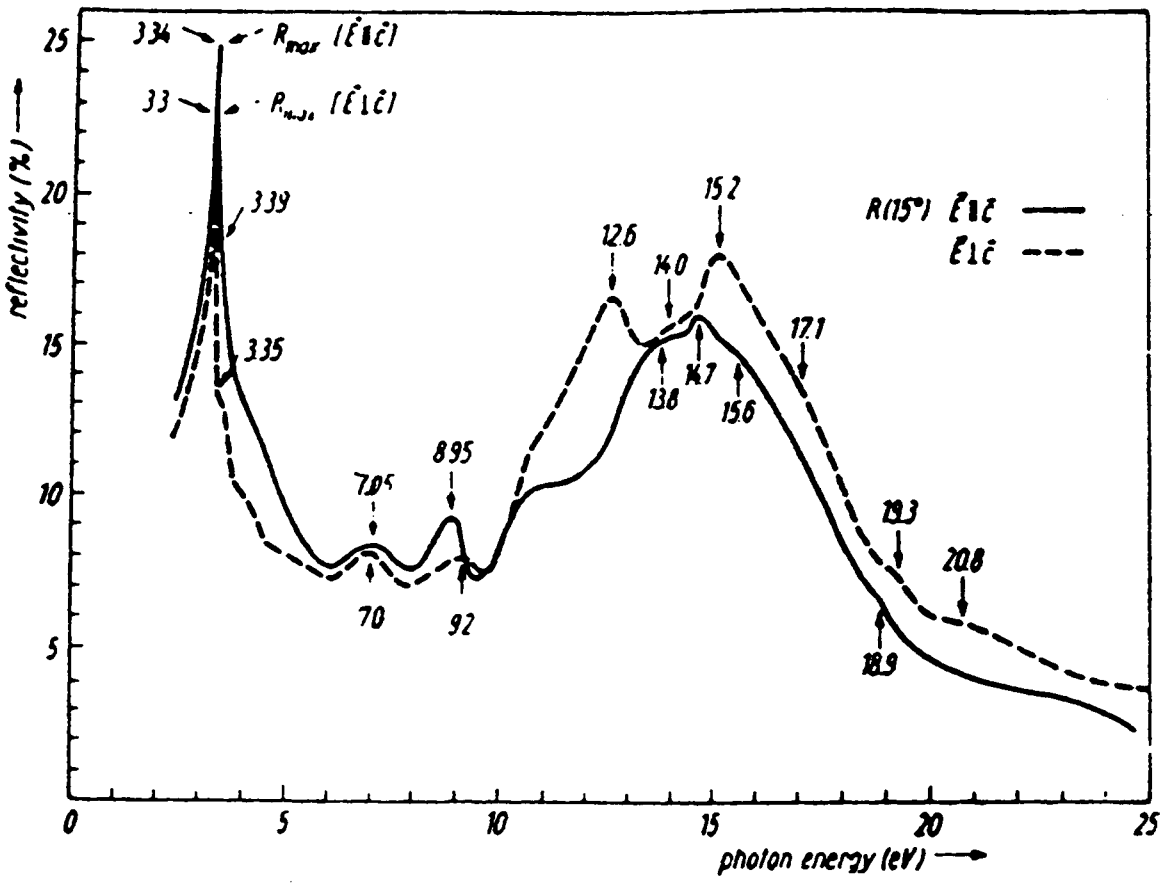

Figure 6.12 Reflectance spectra of ZnO measured by R.Klucker et al[22].

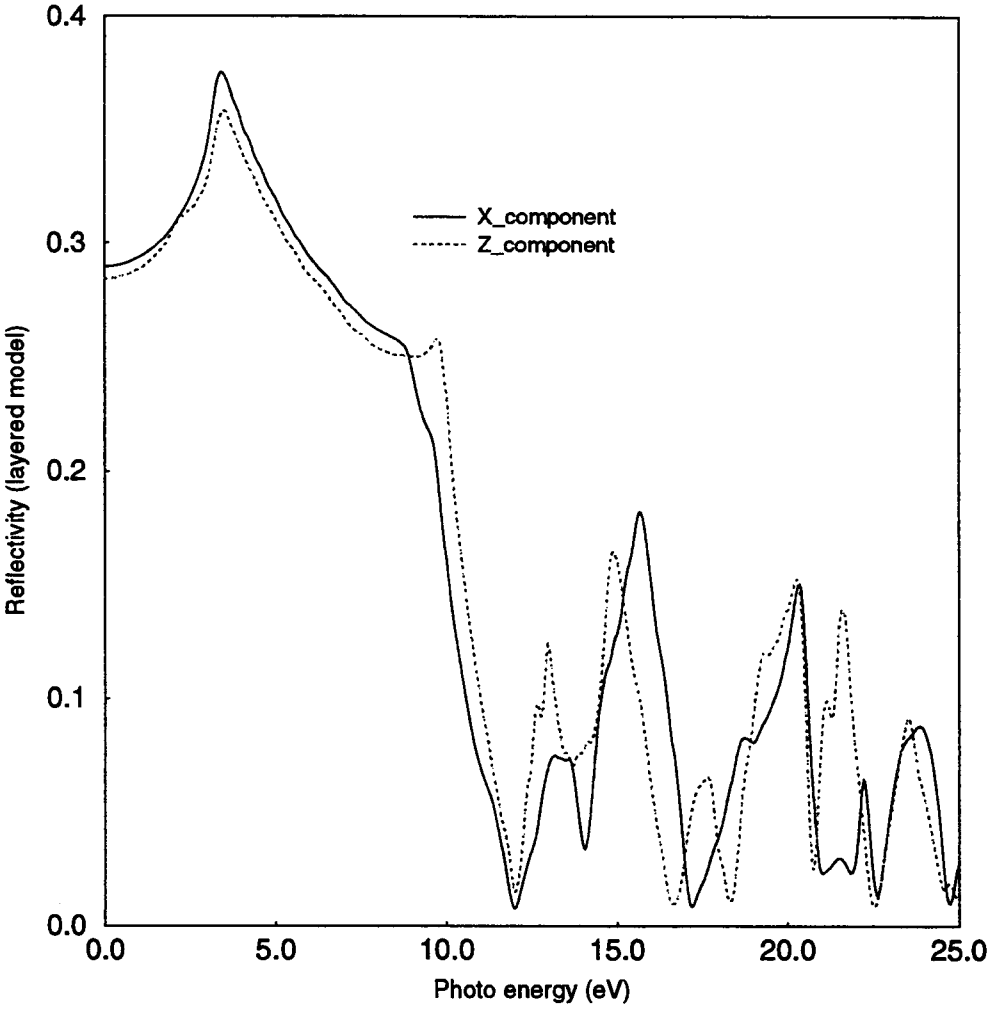

Figure 6.13 Normal-incidence reflectivities calculated using the layered model of 48 layers for photon energies 0-25 eV.

Chapter 7
Second Harmonic Optical Response Functions of ZnO Bulk and ZnO Surface

Second harmonic generation is a special case of sum frequency generation in nonlinear optical phenomena. It results from the second order nonlinear response $\bar{p}^{(2)}(\omega,\bar{k})$ of the medium to the incident laser beam. In chapter two, we defined $\bar{p}^{(2)}(\omega,\bar{k})$ in terms of the second order susceptibility tensor $\bar{\bar{\chi}}^{(2)}$ and expressed $\bar{\bar{\chi}}^{(2)}$ in terms of eigen energies and wave functions of the medium. In this chapter, we will derive an expression for the imaginary part of $\bar{\bar{\chi}}^{(2)}$ in a form suitable for numerical calculation. We will also discuss our numerical integration methods for evaluating these expressions for ZnO bulk and ZnO layered model respectively. The results for $\bar{\bar{\chi}}^{(2)}(2\omega)$ from ZnO bulk calculations and ZnO layered model calculations will be presented, compared, and discussed.

7.1 The Susceptibility Tensor $\bar{\bar{\chi}}^{(2)}$

$\bar{\bar{\chi}}^{(2)}$, like $\bar{\bar{\chi}}^{(1)}$, has complex values. Its real part is related to its imaginary part by the same Kramers-Kronig relation[3]:

$$\mathrm{Re}\,\bar{\bar{\chi}}^{(2)}(\omega) = \frac{2}{\pi} P \int_0^{\infty} \frac{\omega' \,\mathrm{Im}\,\bar{\bar{\chi}}^{(2)}(\omega')}{\omega'^{2} - \omega^{2}} d\omega' \qquad (7.1)$$

where P means principal part, Re means real part, and Im means imaginary part. To compute the second order susceptibility tensor $\bar{\bar{\chi}}^{(2)}$, we first calculate the imaginary part

of $\vec{\vec{\chi}}^{(2)}$, then we use the Kramers-Kronig relation (7.1) to obtain the real part of $\vec{\vec{\chi}}^{(2)}$ from the imaginary part.

In chapter two, we have expressed the second order nonlinear polarization as

$$\vec{P}_a^{(2)}(t) = \sum_{b,c;\alpha,\beta} \vec{\vec{\chi}}^{(2)}_{abc}\left(\omega_\alpha + \omega_\beta\right) \vec{E}_b^{\alpha} \vec{E}_c^{\beta} e^{-i(\omega_\alpha+\omega_\beta)t} \qquad (7.2)$$

where the susceptibility tensor $\vec{\vec{\chi}}^{(2)}_{abc}\left(\omega_\alpha + \omega_\beta\right)$ is defined from equation (2.73) and (2.66) as

$$\vec{\vec{\chi}}^{(2)}_{abc}\left(\omega_\alpha + \omega_\beta\right) = -\sum_{i,j,k} \frac{ie^3}{m^3 \omega_\alpha \omega_\beta \left(\omega_\alpha + \omega_\beta\right)} \frac{p^a_{ij} p^b_{jk} p^c_{ki}}{\hbar\left(\omega_\alpha + \omega_\beta - \omega_{ji}\right)} \left[\frac{f^{(0)}_{ik}}{\hbar\left(\omega_\beta - \omega_{ki}\right)} + \frac{f^{(0)}_{jk}}{\hbar\left(\omega_\alpha - \omega_{jk}\right)} \right] \qquad (7.3)$$

and we use the same notations as in chapter two. For second harmonic generation, we have

$$\omega_\alpha = \omega_\beta \equiv \omega,$$

So, equation (7.3) becomes:

$$\vec{\vec{\chi}}^{(2)}_{abc}(2\omega) = -\sum_{i,j,k} \frac{ie^3}{2m^3\omega^3} \frac{p^a_{ij} p^b_{jk} p^c_{ki}}{\hbar\left(2\omega - \omega_{ji}\right)} \left[\frac{f^{(0)}_{ik}}{\hbar\left(\omega - \omega_{ki}\right)} + \frac{f^{(0)}_{jk}}{\hbar\left(\omega - \omega_{jk}\right)} \right] \qquad (7.4)$$

where $\vec{\vec{\chi}}^{(2)}_{abc}(2\omega)$ is called the second harmonic optical response function. If we introduce the perturbation adiabatically, we should write $\vec{\vec{\chi}}^{(2)}_{abc}(2\omega)$ as

$$\vec{\vec{\chi}}^{(2)}_{abc}(2\omega) = -\sum_{i,j,k} \frac{ie^3}{2m^3\omega^3} \frac{p^a_{ij} p^b_{jk} p^c_{ki}}{2\hbar\omega - E_{ji} + i\varepsilon} \left[\frac{f^{(0)}_{ik}}{\hbar\omega - E_{ki} + i\varepsilon} + \frac{f^{(0)}_{jk}}{\hbar\omega - E_{jk} + i\varepsilon} \right] \qquad (7.5)$$

where $E_{ji} = \hbar\omega_{ji}$. Using the following identity

$$\lim_{\varepsilon \to 0} \frac{1}{(x + i\varepsilon)(x + y + i\varepsilon)} = \frac{1}{y}\left[P\left(\frac{1}{x}\right) - P\left(\frac{1}{x+y}\right) - i\pi\delta(x) + i\pi\delta(x+y) \right] \qquad (7.6)$$

where P indicates principal value, and writing $\vec{\vec{\chi}}^{(2)}_{abc}(2\omega)$ as

$$\vec{\vec{\chi}}^{(2)}_{abc}(2\omega) = \vec{\vec{\chi}}^{(2)\,\prime}_{abc}(2\omega) + i\vec{\vec{\chi}}^{(2)\,\prime\prime}_{abc}(2\omega), \tag{7.7}$$

we obtain the imaginary part $\vec{\vec{\chi}}^{(2)\,\prime\prime}_{abc}(2\omega)$

$$\vec{\vec{\chi}}^{(2)\,\prime\prime}_{abc}(2\omega) = \sum_{i,j,k}\frac{\pi}{2}\left[\frac{e}{m\omega}\right]^3 \frac{\mathrm{Im}(P^a_{ij}P^b_{jk}P^c_{ki})}{E_{ki}+E_{kj}}\left\{2f^{(0)}_{ij}\delta(2\hbar\omega - E_{ji}) + f^{(0)}_{jk}\delta(\hbar\omega - E_{jk}) - f^{(0)}_{ik}\delta(\hbar\omega - E_{ki})\right\} \tag{7.8}$$

where Im means the imaginary part; i, j, and k run over all single-particle electronic states. In our band structure calculation, i(and j,k) is replaced by n and $\vec{k}$; n is the band index; $\vec{k}$ is a reciprocal wave vector. When i runs over all the single-particle states, it corresponds to n and $\vec{k}$ running over every band and every possible wave vector. As we did in chapter six, we make the zero temperature approximation and continue to assume $\nabla^b_{n\vec{k},n'\vec{k}'} \propto \delta_{\vec{k}\vec{k}'}$. Then, the expressions for the imaginary part of $\vec{\vec{\chi}}^{(2)}_{abc}(2\omega)$ for ZnO bulk and ZnO layered model can be obtained from equation (7.8).

For ZnO bulk, the $\vec{k}$ space is three dimensional and we have:

$$\begin{aligned}\vec{\vec{\chi}}^{(1)\,\prime\prime}_{ab}(\omega) = \pi \sum_{i(occupied)}\sum_{j(empty)}\sum_{k(all)}\left[\frac{e\hbar}{2\pi m\omega}\right]^3 \int_{BZ} d^3\vec{k}\,\{ \\ -\frac{2\delta(2\hbar\omega - E_{ji})}{\hbar\omega - E_{ki}}\mathrm{Re}\left(\nabla^a_{ij}\nabla^b_{jk}\nabla^c_{ki}\right) \\ +\frac{\delta(\hbar\omega - E_{ji})}{\hbar\omega - E_{ik}}\mathrm{Re}\left(\nabla^a_{kj}\nabla^b_{ji}\nabla^c_{ik}\right) \\ -\frac{\delta(\hbar\omega - E_{ji})}{\hbar\omega - E_{kj}}\mathrm{Re}\left(\nabla^a_{ik}\nabla^b_{kj}\nabla^c_{ji}\right)\Big\}\end{aligned} \tag{7.9}$$

where the matrix elements ∇^a_{ij} and transition energies E_{ji} are implicit functions of the wave vector $\vec{k}$. The summation of index i runs over only valence bands. The summation of index j runs over only conduction bands. However, the summation of index k runs over both valence and conduction bands. The integral is over a primitive unit cell in the 3D $\vec{k}$ space.

For ZnO layered model, the $\vec{k}$ space is two dimensional and we have:

$$\bar{\bar{\chi}}^{(1)}_{ab}{}''(\omega) = \frac{1}{\pi L c} \sum_{i(occupied)} \sum_{j(empty)} \sum_{k(all)} \left[\frac{e\hbar}{m\omega}\right]^3 \int_{BZ} d^2\vec{k}\{$$

$$-\frac{2\delta(2\hbar\omega - E_{ji})}{\hbar\omega - E_{ki}} \mathrm{Re}\left(\nabla^a_{ij}\nabla^b_{jk}\nabla^c_{ki}\right)$$

$$+\frac{\delta(\hbar\omega - E_{ji})}{\hbar\omega - E_{ik}} \mathrm{Re}\left(\nabla^a_{kj}\nabla^b_{ji}\nabla^c_{ik}\right)$$

$$-\frac{\delta(\hbar\omega - E_{ji})}{\hbar\omega - E_{kj}} \mathrm{Re}\left(\nabla^a_{ik}\nabla^b_{kj}\nabla^c_{ji}\right)\} \qquad (7.10)$$

where L is the number of layers of our layered model; c is the height of a ZnO crystal unit cell. The integration is over a primitive unit cell in the two dimensional $\vec{k}$ space. This $\bar{\bar{\chi}}^{(2)}_{abc}(2\omega)$ has been divided by the volume $V = \frac{L}{4}cA$.

We can see from equations (7.9) and (7.10), that resonances can occur when either ω or 2ω is the frequency difference between an unoccupied single-particle state and the occupied single-particle state. The ZnO symmetry point group is C_{6v} in the Shoenflies notation, or $6mm$ in the international symbolism. Because of this symmetry, only seven out of the total twenty seven tensor elements of $\bar{\bar{\chi}}^{(2)}_{abc}(2\omega)$ are nonzero and only four of the seven are independent. The nonvanishing elements and the relations between them are as follows:

$$\bar{\bar{\chi}}^{(2)}_{zzz}, \quad \bar{\bar{\chi}}^{(2)}_{xzx} = \bar{\bar{\chi}}^{(2)}_{yzy}, \quad \bar{\bar{\chi}}^{(2)}_{xxz} = \bar{\bar{\chi}}^{(2)}_{yyz}, \quad \bar{\bar{\chi}}^{(2)}_{zxx} = \bar{\bar{\chi}}^{(2)}_{zyy}.$$

In chapter six, we have discussed how to evaluate the matrix element ∇^b_{ij}. In next two sections of this chapter, we will discuss how to evaluate the integrals in equations (7.9) and (7.10) respectively.

7.2 Calculation of ZnO Bulk Second Harmonic Response Functions

The imaginary part of the second harmonic function of ZnO bulk is given by equation (7.9). If we make $a,b,$ and c all equal to z in equation (7.9), we obtain the formula for $\vec{\vec{\chi}}^{(2)}_{zzz}(2\omega)$. The formulas for other nonvanishing elements can also be obtained by properly assigning values to $a,b,$ and c in equation (7.9).

One way to evaluate the integral of equation (7.9) is to assume that $\frac{\mathrm{Re}(\nabla^a_{ij}\nabla^b_{jk}\nabla^c_{ki})}{\hbar\omega - E_{ki}}$, $\frac{\mathrm{Re}(\nabla^a_{kj}\nabla^b_{ji}\nabla^c_{ik})}{\hbar\omega - E_{ik}}$, and $\frac{\mathrm{Re}(\nabla^a_{ik}\nabla^b_{kj}\nabla^c_{ji})}{\hbar\omega - E_{kj}}$ are all constants over a triangle or a quadrilateral plane of either $2\hbar\omega = E_{ji}$ or $\hbar\omega = E_{ji}$ so that the linear analytic tetrahedron method introduced in chapter six can be used here exactly the same way. Although the resonant-energy denominators of $\hbar\omega - E_{ki}$, $\hbar\omega - E_{ik}$, and $\hbar\omega - E_{kj}$ do not give any ill-behaved contributions to the response functions in our calculation, we find that we obtain better convergence if we take only the matrix elements as constants and integrate $\frac{1}{\hbar\omega - E_{ki}}$, $\frac{1}{\hbar\omega - E_{ik}}$, and $\frac{1}{\hbar\omega - E_{kj}}$ analytically.

To integrate $\frac{1}{\hbar\omega - E_{ki}}$ analytically, we first obtain E_{ki} values at the three vertices of the triangular plane contained inside the tetrahedron by interpolating linearly from the values at the four vertices of the tetrahedron. Then, we obtain the function of E_{ki} over the triangle plane by linearly interpolating from the E_{ki} values at the three vertices of the triangle. If $-E_{ki}$ has values f_1, f_2, and f_3 at the three vertices of the triangle respectively, the results of the integral $\frac{1}{\Delta s}\int_{triangle\ plane}\frac{ds}{\hbar\omega - E_{ki}}$, where Δs is the area of the triangular plane in the $\vec{k}$ space, are as follows:

1. if $f_1 \neq f_2 \neq f_3$:
$$\frac{\hbar\omega + f_3}{(f_3 - f_2)(f_3 - f_1)} \ln|\hbar\omega + f_3| - \frac{\hbar\omega + f_2}{(f_3 - f_2)(f_2 - f_1)} \ln|\hbar\omega + f_2| + \frac{\hbar\omega + f_1}{(f_3 - f_1)(f_2 - f_1)} \ln|\hbar\omega + f_1|$$

2. if $f_1 = f_2 \neq f_3$: $\dfrac{\hbar\omega + f_3}{(f_3 - f_1)^2} \ln\left|\dfrac{\hbar\omega + f_3}{\hbar\omega + f_1}\right| - \dfrac{1}{(f_3 - f_1)}$

3. if $f_1 = f_3 \neq f_2$: $\dfrac{\hbar\omega + f_2}{(f_2 - f_1)^2} \ln\left|\dfrac{\hbar\omega + f_2}{\hbar\omega + f_1}\right| - \dfrac{1}{(f_2 - f_1)}$

4. if $f_1 \neq f_2 = f_3$: $\dfrac{\hbar\omega + f_1}{(f_2 - f_1)^2} \ln\left|\dfrac{\hbar\omega + f_1}{\hbar\omega + f_2}\right| - \dfrac{1}{(f_1 - f_2)}$

5. if $f_1 = f_2 = f_3$: $\dfrac{1}{2}\dfrac{1}{\hbar\omega + f_1}$

We divide the IBZ into about 100,000 tetrahedrons. Our results for the imaginary parts of the nonvanishing elements of $\vec{\vec{\chi}}^{(2)}_{abc}(2\omega)$ are presented in figures (7.1), (7.3), (7.5), and (7.7). The real parts are obtained from the imaginary parts using the Kramers-Kronig relation. The results for the real parts are presented in figures (7.2), (7.4), (7.6), and (7.8).

7.3 Calculation of Second Harmonic Response Functions for the ZnO Layered Model

The imaginary part of the second harmonic response coefficients for ZnO layered model is given by equation (7.10). To evaluate the integral in equation (7.10), we use exactly the same method discussed above for the zinc oxide bulk calculation. The only difference is that we do the integral now in two dimensions instead of three

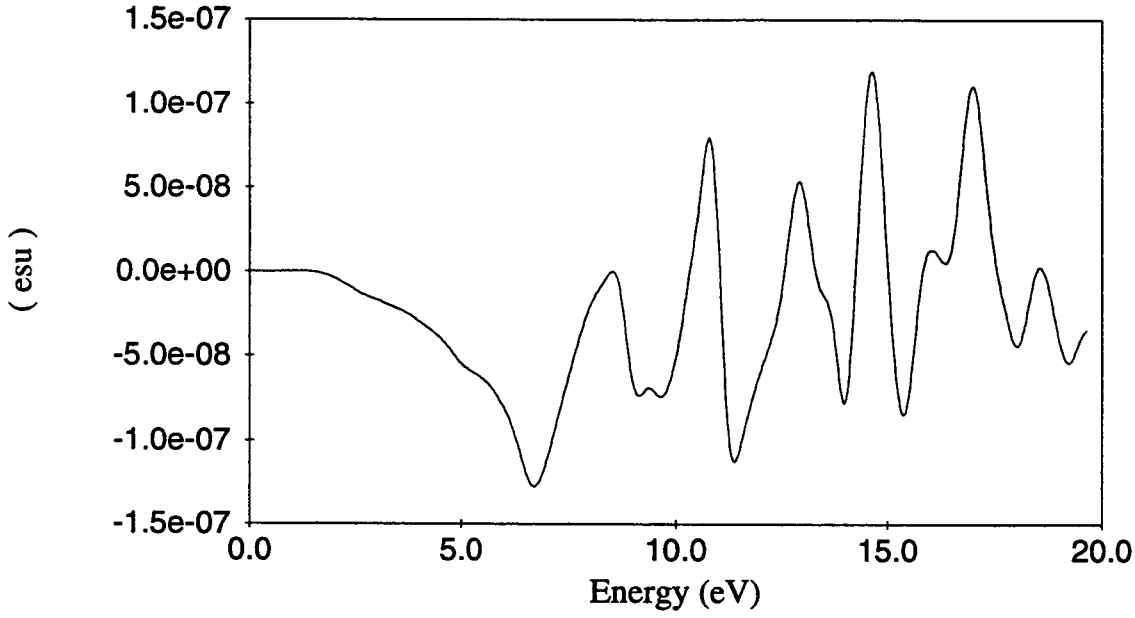

Figure 7.1 Bulk crystal Im $\chi_{xxz}^{(2)}(2\varpi)$.

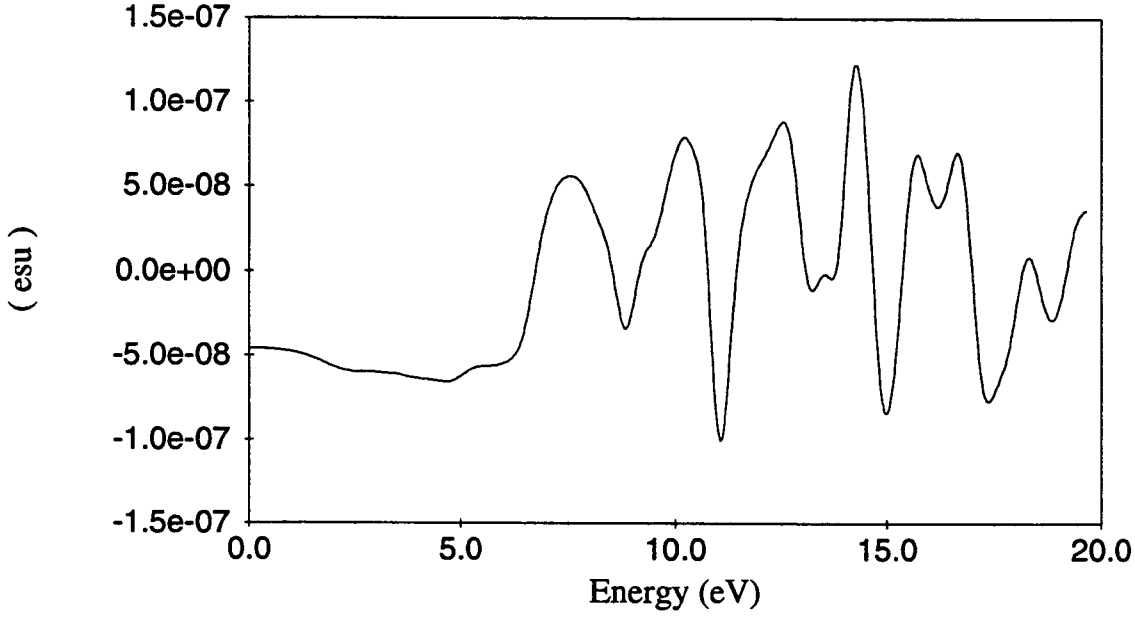

Figure 7.2 Bulk crystal Re $\chi_{xxz}^{(2)}(2\varpi)$.

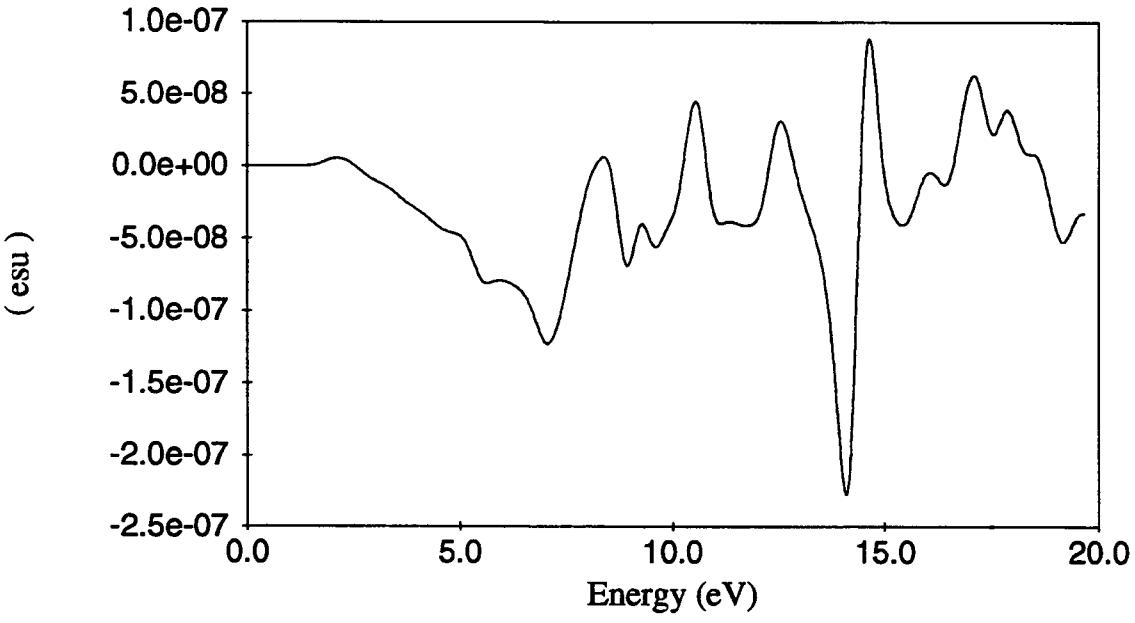

Figure 7.3 Bulk crystal Im $\chi_{xzx}^{(2)}(2\varpi)$.

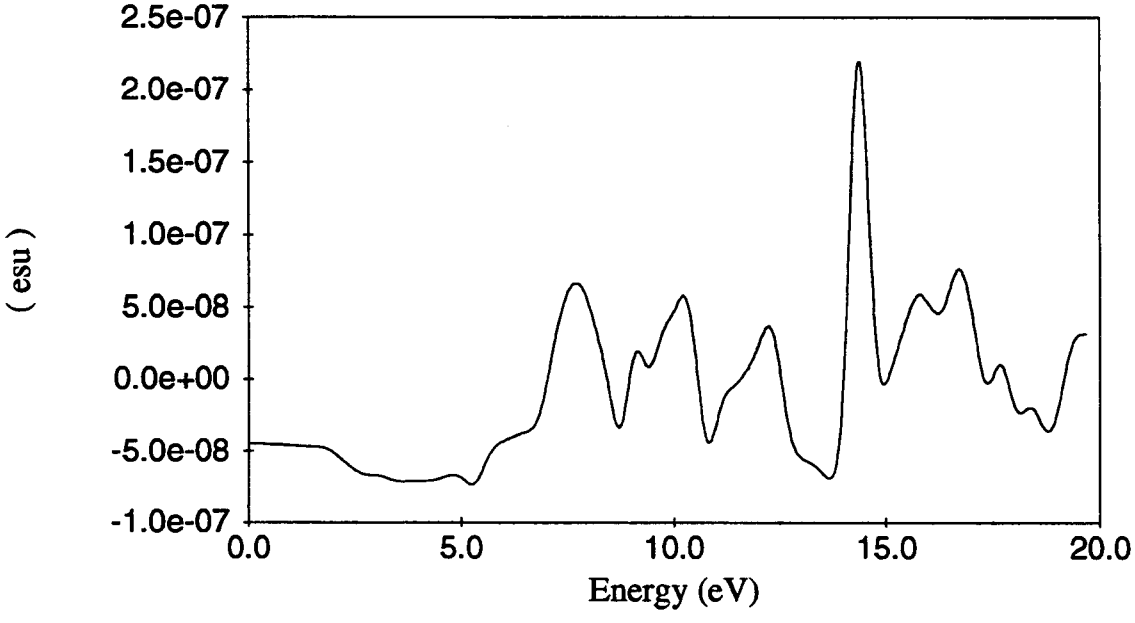

Figure 7.4 Bulk crystal Re $\chi_{xzx}^{(2)}(2\varpi)$.

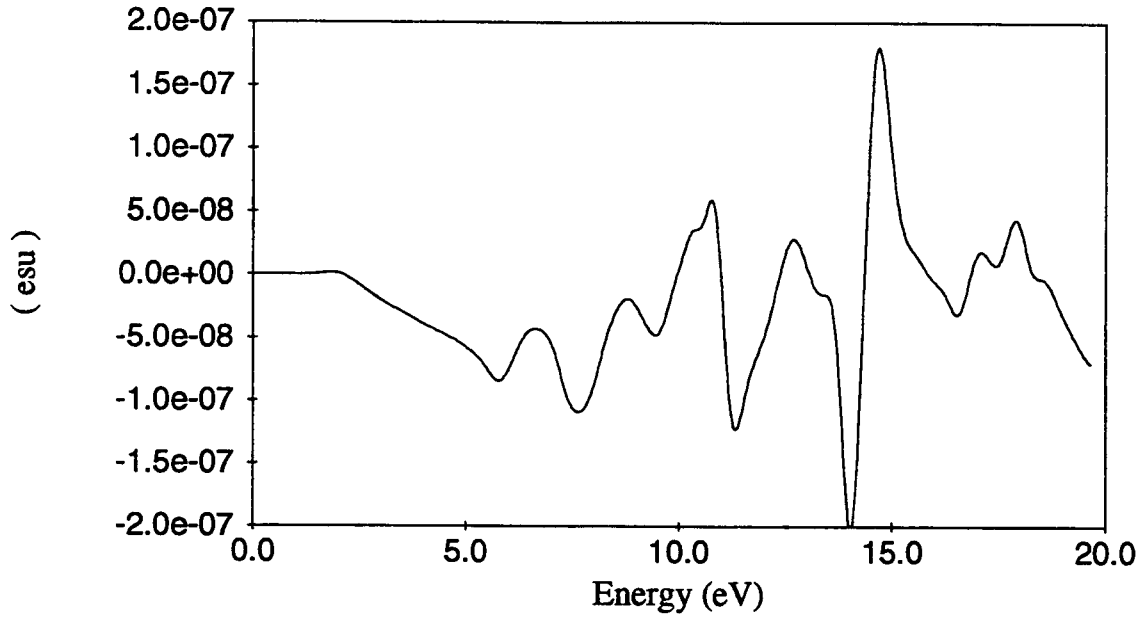

Figure 7.5 Bulk crystal Im $\chi_{zxx}^{(2)}(2\varpi)$.

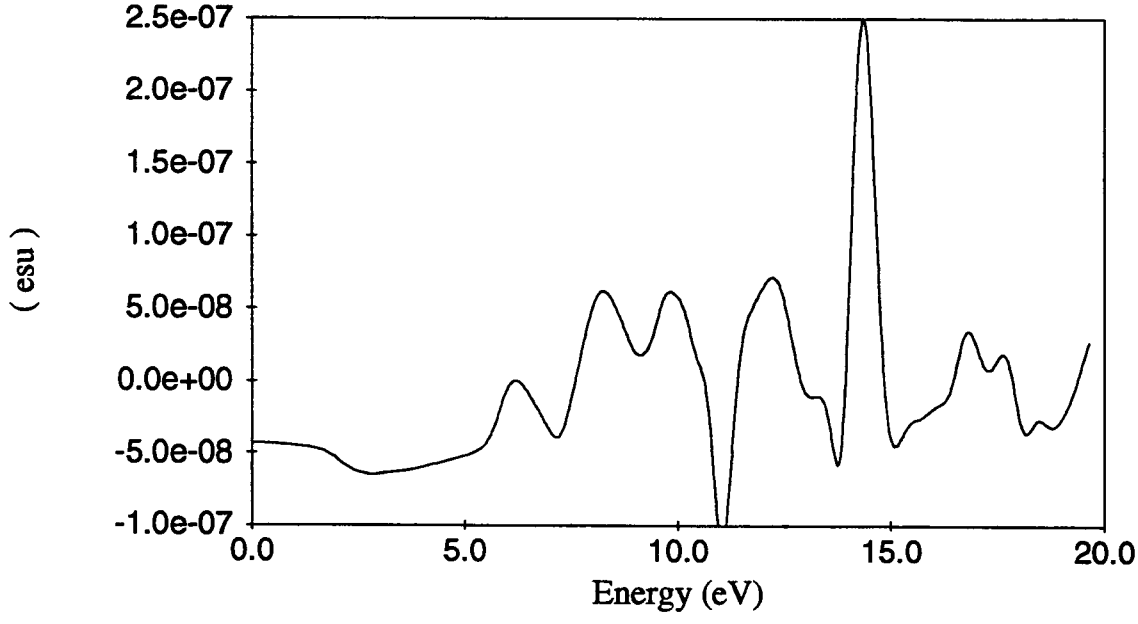

Figure 7.6 Bulk crystal Re $\chi_{zxx}^{(2)}(2\varpi)$.

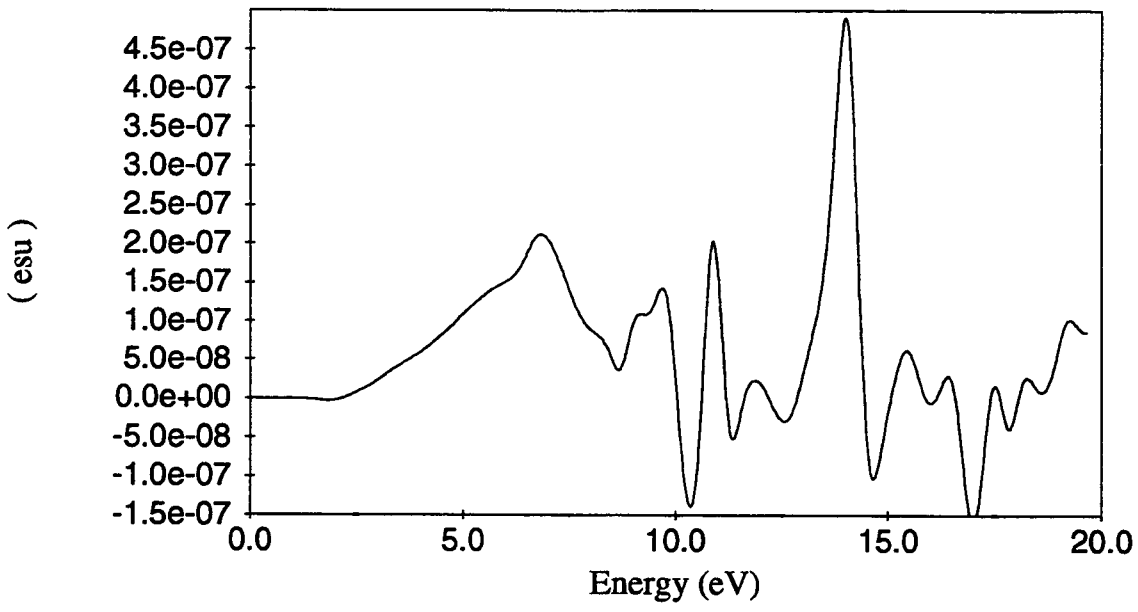

Figure 7.7 Bulk crystal Im $\chi_{zzz}^{(2)}(2\varpi)$.

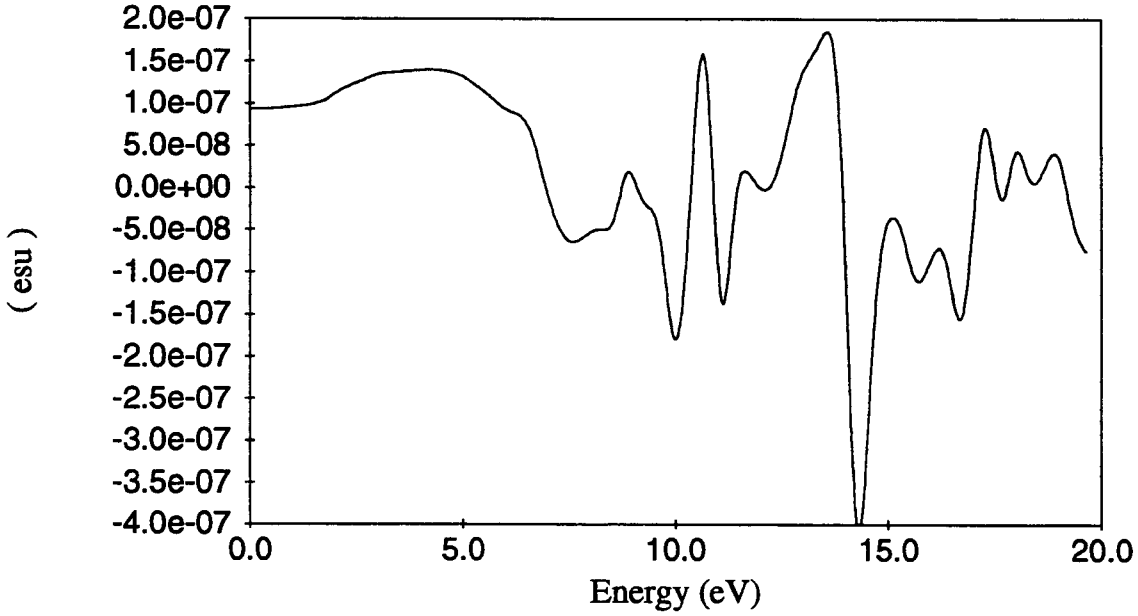

Figure 7.8 Bulk crystal Re $\chi_{zzz}^{(2)}(2\varpi)$.

dimensions. In this two dimensional case, we integrate $\frac{1}{\hbar\omega - E_{ki}}$, $\frac{1}{\hbar\omega - E_{ik}}$, and $\frac{1}{\hbar\omega - E_{kj}}$ analytically over a line segment instead of a triangular plane in the three dimensional case.

We divide the two dimensional IBZ into about 3,000 triangles and we take $0.028\ eV$ to be the energy resolution in all the second harmonic response coefficients calculations for the bulk and the layered model. Figures (7.9), (7.11), (7.13), and (7.15) show the imaginary parts of the second harmonic response functions $\bar{\bar{\bar{\chi}}}^{(2)}_{zzz}(2\omega)$, $\bar{\bar{\bar{\chi}}}^{(2)}_{zxx}(2\omega)$, $\bar{\bar{\bar{\chi}}}^{(2)}_{xzx}(2\omega)$, and $\bar{\bar{\bar{\chi}}}^{(2)}_{xxz}(2\omega)$ calculated from our ZnO layered model with 48 layers. The real parts obtained using the Kramers-Kronig relation from the calculated imaginary parts are shown in figures (7.10), (7.12), (7.14), and (7.16).

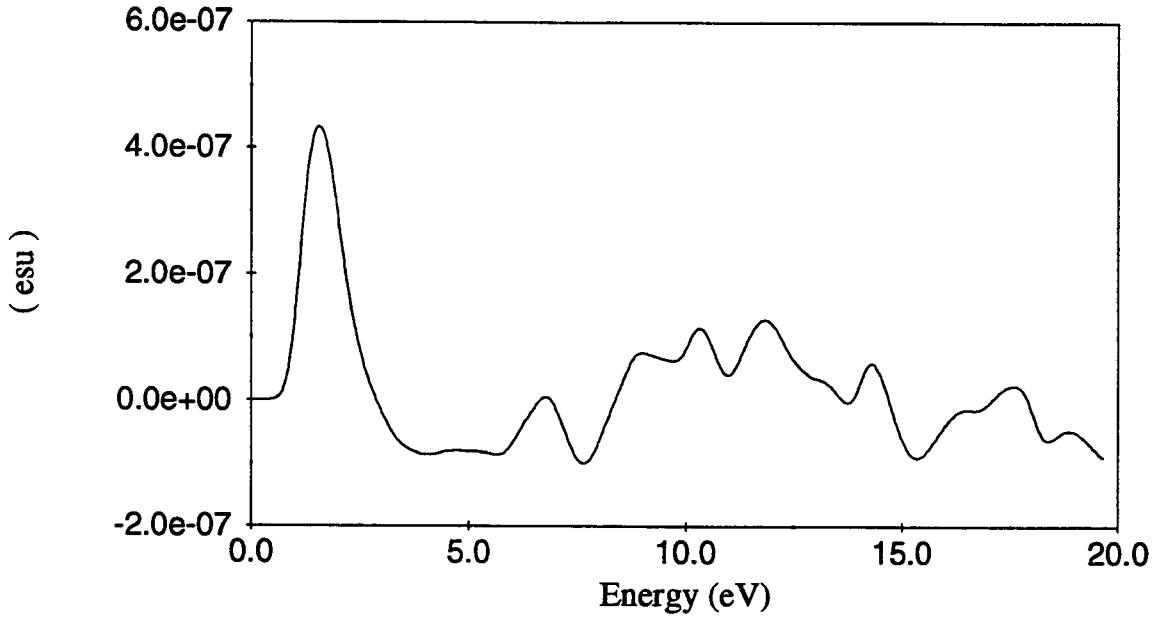

Figure 7.9 Im $\chi_{xxz}^{(2)}(2\varpi)$ for the layered model of 48 layers.

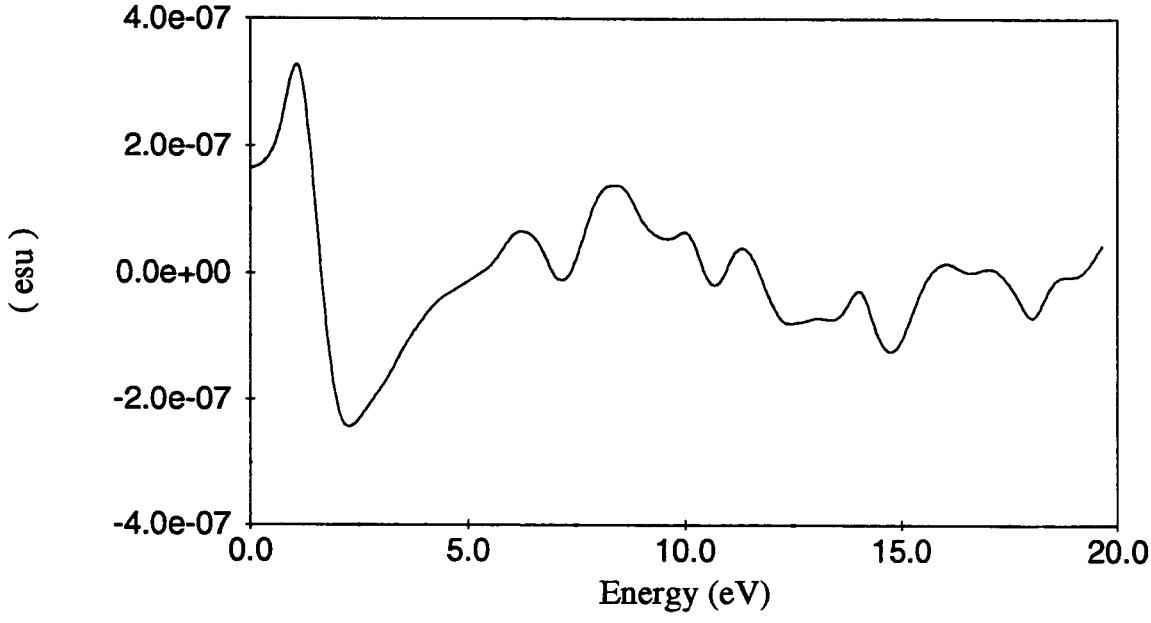

Figure 7.10 Re $\chi_{xxz}^{(2)}(2\varpi)$ for the layered model of 48 layers.

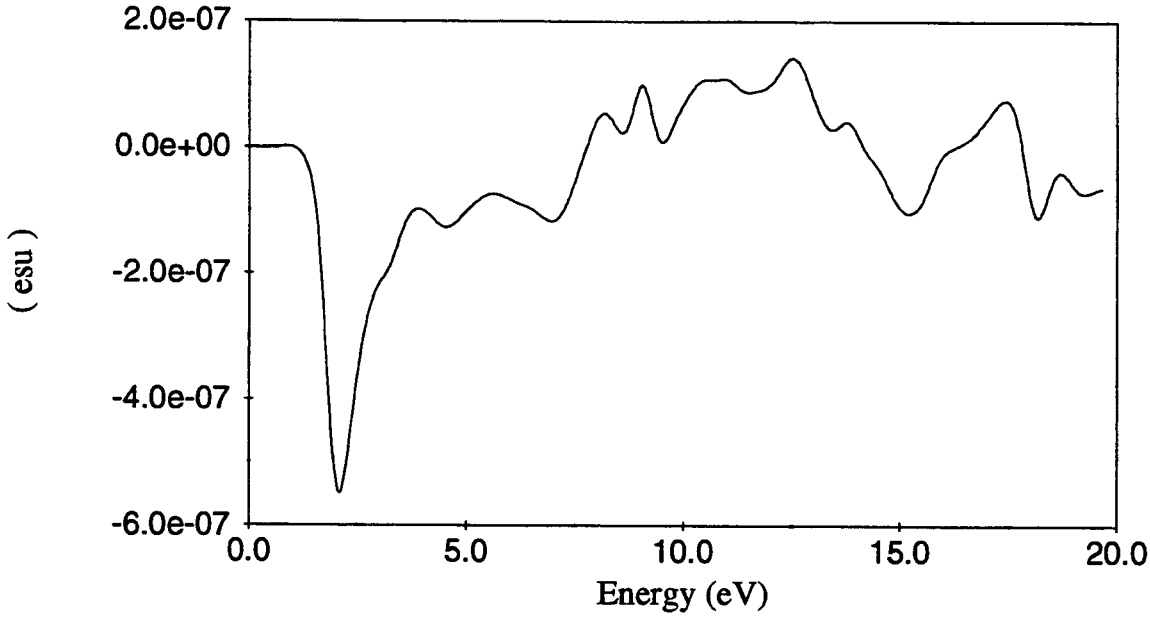

Figure 7.11 Im $\chi_{xzx}^{(2)}(2\varpi)$ for the layered mdel of 48 layers.

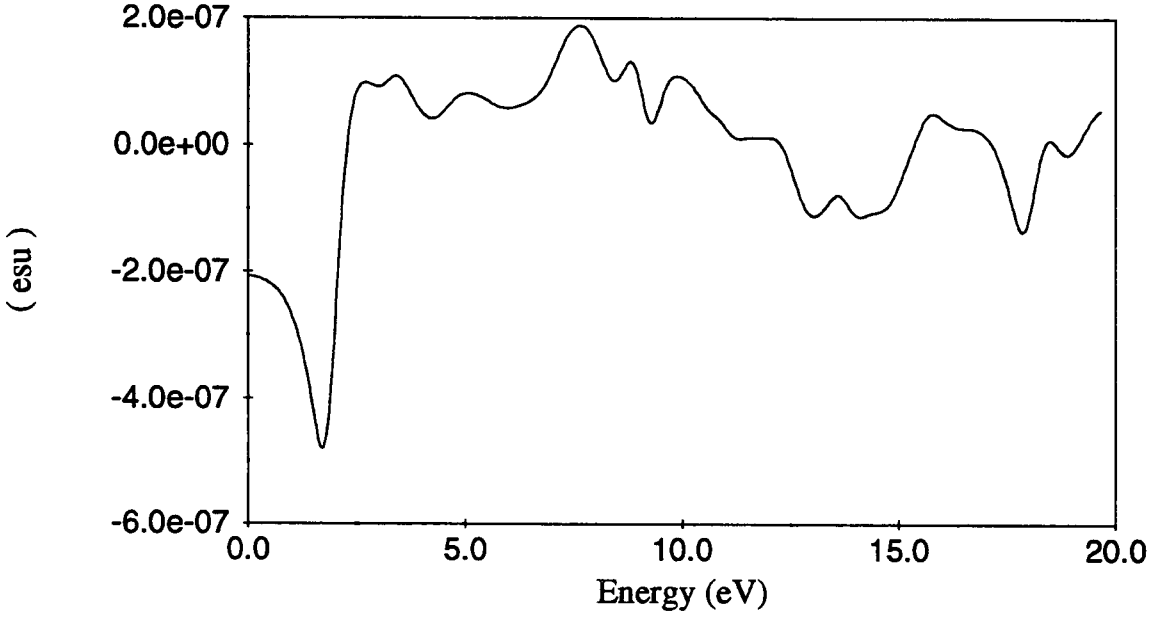

Figure 7.12 Re $\chi_{xzx}^{(2)}(2\varpi)$ for the layered model of 48 layers.

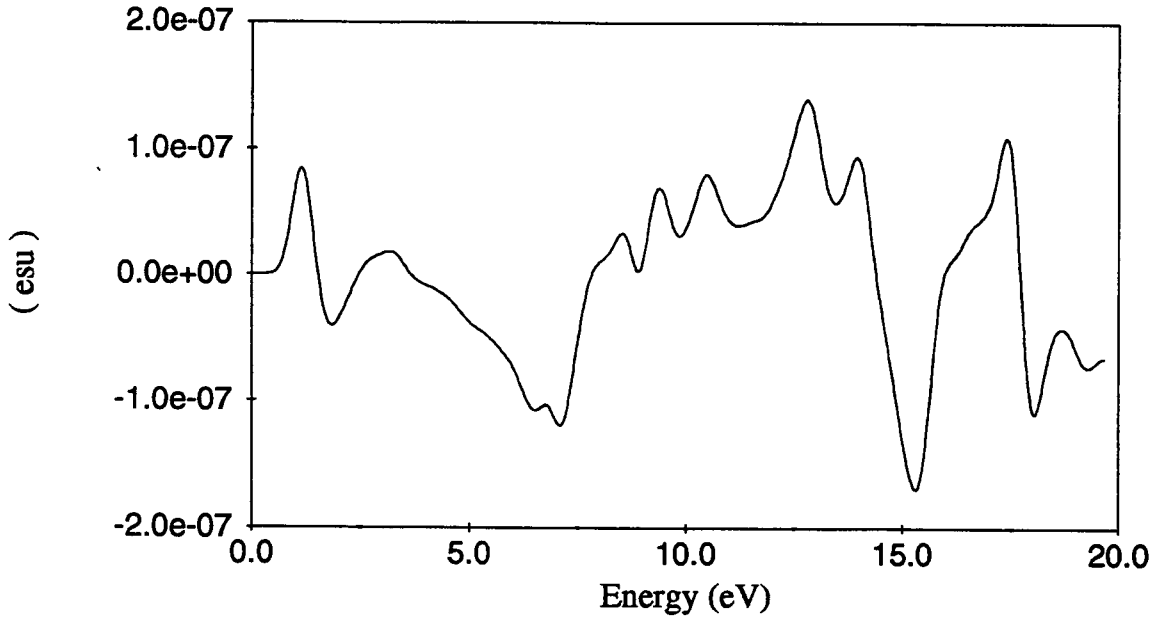

Figure 7.13 Im $\chi_{zxx}^{(2)}(2\varpi)$ for the layered model of 48 layers.

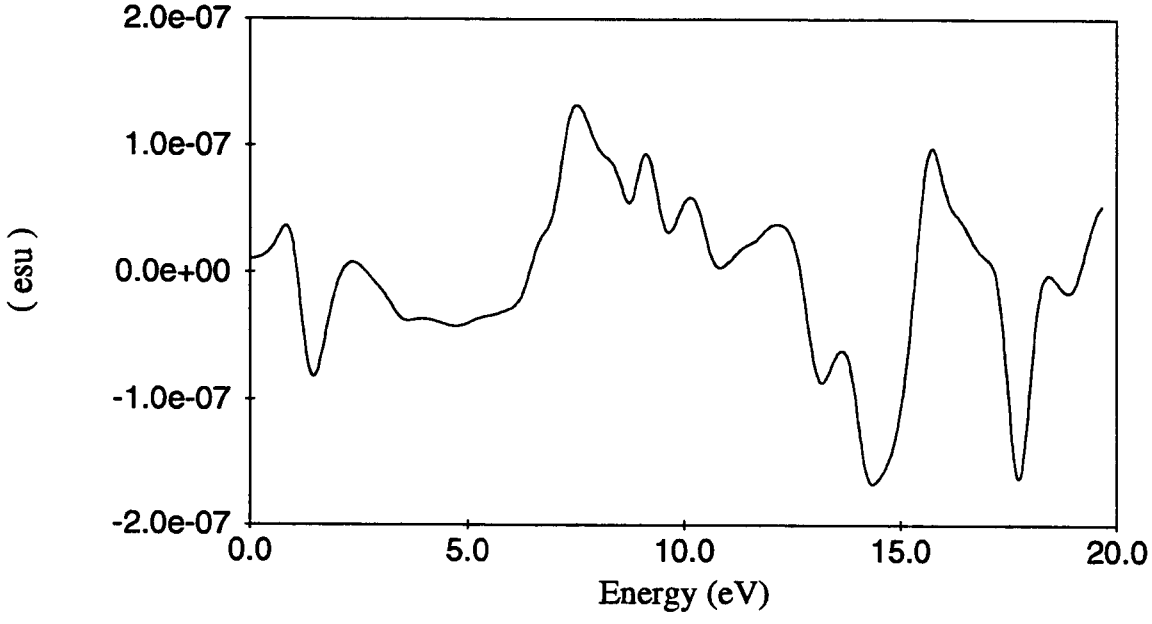

Figure 7.14 Re $\chi_{zxx}^{(2)}(2\varpi)$ for the layered model of 48 layers.

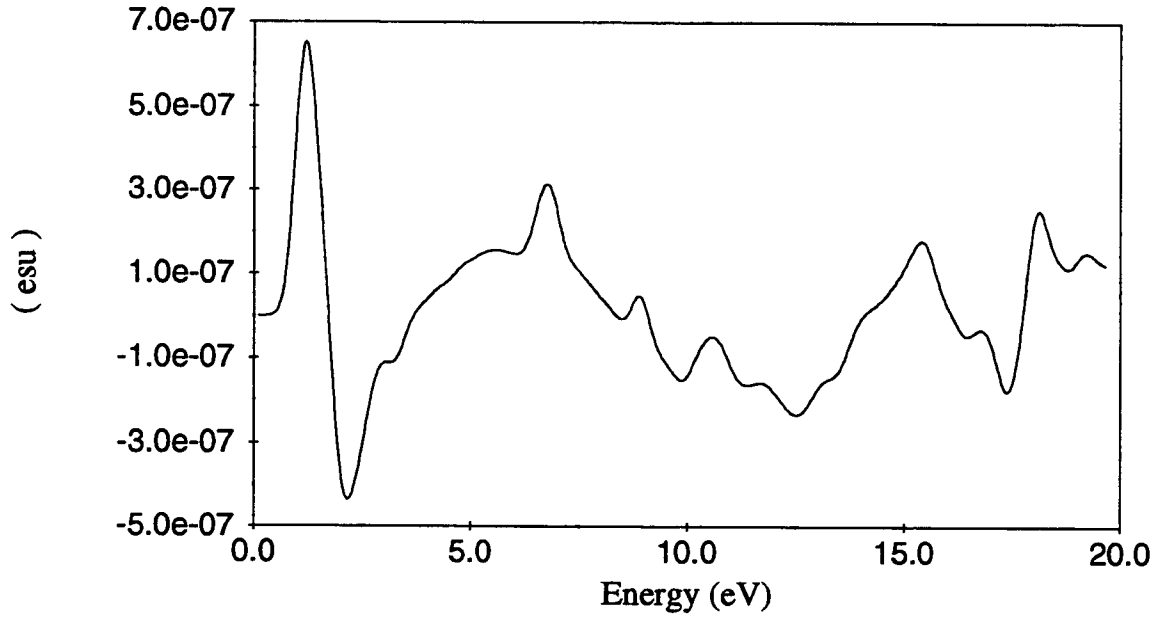

Figure 7.15 Im $\chi_{zzz}^{(2)}(2\varpi)$ for the layered model of 48 layers.

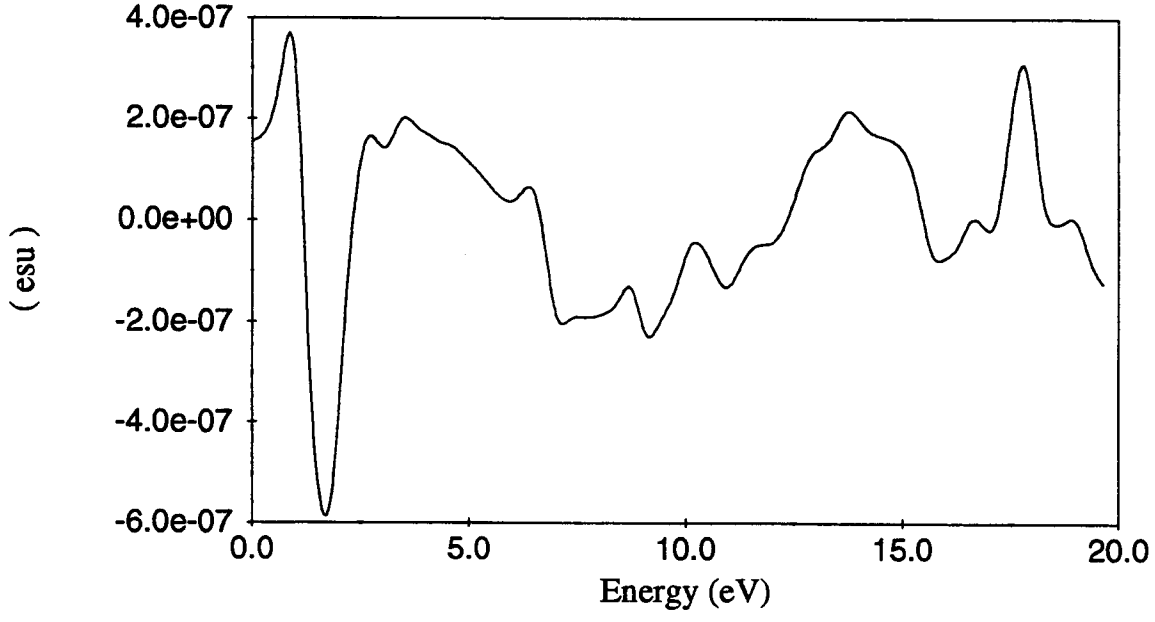

FIgure 7.16 Re $\chi_{zzz}^{(2)}(2\varpi)$ for the layered model of 48 layers.

7.4 Comparison and Discussion

In order to compare the results from the bulk calculation to the results from the layered model calculation, we plot them together in figures (7.17)-(7.20) for each of the four second harmonic optical response functions $\vec{\vec{\chi}}^{(2)}_{zzz}(2\omega)$, $\vec{\vec{\chi}}^{(2)}_{zxx}(2\omega)$, $\vec{\vec{\chi}}^{(2)}_{xzx}(2\omega)$, and $\vec{\vec{\chi}}^{(2)}_{xxz}(2\omega)$. Although the ZnO second harmonic response spectrum calculated using the layered model shows patterns similar to the spectrum calculated for the bulk crystal, the peaks are shifted and the magnitudes are different. The significant differences between the results of the bulk calculation and of the layered model calculation tell us that the surface plays a very important role in the second harmonic optical response of ZnO to the electromagnetic fields. To understand the nonlinear optical phenomena of the second harmonic generation of ZnO, one has to somehow include surface effects.

The contributions from surface states to the second harmonic optical response functions should decrease as the number of layers in our layered model increases. This is because the number of surface states remains unchanged while the total number of states increased if we increase the number of layers in our layered model. To check out which features are mostly due to pure surface states in the spectrum, we constructed our layered model with various number of layers and calculated the spectrum for each nonvanishing element of $\vec{\vec{\chi}}^{(2)}_{abc}(2\omega)$. The results are shown in figures (7.21)-(7.24).

From figures (7.21) to (7.24), we see where the spectrum scales inversely with the number of layers. The spectrum does not, however, scale with the number of layers in most regions of the spectrum. One might naively expect that in these regions, the layered model calculation should give the same results as the bulk crystal calculation. They are, however, significantly different from one another. Taking the surface into account, we not only obtained the surface states but also changed the bulk-like state wave functions. It is these changed wave functions that cause the differences

between the layered model calculation and the bulk crystal calculation in the region of the spectrum where there is a negligible direct contribution from the surface states.

Why do the changed bulk-like wave functions have such a significant impact on the second order harmonic response but almost no effects at all on the first order response? Why are similar patterns found in the bulk crystal calculations and the layered model calculations, but why do the peaks shift their positions and magnitudes so significantly? We leave these questions unanswered.

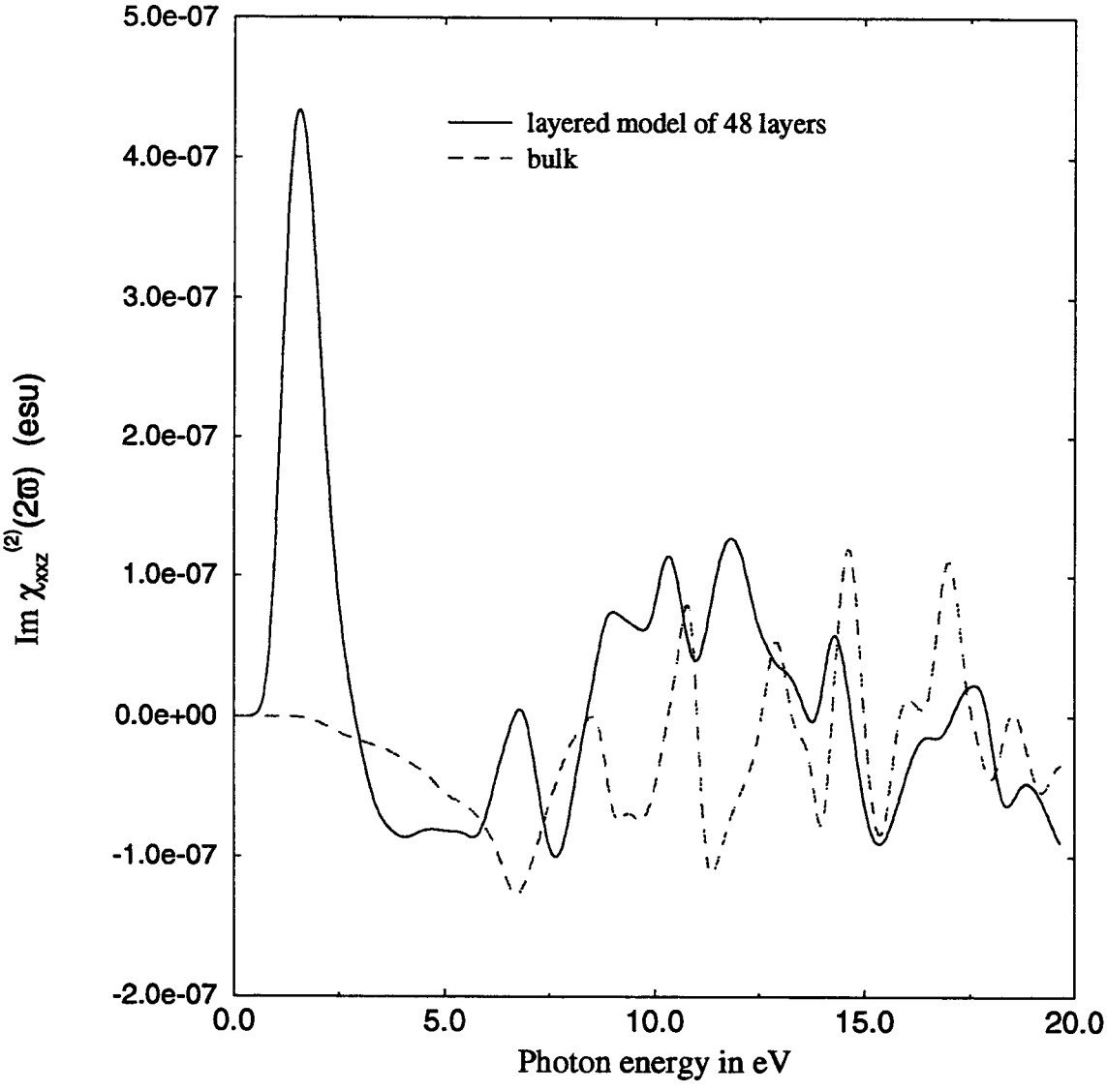

Figure 7.17 Comparison between bulk and layered model Im $\chi_{xxz}^{(2)}(2\varpi)$.

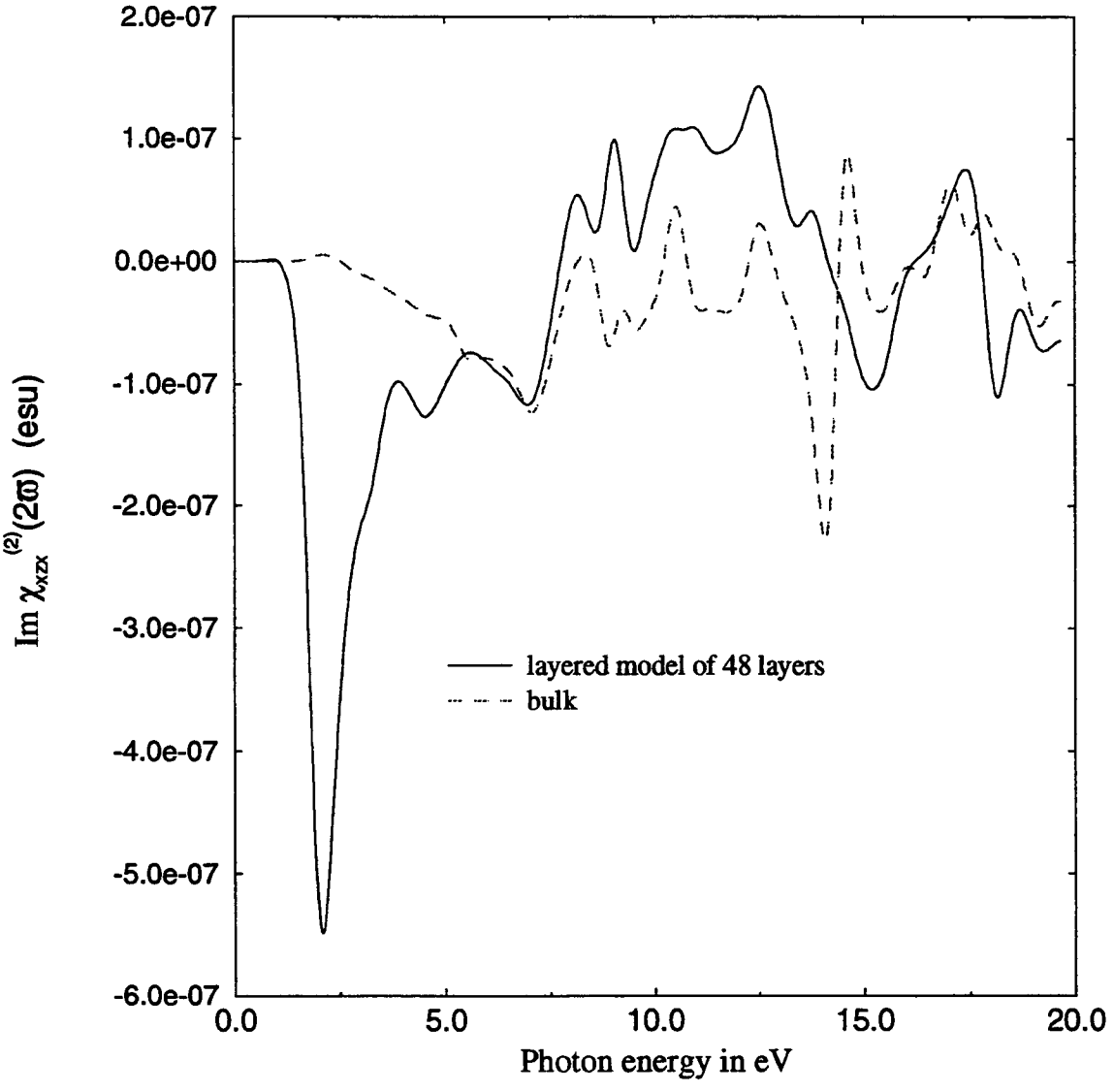

Figure 7.18 Comparison between bulk and layered model Im $\chi_{xzx}^{(2)}(2\varpi)$.

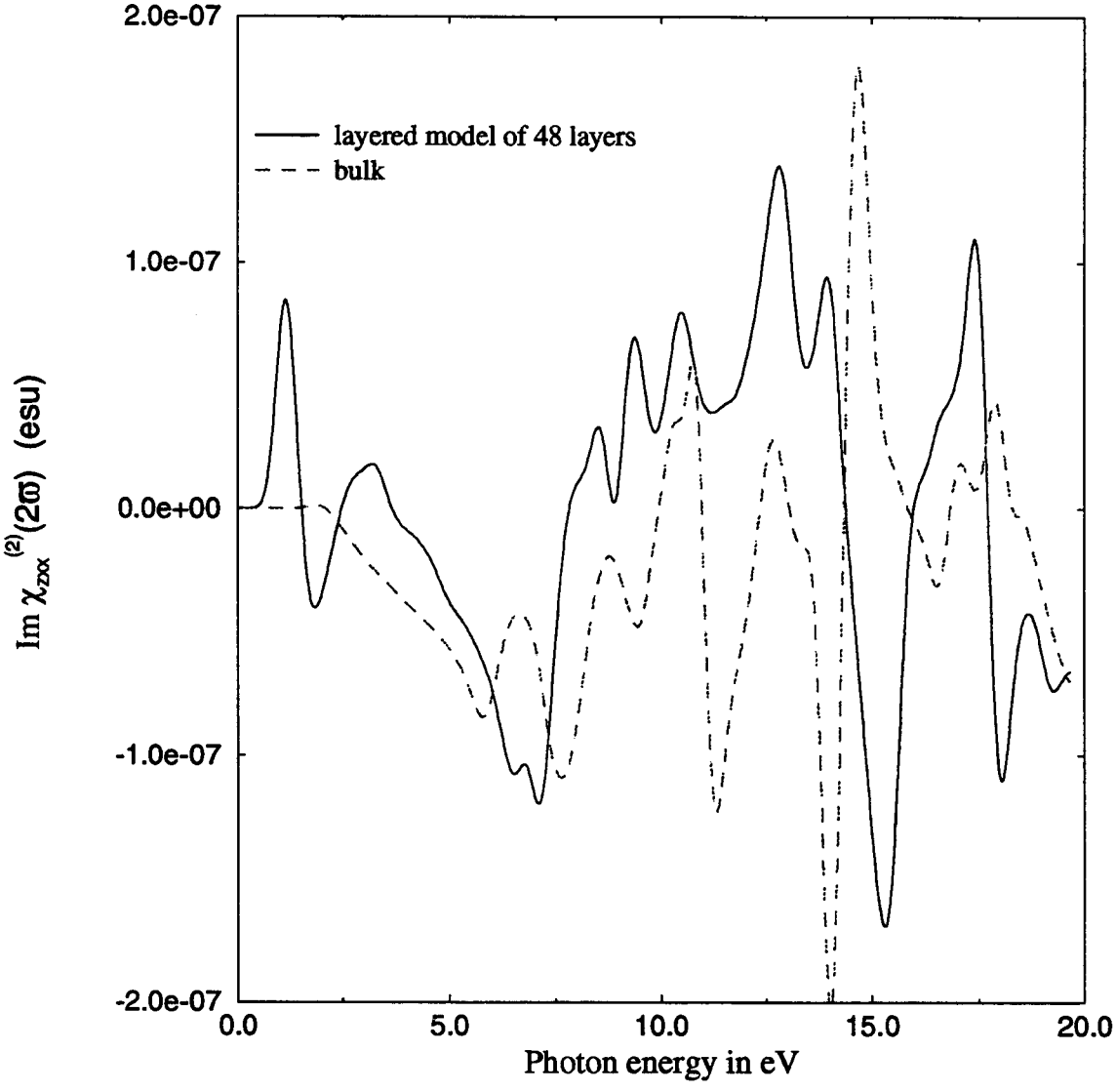

Figure 7.19 Comparison between bulk and layered model Im $\chi_{zxx}^{(2)}(2\varpi)$.

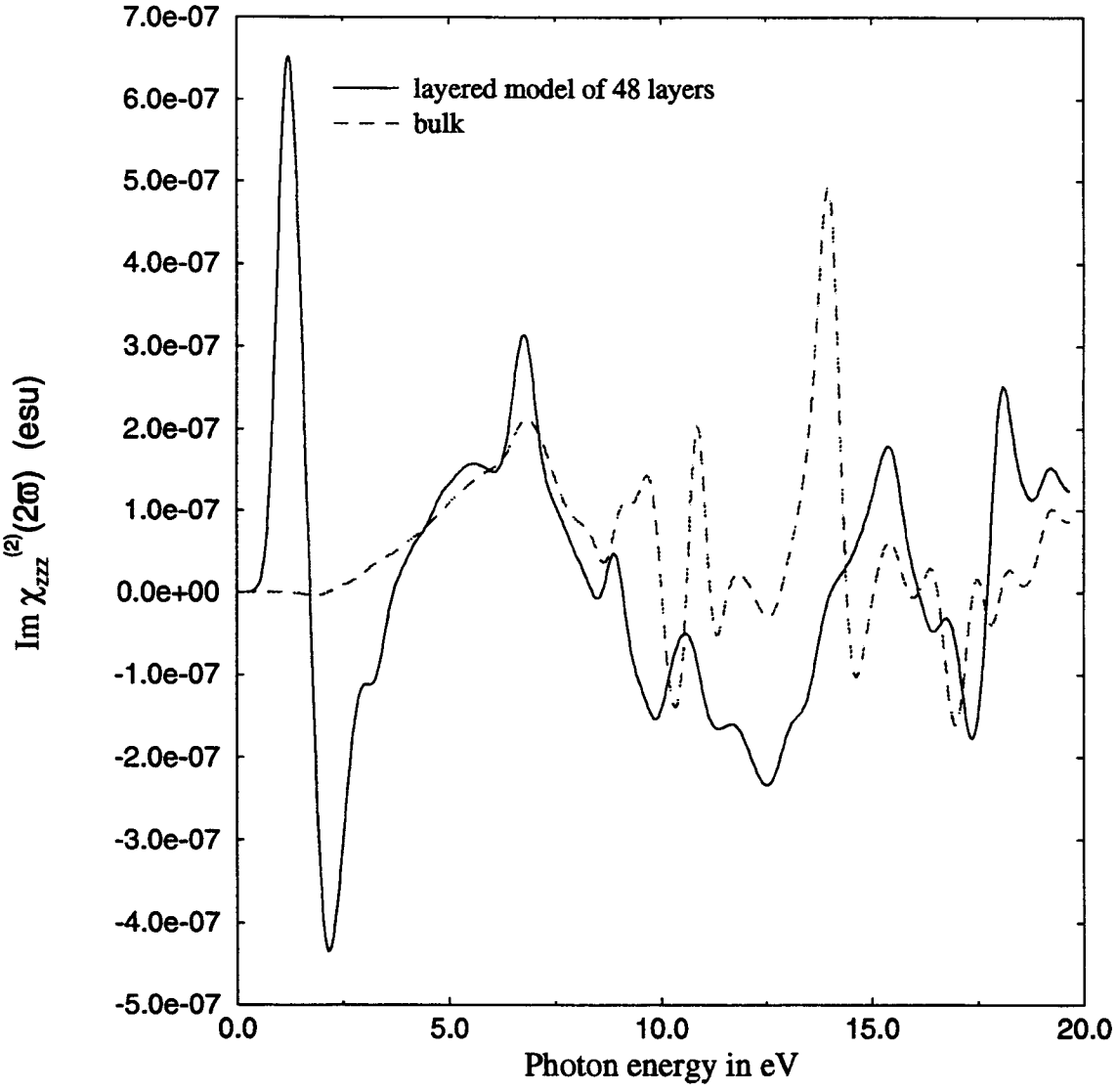

Figure 7.20 Comparison between bulk and layered model Im $\chi_{zzz}^{(2)}(2\varpi)$.

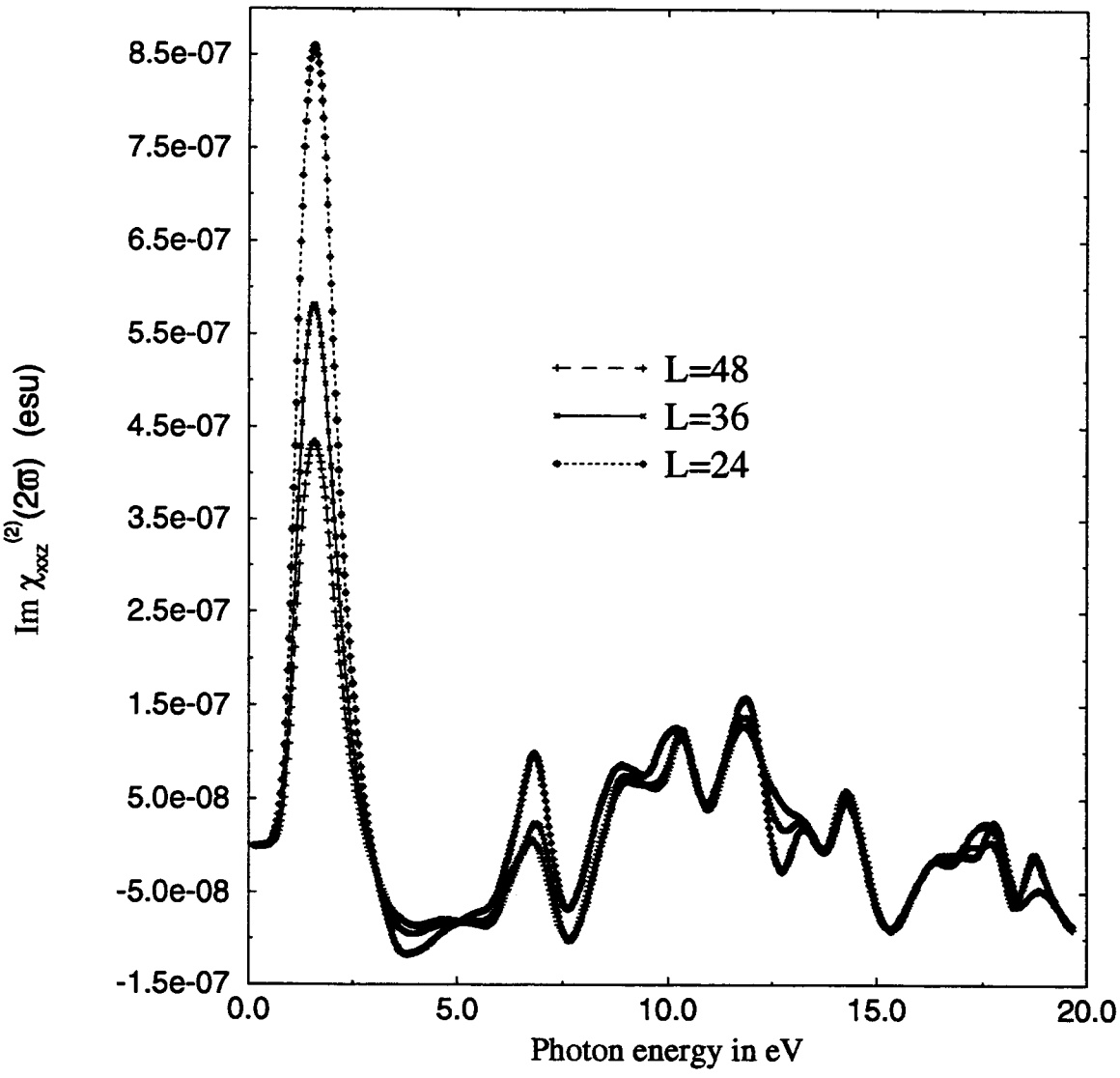

Figure 7.21 The results of $\chi_{xxz}^{(2)}(2\varpi)$ for the ZnO layered models with three different total numbers (L) of layers.

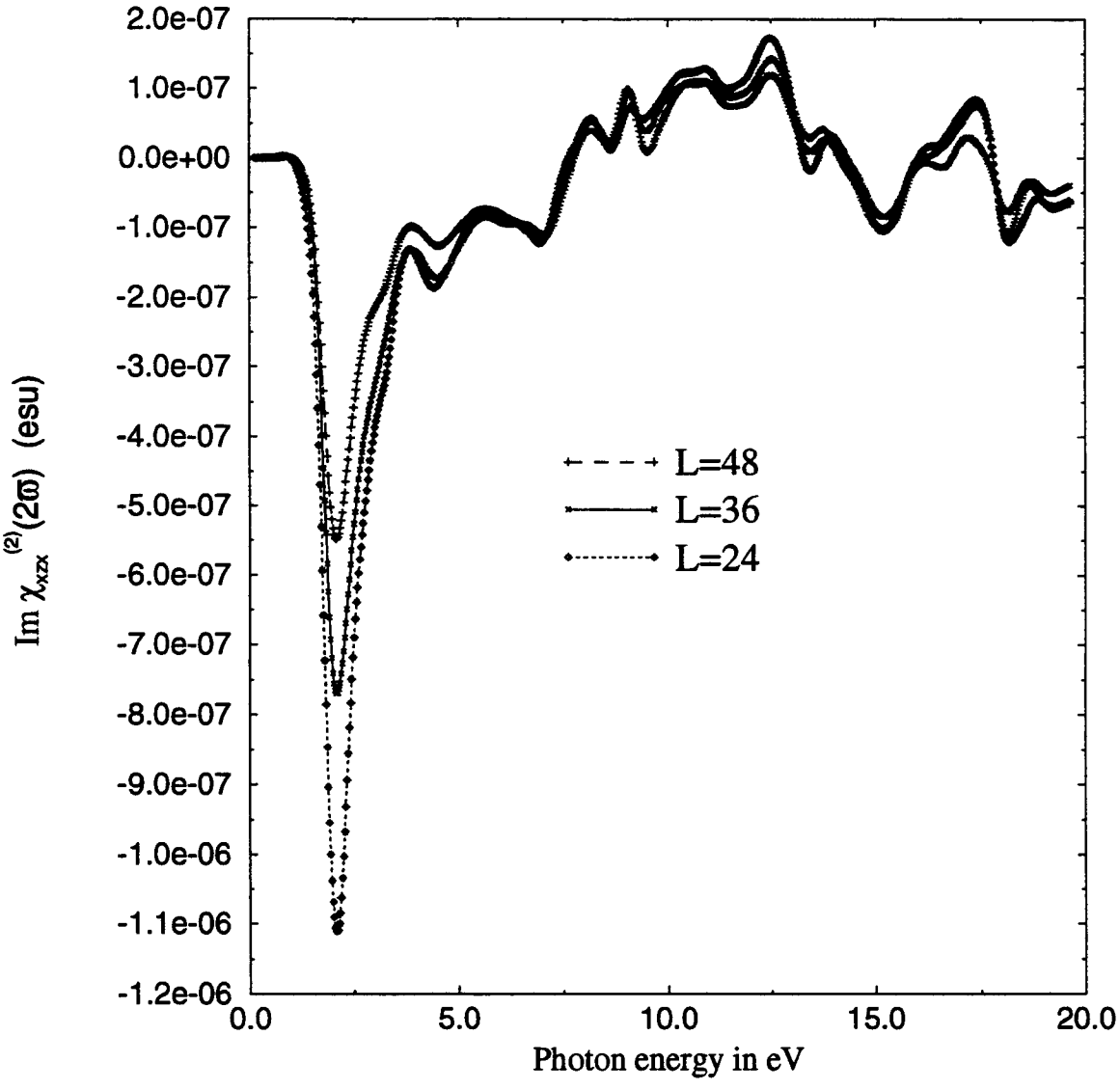

Figure 7.22 The results of $\chi_{xzx}^{(2)}(2\varpi)$ for the ZnO layered models with three different numbers (L) of layers.

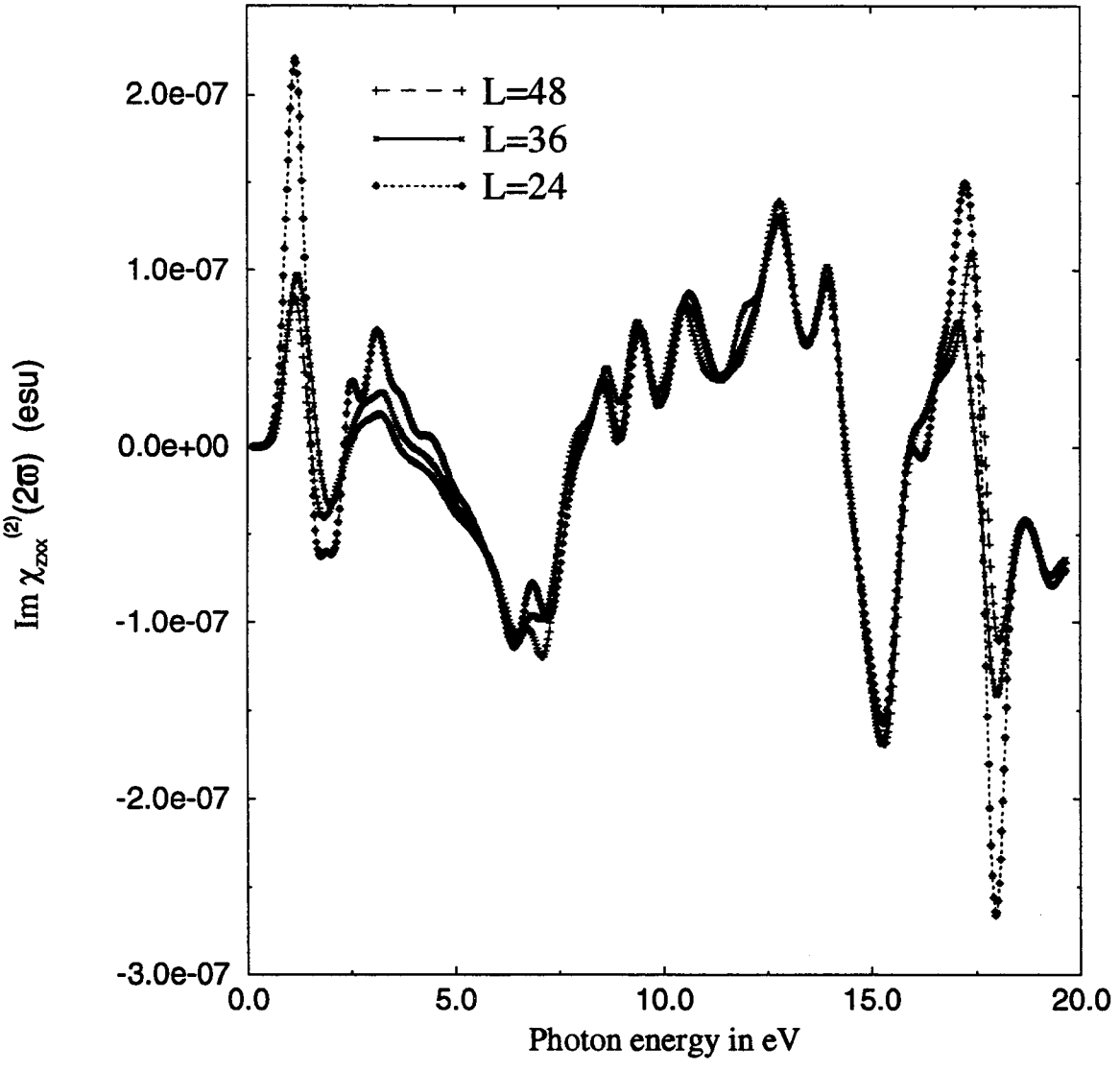

Figure 7.23 The results of $\chi_{zxx}^{(2)}(2\varpi)$ for the ZnO layered models with three different numbers (L) of layers.

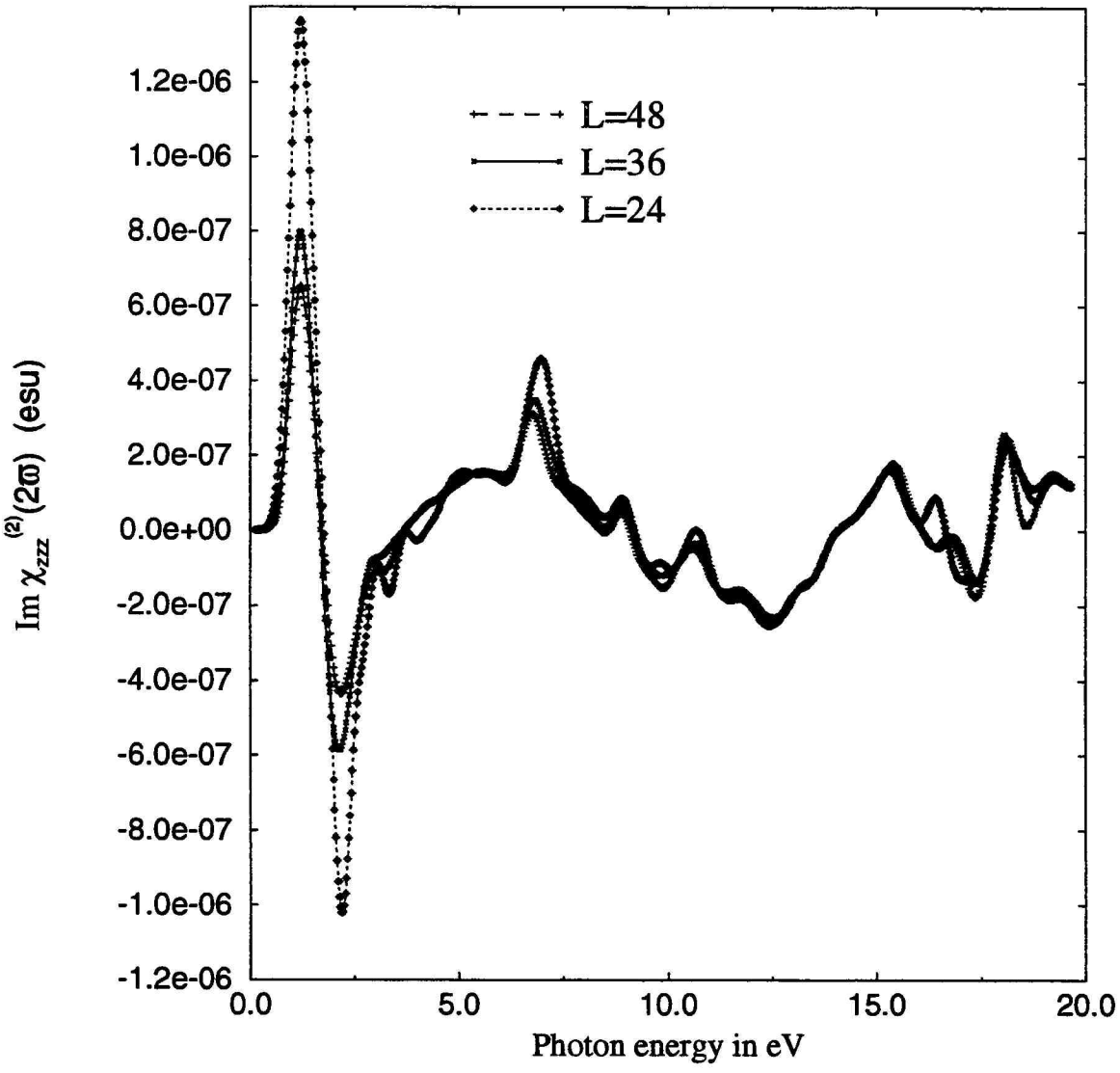

Figure 7.24 The results of $\chi_{zzz}^{(2)}(2\varpi)$ for the ZnO layered models with three different numbers (L) of layers.

Bibliography

1. P.A.Franken, A.E.Hill, C.W.Peters, and G.Weinreich, Phys. Rev. Lett. 7, 118 (1961).
2. Ed Ghahramani, D.J.Moss, J.E.Sipe, Phys. Rev. B43, 9269(1991).
3. Ed Ghahramani, D.J.Moss, J.E.Sipe, Phys. Rev. B43, 8990(1991).
4. Yong-Nian Xu, W.Y.Ching, preprint, 1993.
5. Y.R.Shen, The Principles of Nonlinear Optics (Wiley-Interscience, New York, 1984).
6. J.A.Armstrong, N.Bloembergen, J.Ducuing, and P.S.Pershan, Phys. Rev. 127, 1918(1962).
7. W.A.Harrison, Electronic Structure and the Properties of Solids (W.H. Freeman and Company, San Francisco, 1980).
8. J.D.Jackson, Classical Electrodynamics (John Wiley & Sons, New York, 1975).
9. L.D.Landau and E.M.Lifshitz, Eletrodynamics of Continuous Media (Pergamon Press, New York, 1984).
10. D.J.Moss, E.Ghahramani, J.E.Sipe, and H.M.van Driel, Phys. Rev. B41, 1542(1990).
11. N.Bloembergen, Nonliear Optics (W.A. Benjamin, New York, 1965).
12. R.J.Glauber, Phys. Rev. 131, 2766(1963).
13. R.J.Glauber, Phys. Rev. 130, 2529(1963).
14. W.A.Harrison, and S.T.Pantelides, Phys. Rev. B14 (691). 101, 102, 111 (1976).
15. N.W.Ashcroft, N.D. Mermin, Solid State Physics (W.B. Saunders Company, New York, 1976).
16. M.Rosenbauer, Parametrization of Energy bands in Zirconia, M.S. thesis, OSU, 1991.

17. D.W.Marquardt, An algorithm for least-squares estimation of nonlinear parameters; Journal O. Soc. for Industrial and Applied Mathematics 11, 431 (1963).

18. A.Kobayashi, O.F.Sankey, S.M.Volz, and J.D.Dow, Semiempirical tight-banding band structures of wurtzite semiconductors, Phys.Rev. B28, 935 (1983).

19. P.Vogl, H.D.Hjalmarson, and J.D.Dow, J. Phys. Chem. Solids, 44, 365(1983).

20. L.I.Schiff, Quantum Mechanics (McGraw-Hill, New York, 1968).

21. J.Rath, A.J.Freeman, Phys. Rev. B11, 2109 (1975)

22. R. Klucker, H. Nelkowski, Y.S.Park, M.Skibowski, and T.S. Wagner, Phys. Stat. Sol. (b) 45, 265 (1971)

23. John L. Freeouf, Phys. Rev. B7, 3810 (1973)

Appendix

Appendix A The C program computing the Hamiltonian of ZnO

```
/*********************************************************************
This program accepts Bloch wave vector (k[1],k[2],k[3]) defined as
k=2*pi*(k[1]/a,k[2]/a,k[3]/c) as inputs where 'a' & 'c' are the lengths of unit cell in
hexagonal Bravis Lattice and k is the Bloch wave vector. Then, it calculates the 16x16
Hamiltonian matrix elements of ZnO crystal bulk and stores the results in the two 16x16
matrices of "mtrx" and "imtrx" for real and imaginary parts respectively.
*********************************************************************/

#include <math.h>
#include <stdio.h>

void wrztmtrx(mtrx,imtrx,k)
double mtrx[16][16],imtrx[16][16],k[4];
{
  static int    IsFirst=1;
  static double  A1S,A2S,C1S,C2S,A1P,A2P,C1P,C2P;   /* Parameters of the */
  static double  vss,vsp,vps,vpp,vppi;                /* Hamiltonian matrix */

  int i,j;
  double xp,ratio,cfi,cfi2,sfi,sfi2,pi,u,x1,d[5][4],dy[5][4],kd[5],kdy[5];
  double exc2,exc3,exs2,exs3,eyc2,eyc3,eys2,eys3;
  extern FILE *fpInput;

  if(IsFirst) {
                IsFirst=0;
                fscanf(fpInput,"%lf",&A1S);
                fscanf(fpInput,"%lf",&A2S);
                fscanf(fpInput,"%lf",&C1S);
                fscanf(fpInput,"%lf",&C2S);
                fscanf(fpInput,"%lf",&A1P);
                fscanf(fpInput,"%lf",&A2P);
                fscanf(fpInput,"%lf",&C1P);
                fscanf(fpInput,"%lf",&C2P);

                fscanf(fpInput,"%lf",&vss);
                fscanf(fpInput,"%lf",&vpp);
                fscanf(fpInput,"%lf",&vppi);
                fscanf(fpInput,"%lf",&vsp);
                fscanf(fpInput,"%lf",&vps);
                }
```

```
for(i=1;i<=4;i++)
  {
   kd[i]=0.0;
   kdy[i]=0.0;
   for(j=1; j<=3; j++)
        {
         d[i][j]=0.0;
         dy[i][j]=0.0;
         }
    }

for(i=0; i<16; i++)
   for(j=0;j<16;j++)
   {
        mtrx[i][j]=0.0;
        imtrx[i][j]=0.0;
        }

xp=0.5*sqrt(3.0);
ratio=sqrt(8.0/3.0);
u=3.0/8.0;
pi=4.*atan(1.0);
cfi2=1.0/(1.0+3.0*ratio*ratio*(0.5-u)*(0.5-u));
cfi=sqrt(cfi2);
sfi2=1.0-cfi2;
sfi=sqrt(sfi2);

d[1][1]=0.5;
d[1][2]=d[2][2]=sqrt(3.0)/6.0;
d[2][1]=-0.5;
d[1][3]=d[2][3]=d[3][3]=0.5-u;
d[3][1]=d[4][1]=d[4][2]=0.0;
d[3][2]=-1.0/sqrt(3.0);
d[4][3]=-u;

for(i=1;i<5;i++)
        for(j=1;j<4;j++)
            {
               dy[i][j]=d[i][j];
               if(j==2)  dy[i][j]=-d[i][j];
          }
for (i=1;i<5;i++)
      for (j=1;j<4;j++)
```

```
        {
         kd[i]+=d[i][j]*k[j]*2.0*pi;
         kdy[i]+=dy[i][j]*k[j]*2.0*pi;
      }

exc2=cos(kd[1])+cos(kd[2]);
exs2=sin(kd[1])+sin(kd[2]);
exc3=cos(kd[3])+exc2;
exs3=sin(kd[3])+exs2;
eyc2=cos(kdy[1])+cos(kdy[2]);
eyc3=eyc2+cos(kdy[3]);
eys2=sin(kdy[1])+sin(kdy[2]);
eys3=eys2+sin(kdy[3]);

mtrx[0][0]=A1S;
mtrx[0][4]=vss*exc3;
imtrx[0][4]=vss*exs3;
mtrx[0][5]=vsp*xp*cfi*(cos(kd[1])-cos(kd[2]));
imtrx[0][5]=vsp*xp*cfi*(sin(kd[1])-sin(kd[2]));
mtrx[0][6]=vsp*cfi*(0.5*exc2-cos(kd[3]));
imtrx[0][6]=vsp*cfi*(0.5*exs2-sin(kd[3]));
mtrx[0][7]=vsp*sfi*exc3;
imtrx[0][7]=vsp*sfi*exs3;
mtrx[0][12]=vss*cos(kd[4]);
imtrx[0][12]=vss*sin(kd[4]);
mtrx[0][15]=-vsp*cos(kd[4]);
imtrx[0][15]=-vsp*sin(kd[4]);

mtrx[1][1]=A1P;
mtrx[1][4]=-vps*xp*cfi*(cos(kd[1])-cos(kd[2]));
imtrx[1][4]=-vps*xp*cfi*(sin(kd[1])-sin(kd[2]));
mtrx[1][5]=(vppi*(0.75*sfi2+0.25)+0.75*cfi2*vpp)*exc2+vppi*cos(kd[3]);
imtrx[1][5]=(vppi*(.75*sfi2+.25)+0.75*cfi2*vpp)*exs2+vppi*sin(kd[3]);
mtrx[1][6]=0.5*xp*cfi2*(vpp-vppi)*(cos(kd[1])-cos(kd[2]));
imtrx[1][6]=0.5*xp*cfi2*(vpp-vppi)*(sin(kd[1])-sin(kd[2]));
mtrx[1][7]=xp*sfi*cfi*(vpp-vppi)*(cos(kd[1])-cos(kd[2]));
imtrx[1][7]=xp*sfi*cfi*(vpp-vppi)*(sin(kd[1])-sin(kd[2]));
mtrx[1][13]=vppi*cos(kd[4]);
imtrx[1][13]=vppi*sin(kd[4]);

mtrx[2][2]=A1P;
mtrx[2][4]=-vps*cfi*(0.5*exc2-cos(kd[3]));
imtrx[2][4]=-vps*cfi*(0.5*exs2-sin(kd[3]));
mtrx[2][5]=0.5*xp*cfi2*(vpp-vppi)*(cos(kd[1])-cos(kd[2]));
imtrx[2][5]=0.5*xp*cfi2*(vpp-vppi)*(sin(kd[1])-sin(kd[2]));
```

```
mtrx[2][6]=(.25*cfi2*vpp+(.25*sfi2+.75)*vppi)*exc2;
mtrx[2][6]+=(cfi2*vpp+sfi2*vppi)*cos(kd[3]);
imtrx[2][6]=(.25*cfi2*vpp+(.25*sfi2+.75)*vppi)*exs2;
imtrx[2][6]+=(cfi2*vpp+sfi2*vppi)*sin(kd[3]);
mtrx[2][7]=(vpp-vppi)*(0.5*exc2-cos(kd[3]))*sfi*cfi;
imtrx[2][7]=(vpp-vppi)*(0.5*exs2-sin(kd[3]))*sfi*cfi;
mtrx[2][14]=vppi*cos(kd[4]);
imtrx[2][14]=vppi*sin(kd[4]);

mtrx[3][3]=A1P;
mtrx[3][4]=-vps*sfi*exc3;
imtrx[3][4]=-vps*sfi*exs3;
mtrx[3][5]=xp*sfi*cfi*(vpp-vppi)*(cos(kd[1])-cos(kd[2]));
imtrx[3][5]=xp*sfi*cfi*(vpp-vppi)*(sin(kd[1])-sin(kd[2]));
mtrx[3][6]=sfi*cfi*(vpp-vppi)*(.5*exc2-cos(kd[3]));
imtrx[3][6]=sfi*cfi*(vpp-vppi)*(.5*exs2-sin(kd[3]));
mtrx[3][7]=(sfi2*vpp+cfi2*vppi)*exc3;
imtrx[3][7]=(sfi2*vpp+cfi2*vppi)*exs3;
mtrx[3][12]=vps*cos(kd[4]);
imtrx[3][12]=vps*sin(kd[4]);
mtrx[3][15]=vpp*cos(kd[4]);
imtrx[3][15]=vpp*sin(kd[4]);

mtrx[4][4]=C1S;
mtrx[4][8]=vss*cos(kd[4]);
imtrx[4][8]=-vss*sin(kd[4]);
mtrx[4][11]=vps*cos(kd[4]);
imtrx[4][11]=-vps*sin(kd[4]);

mtrx[5][5]=C1P;
mtrx[5][9]=vppi*cos(kd[4]);
imtrx[5][9]=-vppi*sin(kd[4]);

mtrx[6][6]=C1P;
mtrx[6][10]=vppi*cos(kd[4]);
imtrx[6][10]=-vppi*sin(kd[4]);

mtrx[7][7]=C1P;
mtrx[7][8]=-vsp*cos(kd[4]);
imtrx[7][8]=vsp*sin(kd[4]);
mtrx[7][11]=vpp*cos(kd[4]);
imtrx[7][11]=-vpp*sin(kd[4]);

mtrx[8][8]=A2S;
mtrx[8][12]=vss*eyc3;
```

```
imtrx[8][12]=vss*eys3;
mtrx[8][13]=vsp*xp*cfi*(cos(kdy[1])-cos(kdy[2]));
imtrx[8][13]=vsp*xp*cfi*(sin(kdy[1])-sin(kdy[2]));
mtrx[8][14]=-vsp*cfi*(0.5*eyc2-cos(kdy[3]));
imtrx[8][14]=-vsp*cfi*(0.5*eys2-sin(kdy[3]));
mtrx[8][15]=vsp*sfi*eyc3;
imtrx[8][15]=vsp*sfi*eys3;

mtrx[9][9]=A2P;
mtrx[9][12]=-vps*xp*cfi*(cos(kdy[1])-cos(kdy[2]));
imtrx[9][12]=-vps*xp*cfi*(sin(kdy[1])-sin(kdy[2]));
mtrx[9][13]=(vppi*(0.75*sfi2+0.25)+0.75*cfi2*vpp)*eyc2+vppi*cos(kdy[3]);
imtrx[9][13]=(vppi*(.75*sfi2+.25)+0.75*cfi2*vpp)*eys2+vppi*sin(kdy[3]);
mtrx[9][14]=-0.5*xp*cfi2*(vpp-vppi)*(cos(kdy[1])-cos(kdy[2]));
imtrx[9][14]=-0.5*xp*cfi2*(vpp-vppi)*(sin(kdy[1])-sin(kdy[2]));
mtrx[9][15]=xp*sfi*cfi*(vpp-vppi)*(cos(kdy[1])-cos(kdy[2]));
imtrx[9][15]=xp*sfi*cfi*(vpp-vppi)*(sin(kdy[1])-sin(kdy[2]));

mtrx[10][10]=A2P;
mtrx[10][12]=vps*cfi*(0.5*eyc2-cos(kdy[3]));
imtrx[10][12]=vps*cfi*(0.5*eys2-sin(kdy[3]));
mtrx[10][13]=-.5*xp*cfi2*(vpp-vppi)*(cos(kdy[1])-cos(kdy[2]));
imtrx[10][13]=-.5*xp*cfi2*(vpp-vppi)*(sin(kdy[1])-sin(kdy[2]));
mtrx[10][14]=.25*(cfi2*vpp+(sfi2+3.)*vppi)*eyc2;
mtrx[10][14]+=(cfi2*vpp+sfi2*vppi)*cos(kdy[3]);
imtrx[10][14]=.25*(cfi2*vpp+(sfi2+3.)*vppi)*eys2;
imtrx[10][14]+=(cfi2*vpp+sfi2*vppi)*sin(kdy[3]);
mtrx[10][15]=sfi*cfi*(vpp-vppi)*(cos(kdy[3])-.5*eyc2);
imtrx[10][15]=sfi*cfi*(vpp-vppi)*(sin(kdy[3])-.5*eys2);

mtrx[11][11]=A2P;
mtrx[11][12]=-vps*sfi*eyc3;
imtrx[11][12]=-vps*sfi*eys3;
mtrx[11][13]=xp*sfi*cfi*(vpp-vppi)*(cos(kdy[1])-cos(kdy[2]));
imtrx[11][13]=xp*sfi*cfi*(vpp-vppi)*(sin(kdy[1])-sin(kdy[2]));
mtrx[11][14]=sfi*cfi*(vpp-vppi)*(cos(kdy[3])-.5*eyc2);
imtrx[11][14]=sfi*cfi*(vpp-vppi)*(sin(kdy[3])-.5*eys2);
mtrx[11][15]=(sfi2*vpp+cfi2*vppi)*eyc3;
imtrx[11][15]=(sfi2*vpp+cfi2*vppi)*eys3;

mtrx[12][12]=C2S;
mtrx[13][13]=C2P;
mtrx[14][14]=C2P;
mtrx[15][15]=C2P;
```

```
 for (i=1; i<16; i++)
 {
  for (j=0; j<i; j++)
  {
        mtrx[i][j]=mtrx[j][i];
        imtrx[i][j]=-imtrx[j][i];
  }
 }
}
```